



Ryana Carvalho

Encapsulação de nanopartículas de $Gd_2O_3: Eu^{3+}$ @ SiO_2 com agentes RAFT macromoleculares de PAA

Encapsulation of SiO_2 coated $Gd_2O_3: Eu^{3+}$ nanoparticles using PAA macroRAFT agents



Ryana Carvalho

Encapsulação de nanopartículas de $Gd_2O_3: Eu^{3+}$ @ SiO_2 com agentes RAFT macromoleculares de PAA

Encapsulation of SiO_2 coated $Gd_2O_3: Eu^{3+}$ nanoparticles using PAA macroRAFT agents

Dissertação apresentada à Universidade de Aveiro para cumprimento dos requisitos necessários à obtenção do grau de Mestre em Ciência e Engenharia dos Materiais, realizada sob a orientação científica da Dra. Ana Barros Timmons, Professora Auxiliar do Departamento de Química da Universidade de Aveiro

הַשָּׁמַיִם מְסַפְּרִים כְּבוֹד־אֱלֹהִים וּמַעֲשֵׂה יָדָיו מִגִּיד הַרְקִיעַ:

*The heavens declare the glory of God;
and the firmament sheweth his handiwork (Psalm 19:1)*

o júri

presidente

Prof. Dr. Dmitry V. Evtuguin
Associate Professor with Aggregation, Universidade de Aveiro

Prof. Dr. Maria do Rosario Ribeiro
Auxiliary Professor, Universidade Tecnica de Lisboa

Prof. Dr. Ana Magarida Madeira Viegas de Barros Timmons
Auxiliary Professor, Universidade de Aveiro

acknowledgements

First and foremost I would like to express my deepest gratitude to my thesis advisor, Auxiliary Professor **Ana Barros Timmons** for her time, constructive advice, and willingness to share her knowledge and wisdom.

I would also like to thank some other people for their helpful collaborations like **Dr. Duarte Ananias** for his assistance in obtaining the $\text{Gd}_2\text{O}_3:\text{Eu}^{3+}$ fibres and collecting PL data. **Dr. Dmitry Evtuguin** for help concerning GPC. Marta, Violeta, Ricardo for lending a hand during SEM and S-TEM operations and Fabiane Costa Oliveira for the help extended while synthesizing silica.

The assistance of the members of the technical staff is also gratefully acknowledged; especially Belinda for help within the laboratory, Sandra for help with DSC and Celeste for lending a hand in TGA operations. Also a special thanks goes out to Nuno, Andrea, Marina, Natercia and Carla for general assistance in the lab.

I would like to express my gratitude to the **FAME consortium** for their financial support during the course of this Masters Program. Another round of thanks is acknowledged to my family and friends, for their love and support. Last but by no means least, a big thanks to my Lord and Saviour **Jesus Christ** for being with me through the rough storms and smooth sailings.

palavras-chave

polimerização radicalar, nanocompósitos, sílica, $Gd_2O_3:Eu^{3+}@SiO_2$, materiais anisotrópicos, agente RAFT macromolecular, ácido poli(acrílico)

resumo

O desenvolvimento de novos materiais com propriedades funcionais é uma constante necessidade para a maturação e sustentabilidade da sociedade como um todo. No que diz respeito aos nanocompósitos de matriz polimérica, uma das maiores restrições ao seu uso é a preservação e o controlo das propriedades físicas únicas das cargas de dimensões nanométricas, sendo portanto essencial manter a sua integridade e conseguir dispersões uniformes. Tal é particularmente difícil no caso de nanopartículas anisotrópicas, tais como as fibras de $Gd_2O_3:Eu^{3+}$ revestidas com sílica utilizadas nesta tese. Nesse sentido, estudou-se a utilização de agentes RAFT macromoleculares para preparar nanocompósitos de matriz polimérica inorgânicos quer em solução quer em emulsão.

Numa primeira fase estudou-se a preparação do agente RAFT macromolecular a partir do agente RAFT ácido 2-[[dodeciltio]carbonotioil]tio]-2-metilpropanóico (TTCA) e do ácido acrílico para diferentes graus de conversão, tendo-se obtido polímeros controlados e com distribuições de massa moleculares (PDI) estreitas. Seguidamente, verificou-se que o sistema apresenta as características de um sistema vivo por co-polimerização com o acrilato de butilo (BuA) tanto em emulsão como em solução. No entanto, não se obteve controlo no PDI, nomeadamente quando a polimerização foi realizada em emulsão. Apesar de não se ter conseguido otimizar este sistema, a sua utilização foi explorada na preparação de nanocompósitos de sílica e depois estendido a fibras de $Gd_2O_3:Eu^{3+}$ revestidas com sílica. Com o objectivo de aumentar a afinidade entre o polímero e as cargas, as nanopartículas inorgânicas foram funcionalizadas com agentes de acoplamento à base de silano. Os nanocompósitos obtidos foram depois caracterizados por FT-IR, DSC, SEM, e PL. Os resultados obtidos por SEM e FTIR-ATR permitiram confirmar que a preparação dos nanocompósitos foi bem sucedida. Porém os resultados de DSC foram inconclusivos e os de fotoluminescência indicam que após funcionalização com o 3-aminopropilo trimetoxisilano (APS) o sinal é reduzido sendo esse efeito agravado após encapsulamento na matriz polimérica.

Por fim são apresentados alguns resultados relativos à preparação de filmes finos dos nanocompósitos de modo a avaliar a presença de alguma anisotropia.

keywords

radical polymerization, nanocomposites, silica , Gd₂O₃:Eu³⁺, anisotropic materials, macroRAFT agent, poly(acrylic acid)

abstract

New materials with functional properties are a consistent necessity for the maturation and sustainability of society on a whole. One main restriction when polymer based nanocomposites are concerned is the preservation and control of the unique physical properties of the nanometric fillers. However, it is quite essential to maintain their nanoscale integrity and hitherto achieve uniform dispersions, which is extremely challenging especially when anisotropic nanoparticles are brought into the limelight, such as Gd₂O₃:Eu³⁺ fibers coated with silica studied in this thesis. In this regard, polymer nanocomposites were devised using a macroRAFT agent both in solution and emulsion.

Initially, the homopolymerization of acrylic acid (AA) using 2-[[dodecylthio]carbonothioyl]thio-2-methylpropanoic acid (TTC-A), to yield the macroRAFT agent (PAATTC) was studied for varying degrees of conversion and narrow molar mass distributions prevailed. Next, the copolymerization of PAATTC with n-butyl acrylate (nBuA) was carried out in both emulsion and solution conditions to test the livingness of the system which was confirmed, but proved to be uncontrolled. Despite the fact that this system was not optimized, it was utilized in the preparation of silica nanocomposites and extended to the preparation of Gd₂O₃:Eu³⁺@silica nanocomposites. In order to increase the affinity between the polymer and the inorganic nanofillers, the latter was functionalized using suitable silane coupling agents. The nanocomposites obtained were characterized by FTIR, SEM, DSC, and PL. While SEM and FTIR, confirmed the successful formation of nanocomposites, the DSC results were inconclusive and the PL results of Gd₂O₃:Eu³⁺@silica showed a decrease in the signal intensity, upon functionalization with 3-aminopropyl trimethoxysilane (APS), which was further aggravated upon encapsulation in the polymeric matrix.

Finally, some preliminary results regarding the preparation of composite thin films to assess the presence of any anisotropy are documented.

Table Of Contents

	Subject	Page Number
1	Chapter 1:General Introduction and Review of Literature	1-24
	Preface	1
1.1	Nanocomposite Basics	1
1.2	Types of Nanocomposites	2
1.2.1	Polymer Matrix Nanocomposites (PMNs)	2
1.3	The Polymerization Process	7
1.3.1	Brief Introduction	7
1.3.2	Controlled and Living Polymerization	7
1.3.3	Types of Controlled and Living Polymerization	8
1.3.3.1	Addition Fragmentation Chain Transfer Process (AFCT Process)	8
1.3.3.2	Reverse Addition Fragmentation Chain Transfer Process	8
1.3.3.2.1	Thiocarbonylthio RAFT agents	9
1.3.3.2.2	RAFT Mechanism of Thiocarbonylthio Compounds	10
1.3.3.3	RAFT Polymerization System Studies	11
1.3.3.3.1	MacroRAFT agents	11
1.3.3.3.2	The Acrylate System	12
1.3.4	Process Conditions	13
1.3.4.1	Polymerization in Solution	14
1.3.4.2	Polymerization in Emulsion	14
1.4	Nanocomposite Preparation Methodologies	15
1.5	Polymeric encapsulation of Silica Nanoparticles	16

1.6	Anisotropic Nanocomposites (Polymer Encapsulated)	17
1.7	Deposition of Nanocomposites on Glass	18
1.8	Thesis Breakup	19
1.9	Bibliography	20
2	Chapter 2: Polymerization studies Performed under RAFT	25-41
	Preface	25
2.1	Introduction	25
2.2	Preparation of the macroRAFT agent PAA-TTC	26
2.2.1	Characterization of the RAFT and the macroRAFT agent	28
2.3.	Formation of Block Copolymer	31
2.3.1	Block Copolymerization in Solution and Emulsion	32
2.3.2.1	Characterization of (PAA co PBuA) TTC	33
2.4	Preparation of (PAA co PBuA) TTC (5:10 ratios)	37
2.5	General Remarks, Conclusions and Future Work	38
2.6	Bibliography	40
3	Chapter 3: Inorganic Nano Fillers	43-64
	Preface	43
3.1	Silica Nanoparticles	43
3.1.1	Introduction	43
3.1.2	Spherical Silica Nanoparticles	44
3.1.3	Silica Nanofibres (hollow)	45

3.1.4	Modification of SiO ₂ nanoparticles	46
3.1.4.1	Surface Modification with MPS	47
3.1.4.2	Surface Modification with APS	47
3.1.5	Characterization of SiO ₂ particles (unmodified)	48
3.1.6	Characterization of surface modified SiO ₂ particles	52
3.2	Gd ₂ O ₃ :Eu ³⁺ @ Silica Nanorods/Fibres Preparation	53
3.2.1	Inorganic Lanthanide (Ln ³⁺)Series Introduction	53
3.2.2	Gd ₂ O ₃ :Eu ³⁺ Nanorods/Fibres Preparation	54
3.2.2.1	Surface Modification of SiO ₂ coated Gd ₂ O ₃ :Eu ³⁺	54
3.2.3	Characterization of Gd ₂ O ₃ :Eu ³⁺ particles	54
3.3	General Remarks and Conclusions	60
3.4	Bibliography	62
4	Chapter 4: Synthesis and Characterization of Nanocomposites	65-81
	Preface	65
4.1	General Introduction	65
4.2	Silica Nanocomposites Preparation	67
4.2.1	Silica Nanocomposites Characterization	68
4.3	Gd ₂ O ₃ :Eu ³⁺ @Silica nanocomposites preparation and characterization	75
4.4	General Remarks and Conclusions	79
4.5	Bibliography	80

5	Chapter 5: Laboratory Experimentation	83-92
	Preface	83
5.1	Instrumentation	83
5.2	Reagents Used	84
5.3	Laboratory Synthesis	84
5.3.1	Polymerization Processes	84
5.3.1.1	Homopolymerization of Acrylic Acid (PAA-TTC)	84
5.3.1.2	Co-polymerization of PAATTC with Butyl Acrylate	85
5.3.1.2.1	Co-polymerization in Solution	85
5.3.1.2.2	Co-polymerization in Emulsion	85
5.3.1.3	Co-polymerization in Emulsion (5:10 ratios)	86
5.4	Inorganic Nanofillers	86
5.4.1	Silica Nanofillers	84
5.4.1.1	Preparation of Spherical Silica Nanoparticles	86
5.4.1.2	Preparation of hollow SiO ₂ fibres	87
5.4.1.3	Surface Modification of Silica	87
5.4.1.3.1	Surface Modification of Silica with MPS	87
5.4.1.3.2	Surface Modification of Silica with APS	88
5.4.2	Gd ₂ O ₃ :Eu ³⁺ @ Silica APS nanorods/fibers Nanocomposites	88
5.4.2.1	Gd (OH) ₃ : Eu ³⁺ nano rods/fibres preparation	88
5.4.2.2	Gd ₂ O ₃ :Eu ³⁺ @ silica Nanorods Preparation	89
5.4.2.3	Gd ₂ O ₃ :Eu ³⁺ @ silica APS preparation	89
5.5	Preparation of Nanocomposites	89

5.5.1	Nanocomposites in emulsion (5:10 ratio)	89
5.6	Preparation of Polymeric films	90
5.6.1	Casting	90
5.6.2	Spin Coating	90
5.7	Sample Preparation Techniques	90
5.7.1	Preparing polymeric samples for GPC analysis, methylation process	90
5.7.1.1	The GPC Analysis	91
5.8	Bibliography	92
	Annex	93-100

List of Figures

	Subject	Page Number
1	Chapter 1: General Introduction and Review of Literature	
Fig 1.1	Filler nano material in a polymer matrix	3
Fig 1.2	Nano fillers	4
Fig 1.3	Rare Earth Elements	4
Fig 1.4	Pictorial representation of the proposed study	6
Fig 1.5	General Structure of AFCTA	8
Fig 1.6	General Structure of RAFT agents	9
Fig 1.7	Initiation Mechanism	10
Fig 1.8	Propagating Mechanism	10
Fig 1.9	Reinitiation Mechanism	10
Fig 1.10	Chain equilibrium Mechanism	11
Fig 1.11	Overall chain mechanism	11
Fig 1.12	Formation of macroRAFT agents	12
Fig 1.13	Emulsion Process	15
Fig 1.14	Methods of Preparing Nanocomposites	15
Fig 1.15	Encapsulation of inorganic nanoparticles	16

Fig 1.16	Nanocomposite formations in solution and emulsion conditions	17
Fig 1.17	Formation of Anisotropic Film Nanocomposite	18
Fig 1.18	Work Chronology	19

2 Chapter 2: Polymerization studies performed under RAFT

Fig 2.1	The synthesis of PAATTC	27
Fig 2.2	Kinetic studies performed on PAATTC	27
Fig 2.3	GPC chromatogram of PAATTC (100% conversion)	29
Fig 2.4	GPC chromatogram of PAATTC (20%, 50% and 70% systems)	29
Fig 2.5	Synthetic Approach to the preparation of P(AAcoBuA)-TTC	32
Fig 2.6	Snapshot of copolymers P(AAcoBuA)TTC	33
Fig 2.7	TGA of P(AA co BuA) TTCA (80% conversion)	33
Fig 2.8	Systematic Degradation of PBuA at 292°C	34
Fig 2.9	GPC studies of the P(AA co BuA) TTC copolymer	36
Fig 2.10	GPC studies of the P(AA co BuA) TTCA 50% conversion	36
Fig 2.11	Copolymerization in solution, emulsion and emulsion (5:10)	38

3 Chapter 3: Inorganic Nano Fillers

Fig 3.1	Hydrolysis of TEOS	44
Fig 3.2	Formation of silica	44
Fig 3.3	Stabilization of silica nano particles	45
Fig 3.4	Particle diameter as a function of $\ln [\text{NH}_4\text{OH}]$	45
Fig 3.5	Methacryloxypropyltrimethoxysilane (MPS)-chemical formula	47
Fig 3.6	Surface modification reaction with MPS	47
Fig 3.7	3-aminopropyltrimethoxysilane (APS)-chemical formula	47
Fig 3.8	Surface modification of silica with APS	48
Fig 3.9	DLS result for Si-300 nm spherical particles	48
Fig 3.10	SEM images of SiO_2 particles	49
Fig 3.11	SEM images of SiO_2 spheres (300nm) before and after calcination	51
Fig 3.12	FTIR-ATR analysis of SiO_2 spheres before and after calcination	51
Fig 3.13	The surface modification of $\text{Gd}_2\text{O}_3:\text{Eu}^{3+}@\text{SiO}_2$ with APS	54
Fig 3.14	S-TEM images of $\text{Gd}_2\text{O}_3:\text{Eu}^{3+}$ nanofillers	55
Fig 3.15	S-TEM images of $\text{Gd}_2\text{O}_3:\text{Eu}^{3+}@\text{SiO}_2$	56
Fig 3.16	Chemical Analysis of the sample by EDS	56
Fig 3.17	Excitation Spectra of $\text{Gd}_2\text{O}_3:\text{Eu}^{3+}@\text{SiO}_2$ nanofillers	57

Fig 3.18	Emission Spectra of $\text{Gd}_2\text{O}_3:\text{Eu}^{3+}@\text{SiO}_2$ nanofillers	58
Fig 3.19	Emission Spectra of $\text{Gd}_2\text{O}_3:\text{Eu}^{3+}@\text{SiO}_2$ nanofillers	58
Fig 3.20	XRD analysis of $\text{Gd}_2\text{O}_3:\text{Eu}^{3+}$ and $\text{Gd}_2\text{O}_3:\text{Eu}^{3+}@\text{Silica}$	59
Fig 3.21	FTIR-ATR analysis of modified and unmodified $\text{Gd}_2\text{O}_3:\text{Eu}^{3+}$ samples	60

4 Chapter 4: Synthesis and Characterization of Nanocomposites

Fig 4.1	Methods of producing silica nanocomposites	67
Fig 4.2	Snapshot of Silica (spheres) nanocomposites in solution	69
Fig 4.3	SEM Imagery of Silica nanocomposites in solution and emulsion	70
Fig 4.4	FTIR-ATR analysis of silica@APS spheres nanocomposites	70
Fig 4.5	SEM Imagery of Silica@APS nanocomposites (spheres) thin films	72
Fig 4.6	Snapshot of Silica (fibres) nanocomposites in solution	72
Fig 4.7	SEM Imagery of Silica@APS fibres nanocomposites	73
Fig 4.8	EDS of silica fiber nanocomposites in solution	74
Fig 4.9	SEM Imagery of silica@APS nanocomposites (fibres) thin films	75
Fig 4.10	SEM Images of $\text{Gd}_2\text{O}_3:\text{Eu}^{3+}@\text{silica}$ nanocomposites	76
Fig 4.11	SEM Images of $\text{Gd}_2\text{O}_3:\text{Eu}^{3+}@\text{silica}$ nanocomposites	77
Fig 4.12	Emission Spectra of the $\text{Gd}_2\text{O}_3:\text{Eu}^{3+}@\text{silica APS}$ nanocomposites	78

Fig 4.13 Emission Spectra of the Gd₂O₃: Eu³⁺ @ silica APS nanocomposites 77

5 Chapter 5: Laboratory Experimentation

Fig 5.1 Lab Setup for the preparation of Silica@APS 88

List of Tabular Columns

	Subject	Page Number
1.1	Lanthanides electronic structure of trivalent ions	5
1.2	Thiocarbonylthio RAFT agents general structure	9
1.3	RAFT polymerization of acrylates with various RAFT agents	13
2.1	% Conversion as a function of time	28
2.2	PDI, theoretical and experimental Mn of the PAATTC	30
2.3	Tg values by DSC analysis attempt 1	31
2.4	DSC studies of P(AAcoBuA) TTC	34
2.5	GPC studies of the P(AAcoBuA)TTC copolymer	35
2.6	PDI studies of P(AAcoBuA)TTC system	37
3.1	FTIR-ATR bands of Silica Spheres and Fibers	50
3.2	BET surface areas of Silica Samples	52
3.3	Zeta Potential Measurements	52
4.1	Silica nanocomposite formation attempts	68
4.2	DSC results of Silica @ APS nanocomposite spheres	71
4.3	DSC results of Silica @ APS nanocomposite fibers	74
4.4	DSC analysis of Gd ₂ O ₃ :Eu ³⁺ @Silica APS nanocomposites	77

List Of Abbreviations

AA	Acrylic Acid
AIBN	Azobisisobutyronitrile
AFM	Atomic Force Microscopy
ATRP	Atom transfer radical polymerization
BuA	Butyl Acrylate
CRP	Controlled radical polymerization
DLS	Diffusion Light scattering
DMF	Dimethylformamide
DSC	Differential Scanning Calorimetry
EDS	Energy Dispersive Spectroscopy
FTIR	Fourier Transform Infrared Spectroscopy
LRP	Living radical polymerization
M _n	Number average molecular weight
MPS	Methacryloxypropyltrimethoxysilane
M _w	Weight average molecular weight
NMP	Nitroxide mediated polymerization
NMR	Nuclear Magnetic Resonance
OLED	Organic Light Emitting Diode
PAATTC	Poly Acrylic Acid 2-(Dodecylthiocarbonothioylthio)-2-methyl propanoic acid
PDI	Poly Dispersity Index
PL	Photoluminescence
RAFT	Reversible addition-fragmentation chain transfer
SEM	Scanning Electron Microscopy
TEM	Transmission Electron Microscopy
TEOS	Tetra-ethylorthosilicate
TGA	Thermal Gravimetric Analysis
T _g	Glass Transition Temperature
THF	Tetrahydrofuran
UV/ Vis	Uv-visible Spectroscopy

Chapter 1

General Introduction and Review of Literature

Preface:

In this introductory chapter an attempt to define related concepts and terminology within the boundaries of the thesis has been furnished, alongside strategies and tactics used in the synthesis of nanocomposites. Some of the major topics covered are polymer matrix nanocomposites, anisotropic nanocomposites, types of polymerization processes (homogeneous and heterogeneous), lanthanide (Ln³⁺) nanofillers, RAFT polymerization (introduction and mechanism), macroRAFT agent (formation), polymer encapsulation strategies etc. A short chronology of the work done has also been provided in a diagrammatic format.

1.1 Nanocomposite Basics

The cardinal focus of Science and Technology in the last couple of decades has been in the field of **Nanotechnology** and **Materials**, which was initially characterized as small alterations made to the study of micro and macro materials. Albeit this definition has evolved overtime and today stands as the study of the control of matter at an atomic or molecular level (the nanometer range). Since understanding often induces simplification and clarity, it is no surprise that the availability of better visualization and characterization techniques has made studying the innate nature of the material possible, and lately new strategies for the synthesis of new materials have been sought after and deployed, which leads to better structural and overall control of the material at the atomic scale. All this advancement has given rise to a new interdisciplinary field of study called Nanocomposite Materials.

P.M. Ajayan *et al.* [1] have construed that nanocomposites are solid structures which possess a nanoscale dimensional repeat distance between the different phases, and they demonstrate mechanical, electrical, optical and structural properties quite different from and sometimes better than the individual components. These enhanced properties arise due to the overall interactions between the components at a molecular level which leads to the formation of large interfacial areas, therefore maintaining a high surface to volume ratio or high aspect ratio between the phases, while conventional composite materials possess smaller volume fractions [2, 3, 4]. An example is a nanotube-filler polymer composite where the presence of nanotubes could improve the mechanical

strength of the polymeric matrix if interactive interfaces are present [2]. These novel materials are now opening up new avenues for scientists and researchers to exploit and enrich.

1.2 Types of Nanocomposite Materials

Today, we are cognizant of a variety of nanocomposite materials which are broadly categorized as

- organic-organic type nanocomposites
- inorganic-inorganic type nanocomposites
- organic-inorganic type nanocomposites

The ambit of this study, is bound to the apprehension and fabrication of organic-inorganic nanocomposite materials, wherein the matrix constitutes an organic polymer and the fillers inorganic nanoparticles. These are colloquially termed as Polymer Matrix Nanocomposite or Hybrid Materials, while scientifically there exist certain distinctions between these designations. In this context, Sanchez *et al.* [5] ascertain hybrid materials as homogeneous systems derived from monomers possessing both an organic and an inorganic component, while nanocomposites are heterogeneous systems in which one of its components possesses a nanometric dimension [5].

1.2.1 Polymer matrix nanocomposites (PMNs)

The terminology polymer matrix nanocomposites (PMNs) is new in polymer science, but its conceptualization is age old and evidence of it can be found in nature i.e., bones, animal and human teeth, shells etc., [2]. These are composed of both an inorganic segment like calcium, carbonate and phosphate ((CaCO₃), (Ca₁₀(PO₄)₆(OH)₂)) and an organic segment like carbohydrates, lipids and proteins [2]. Similar to the natural structures mentioned, polymer/clay composites can also be synthetically prepared by intercalation [6] and a brief review of the preparation of bio nanocomposites via this technique has been reported in depth by Chivrac *et al.* [7].

The properties of a polymeric material is largely dependent on two primary factors **a) their molecular structure** and **b) the various manufacturing processes involved** [8]. If the polymer matrix admits even distribution of the inorganic fillers within the matrix, then nanocomposite materials with high processability, homogeneity and low density can be obtained [9,10]. Therefore by altering the matrix, materials with advanced physical characteristics i.e., mechanical properties, thermal stability, optical properties, magnetic properties etc., [11] can be synthesized. Another asset

is the protection of the inorganic particles from harsh environmental conditions like oxygen, humidity, moisture etc., by encapsulating them with a protective layer of polymer. This can also be designated as the inclusion of the inorganic nanoparticles within the polymer matrix [4]. The innumerable encapsulation techniques and strategies for shielding the inorganic nanoparticles will be discussed in Chapter 3.

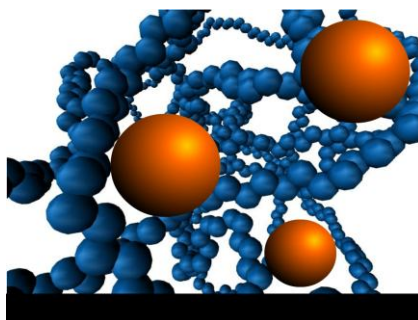


Figure 1.1: Shows the filler nano material in a polymer matrix, reproduced from [12].

Inorganic nanoparticles are preferred filler materials in comparison to conventional fillers due to their possession of high surface-areas [3, 13, 14]. Smaller the size of the filler better is its dispersion in solvents, monomer and/or the polymeric matrix. Today new methods are available for the preparation of nanoparticles with good size control i.e., the sol-gel method, thermal spraying method, templating, chemical vapour deposition, self-assembly, atomic layer deposition, electrospinning etc., however in our series of experiments we made use of the **sol-gel** and the **hydrothermal** synthetic approaches.

Nanoscale filler materials are very different from traditional microscale filler materials due to their reduced dimensions. Due to this factor, they do not scatter light significantly, do not create large stress concentrations, do not compromise the ductility of the polymer, and the individual property of the filler material is retained e.g., single walled nanotubes free from defects, possesses a high modulus of 1TP with strengths as high as 500 Gpa. These can be combined with the polymer to achieve nanocomposites with better overall physical and mechanical properties [1, 2].

Nanoscale fillers come in different shapes and sizes as

- **Nano Fibres** or tubular fillers (diameters <100 nm with aspect ratio of at least 100) [1].
- **Nano Plates** are layered materials with thickness of around 1nm but with an aspect ratio in the other two dimensions of at least 25 [1].

- **3D Nanofillers** are equi-axed particles <100 nm in dimension [1].

For our investigation, we made use of nano spheres and fibres/rods.

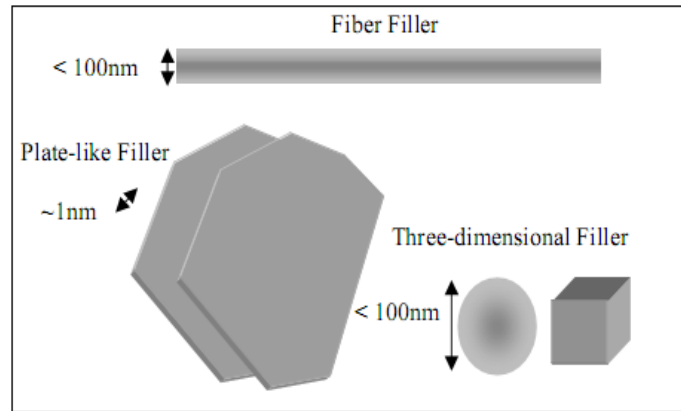


Figure: 1.2 Nano Fillers reproduced in completion from [1].

The use of silica nanoparticles as filler material is relatively new but innumerable published data on the synthesis and the surface chemistry of amorphous silica is readily available. This information is crucial in the preparation of nanocomposites where interfaces play a significant role in the incorporation of the filler material in the polymeric matrix [15, 16]. These studies are further being expanded to incorporate other inorganic fillers such as the rare elements (lanthanide series (Ln^{3+})) due to its striking applications in the field of bio-medical engineering and optics [17-21].



Figure 1.3: Rare Earth elements (lanthanide series) reproduced from [22].

The numerous properties of rare earth lanthanide compounds have fascinated researchers for decades. Some of them are their highly reactive nature (especially with water to liberate hydrogen (H_2)), strong reducing and high paramagnetic tendencies, ability to fluoresce strongly under ultraviolet light, possession of high coordination numbers etc., [22-24].

From the above, their **luminescence ability** is highly attractive due to their line-like emissions, which results in high color purity of the emitted light. The emission color is found to depend only on the lanthanide ion and is independent of the environment, hence these materials can be used as

optical amplifiers, optical waveguides, organic light emission diodes (OLEDs) etc. Most of the studies performed so far have been on inorganic molecular lanthanide compounds, however lately strong interest in lanthanide based organic- inorganic hybrid materials has been taken due to the fact that hybrid materials have superior mechanical properties and better processability than pure molecular lanthanide complexes [23,24].

Tabular Column 1.1: Lanthanides electronic structure of trivalent ions reproduced from [23].

Electronic Structure of the Trivalent Lanthanide Ions				
element	symbol	atomic number (Z)	configuration Ln ³⁺	ground state Ln ³⁺
lanthanum	La	57	[Xe]	¹ S ₀
cerium	Ce	58	[Xe]4f ¹	² F _{5/2}
praseodymium	Pr	59	[Xe]4f ²	³ H ₄
neodymium	Nd	60	[Xe]4f ³	⁴ I _{9/2}
promethium	Pm	61	[Xe]4f ⁴	⁵ I ₄
samarium	Sm	62	[Xe]4f ⁵	⁶ H _{5/2}
europium	Eu	63	[Xe]4f ⁶	⁷ F ₀
gadolinium	Gd	64	[Xe]4f ⁷	⁸ S _{7/2}
terbium	Tb	65	[Xe]4f ⁸	⁷ F ₆
dysprosium	Dy	66	[Xe]4f ⁹	⁶ H _{15/2}
holmium	Ho	67	[Xe]4f ¹⁰	⁵ I ₈
erbium	Er	68	[Xe]4f ¹¹	⁴ I _{15/2}
thulium	Tm	69	[Xe]4f ¹²	³ H ₆
ytterbium	Yb	70	[Xe]4f ¹³	² F _{7/2}
lutetium	Lu	71	[Xe]4f ¹⁴	¹ S ₀

The use of silica-polymer matrix hybrid with rare earth elements as fillers was first described by Yan Bing [25] where he embedded terbium (Tb) into a PMMA matrix and witnessed an emission intensity increase on increasing the concentration of Tb³⁺ with no evidence of concentration quenching [23,25].

Also recently, special interest has been taken in the preparation of anisotropic nanocomposites because these materials provide better mechanical and physical properties than traditional nanocomposites. While the preparation of anisotropic nanocomposites with metallic matrices is well established, the preparation of the same in polymeric matrices is relatively new and not well defined, therefore we decided to explore and see if we were able to prepare anisotropic nanocomposites based on the instructions provided by Ali *et al.* [26] using an acrylate system (PAA and PBuA)

In this work we decided to investigate the luminescence property of gadolinium oxide doped with europium fibres/rods (Gd₂O₃:Eu³⁺ particles or GOED particles). Based on previous experimental

trials performed by the CICECO research group, it was demonstrated that coating $Gd_2O_3:Eu^{3+}$ particles with silica enhances the PL properties [27]. It was also shown that surface modification with MPS followed by conventional radical polymerization in an aqueous medium yielded reasonably stable nanocomposites. Yet, these proposed strategies did not provide means for the formation of ordered/aligned nanocomposites (anisotropic materials) due to their preparation via suspension polymerization. Furthermore the use of stabilizers may cause phase separation upon film formation.

In order to overcome this difficulty, we coated our $Gd_2O_3:Eu^{3+}$ particles with a silica coat and functionalized the surface with a silane coupling agent (APS) for easy insertion within the polymeric matrix. This was polymerized via the RAFT mechanism in both solution and emulsion conditions in an acrylate medium, making use of a suitable initiator and was characterized by standard techniques like FTIR-ATR, SEM, DSC, TEM, BET etc.

Finally, special efforts were taken in the preparation of anisotropic nanocomposites by depositing them on a glass substrate making use of the spin coating and casting technique. A pictorial view of the project proposal is shown in Figure 1.4.

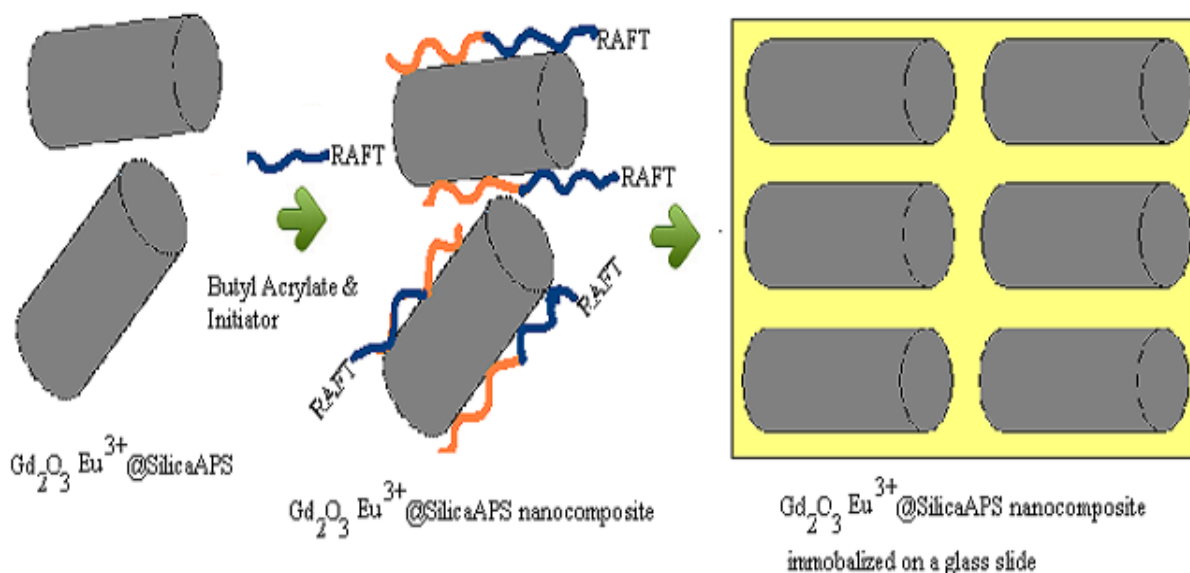


Figure 1.4: Pictorial representation of the proposed study.

1.3 The Polymerization Process

1.3.1 Brief Introduction

Polymer science as a subject of study, originated as a byproduct of the great industrial revolution wherein human curiosity for the better understanding of the physics and chemistry behind plastics, rubber, adhesives, fibers, and coatings formulated [28]. Perhaps due to its lineage, polymer science leans towards a more inter-disciplinary theme than most subject areas, combining chemistry, physics, chemical engineering, materials and others.

Polymers are delineated as long-chain molecules of high molecular weight, often quantified in the hundreds of thousands. For this reason alone, the term “macromolecules” is often used when referrals are made to polymeric materials [28]. Initial polymers were natural products i.e., cotton, starch, proteins, wool etc., and only in the beginning of the earlier twentieth century did synthetic polymers enter mainstream industry. The polymers of importance were Bakelite and Nylon, and they showed tremendous potential but their chemical and physical properties were not entirely understood [28]. We have come a long way since, and now modern techniques of polymer synthesis are available. However, the one which possesses the maximum advantage is the **Controlled and Living Polymerization Process**.

In this work, special emphasis has been given to the Reversible Additional Fragmentation Chain Transfer Process (RAFT Process) which is one of the many Living and Controlled Radical Polymerization processes, due to its tremendous advantages.

1.3.2 Controlled and Living Polymerization

From literature, Controlled and Living Radical Polymerization processes demonstrate good amount of control over the reaction [29] thereby enabling the easy preparation of di and tri block, grafted and star polymers [30]. These processes were initially developed for homogeneous systems but were later altered to work under aqueous dispersed environments by deploying advanced techniques like emulsion and mini emulsion polymerization processes.

Living polymerization is a special form of polymerization wherein the ability of the growing polymer chain to terminate has been minimized [30]. This was achieved by altering the system mechanism by reducing the chain termination and the chain transfer reactions. It also possesses a

rate of chain initiation which is larger than the rate of chain propagation, hence the polymer chains grow at a constant rate and systems with better polydispersity indices are obtained [31]. Nevertheless, this method has its fair share of drawbacks i.e., the system is highly susceptible to small changes in temperature, monomer concentration etc., therefore complete control of the molecular weight, polydispersity, composition, chain length, architecture and site specific functionality is not always possible [29-31].

1.3.3 Types of Controlled and Living Polymerization

There are three types of Controlled and Living Polymerization (CPRs) namely SFRP or NMP-Stable-Free Radical Polymerization, ATRP-Atom Transfer Radical Polymerization and RAFT-Reversible-Addition-Fragmentation-Transfer [29-31].

1.3.3.1 Addition Fragmentation Chain Transfer Process (AFCT Process)

The addition fragmentation chain transfer process is an effective process for controlling the molecular weight and preparing polymers with end functionality. This process is carried out by appending simple organic compounds to AFCT agents. This is versatile and can be used with a wide array of monomers e.g., styrene, vinyls, acrylates etc., and induces functionality at the end terminals. Mono and di functional polymers can be used as a starting point for building block, segmented, grafted and networked polymers. The mechanism of this process was obtained by observing the chemistry of methyl methacrylate macromonomers [32].

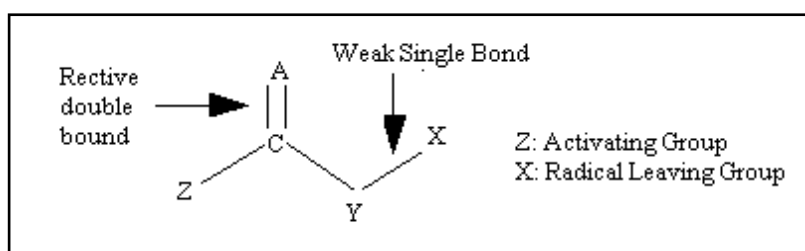


Figure 1.5: General Structure of AFCTA adapted from [32].

1.3.3.2 The Reversible Addition Fragmentation Chain Transfer Process (RAFT)

This is a minor extension of the AFCT Process and was first discovered by a research team in Australia in the year 1998. They made use of the Reversible Addition Fragmentation chain transfer mechanism. This mechanism is highly superior over the other forms of controlled/living free radical polymerization mechanisms, and can be used with a wide range of monomers performed under

different reaction conditions yet provides systems with controlled molecular weight distributions (less than 1.1) [32,33].

1.3.3.2.1 Thiocarbonylthio RAFT agents

The use of macromonomers as RAFT agents was primarily studied by E. Rizzardo *et al.* [33-36] where methacrylate based macromonomers were utilized in the preparation of block copolymers via RAFT. The major disadvantage of using macromonomers, is their low chain transfer values (C_{tr}), which lowers the rate of chain equilibrium and makes the rate of chain transfer slower than the rate of chain propagation, hence the system begins to slow down and becomes uncontrolled. In order to overcome this difficulty RAFT agents with higher C_{tr} values were deployed which possessed the thiocarbonylthio moiety which was responsible for providing the living behavior [37-40] in the free radical polymerization process. Later on, it was incurred that the thiocarbonylthio moiety (S-C=S) not only facilitated livingness but also radical addition, thereby leading to faster chain equilibrium. The four types of thiocarbonylthio RAFT agents are shown in tabular column 1.2.

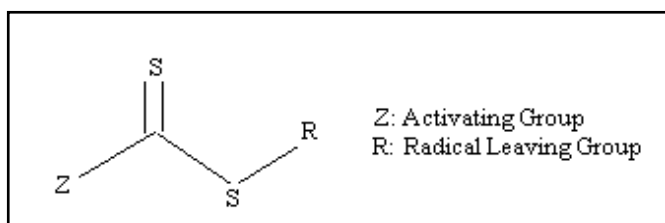
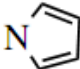
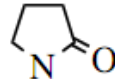


Figure: 1.6: General structure of RAFT agents.

Tabular Column 1.2 : Thiocarbonylthio RAFT agents general structure reproduced from [32].

RAFT agents	Z	R
a) Dithioesters	Ph	CH ₂ Ph
	CH ₃	CH ₂ CN
b) Trithiocarbonates	SCH ₃	C(CH ₂) ₂ CN
c) Xanthates	OEt	C(CH ₂) ₂ Ph
d) Dithiocarbamates		C(CH ₂)(CN)CH ₂ CH ₂ CH ₂ OH
		
	NEt ₂	C(CH ₂)(CN)CH ₂ CH ₂ COOH

1.3.3.2 RAFT mechanism of Thiocarbonylthio Compounds

The RAFT mechanism of a thiocarbonylthio based compound consists of a number of addition-fragmentation steps [32]. There are three crucial steps involved:

a) Initiation and Propagation

The propagating radical is obtained by making use of a suitable conventional initiator.

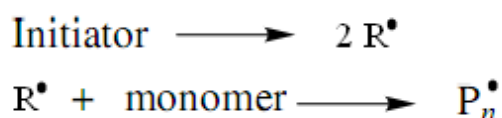


Figure: 1.7 Initiation mechanism, reproduced from [32].

This propagating radical P_n^\bullet is added to the RAFT agent which gives rise to a polymeric RAFT agent and a new radical R^\bullet .

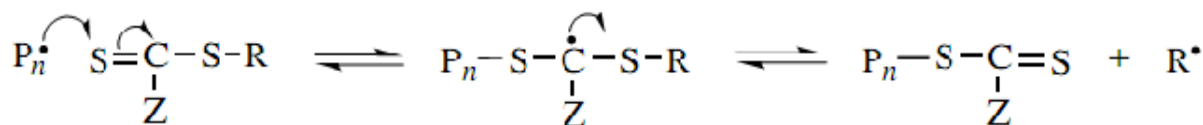


Figure: 1.8 Propagating Mechanism, reproduced from [32].

b) Reinitiation

The radical R^\bullet now combines with the monomer to form a new propagating radical P_m^\bullet .

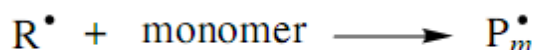


Figure: 1.9 Reinitiation Mechanism, reproduced from [32].

c) Chain equilibrium by reversible addition fragmentation

An equilibrium, now exist between the activated species P_n^\bullet , P_m^\bullet and the dormant RAFT compound thus providing ideal conditions for chain growth in a controlled manner therefore leading to the formation of polymers with narrow polydispersity indices.

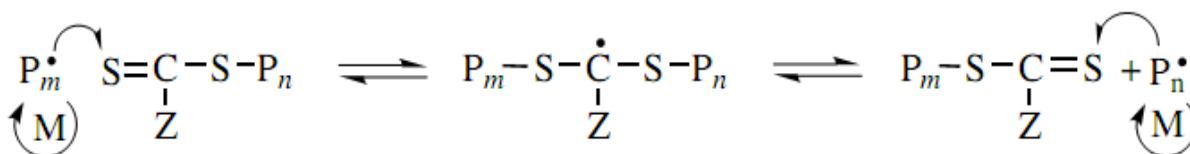


Figure: 1.10 Chain equilibrium Mechanism, reproduced from [32].

The **overall mechanism** of the system is shown below

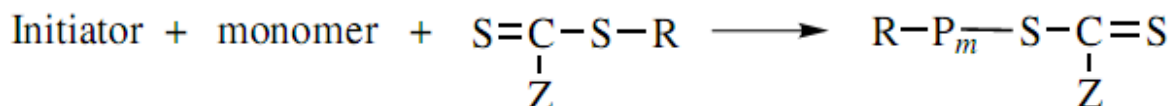


Figure: 1.11 Overall chain mechanism, reproduced from [32].

1.3.3.3 RAFT Polymerization System Studies

RAFT polymerization has been studied for a wide range of systems like a) methacrylate [41, 42] b) styrene [42] c) acrylate [42] d) acrylamide [42,43] e) vinyl ester [42] etc. However in this work emphasis will be given only to the **acrylate system**.

1.3.3.3.1 MacroRAFT agents

Even though the RAFT polymerization process is versatile it has some drawbacks, namely when heterogeneous reactions are carried out slow polymerization rates, low colloidal stability, poor control of the molar mass, or a broad molar mass distribution etc., are observed. Klumperman *et al.* [44] succeeded in overcoming these difficulties by working under starved feed conditions with hydrophilic macroRAFT agents. Their strategy relied in the in-situ formation of an amphiphilic reactive diblock co-polymer self-assembling into micelles, controlled by the RAFT moiety present at the chain end of the hydrophobic block and localized in the inner part of the micelle. Prescott *et al.* [45] also developed a method in which the RAFT agent is located in seed particles before polymerization commences, however this method does not work well with unseeded ab-initio emulsion polymerization. In this context Ferguson *et al.* [46] describes a technique which circumvents this problem using an amphiphilic diblock that self assembles into micelles. This was achieved by the sequential addition of a hydrophilic monomer followed by a hydrophobic monomer in the presence of the RAFT agent i.e., a hydrophilic monomer like acrylic acid can be polymerized in the presence of the RAFT agent to form a macroRAFT agent that possesses the capability of forming micelles. Subsequently, on addition of the hydrophobic monomer, the di-block continues

to grow under RAFT conditions. This technique was further adapted by Jutta Rieger *et al.* [47] who employed a hydrophilic block Polyethyleneoxide (PEO). In our series of experiments we made use of a similar technique, using acrylic acid as the hydrophilic monomer, butyl acrylate as the hydrophobic monomer and TTC-A (2-(dodecylthiocarbonothioylthio)-2-methyl propanoic acid) as our RAFT agent. A diagrammatic representation of the work of Ferguson *et al.* [46] is shown in figure 1.12.

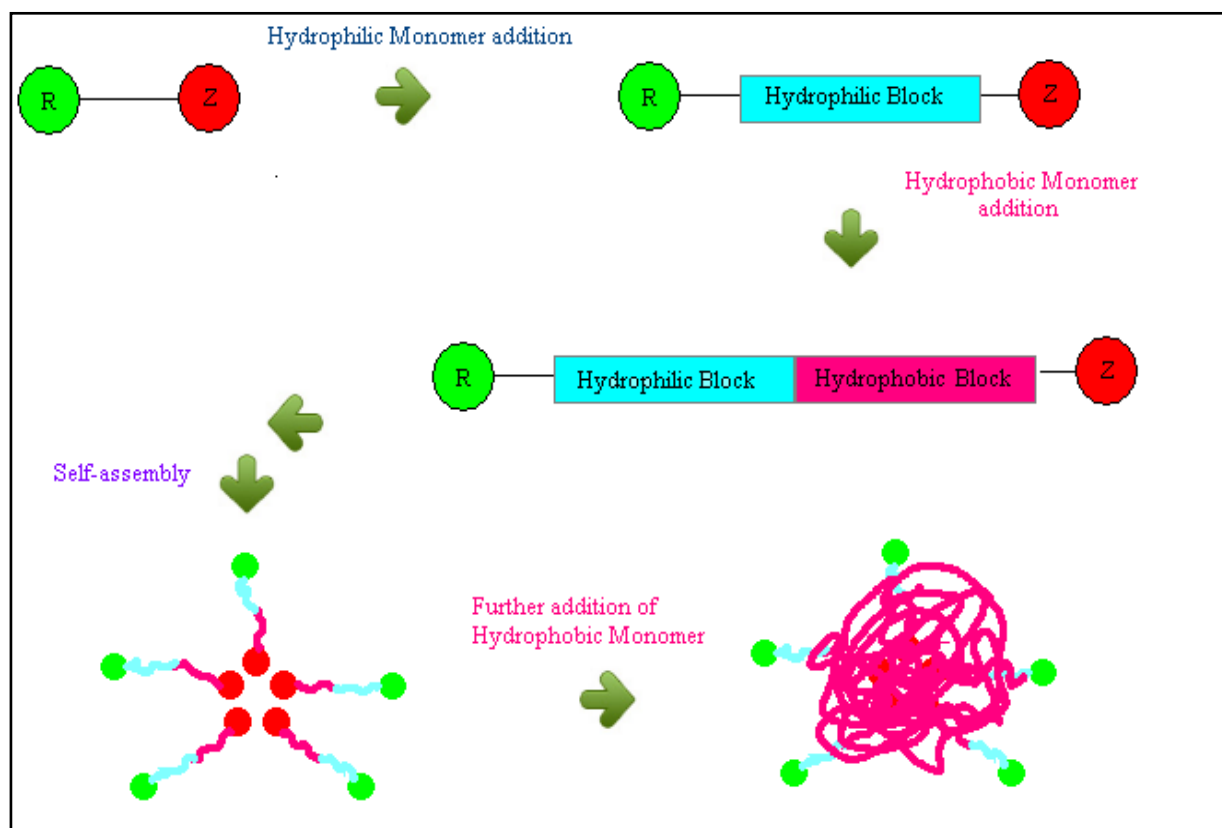


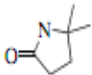
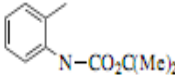
Figure 1.12: Formation of a macroRAFT agents reproduced from [46] and [48].

1.3.3.3.2 The Acrylate System: RAFT polymerization of Acrylates with various RAFT agents

The radicals which are responsible for the propagation in an acrylate system possess low steric hindrance and relatively high reactivity, which are ideal for the addition to the C=S bond and the expulsion of the R group in the RAFT agent. Also a wider choice of both the Z and R groups are available in the polymerization of acrylates. From the tabular column 1.2 we notice that the polydispersity indices of the polymers obtained are <1.2 (acceptable range) except for the last four values in the table. This goes to show that for the majority, good molecular weight control and good

polydispersity indices are observed [32].

Tabular Column 1.3 RAFT polymerization of acrylates with various RAFT agents reproduced in its entirety from [32].

RAFT Agents						
Z	R	Monomer ^a	% Conversion	<i>M_n</i> (GPC)	<i>M_n</i> (Calc)	<i>M_w</i> / <i>M_n</i>
Ph	CH ₂ Ph	<i>n</i> -BA	40	91,700	89,300	1.14
SCH ₃	C(CH ₃) ₂ CN	MA	55	65,400	61,800	1.06
<i>N</i> -Pyrrolo	CH ₂ Ph	MA	74	8,800	9,500	1.17
<i>N</i> -Succinamido	CH ₂ Ph	MA	97	108,200	102,900	1.18
	CH(CO ₂ Et) ^b	EA	69	5,880	7,170	1.19
	CH(CH ₃)CO ₂ Et ^b	EA	87	7,350	7,750	1.20
Ph	C(CH ₃) ₂ CN	AA	53	66,800	73,800	1.13
NEt ₂	CH(CO ₂ Et) ₂ ^c	EA	94	7,800	9,760	2.31
N(Ph)Et	CH(CO ₂ Et) ₂ ^c	EA	99	8,300	8,270	1.86
OEt	C(CH ₃)(SPh)CO ₂ Et ^c	MA	—	3,790	3,500	1.40
OEt	C(CH ₃) ₂ CN	<i>t</i> -BA	72	11,000	10,100	1.77

^a *n*-BA, *n*-butyl acrylate; MA, methyl acrylate; EA, ethyl acrylate, AA, acrylic acid; *t*-BA, *t*-butyl acrylate.

1.3.4 Process Conditions

The two major process conditions under which controlled and living polymerizations reactions are carried out are the homogenous and the heterogeneous processes. These are based on whether the initial reaction mixtures are homogeneous or heterogeneous in nature [49]. Generally mass/bulk and solution polymerization are classified under the homogeneous process category, while dispersion, suspension, emulsion and mini emulsion polymerizations fall under the heterogeneous process category [49].

In this work both homogeneous (solution polymerization) and heterogeneous (emulsion polymerization) process modes were chosen to study the acrylate system and the results obtained were expanded upon and used in the preparation of nanocomposites.

1.3.4.1 Polymerization in Solution

The bulk/mass polymerization technique is the most common method for carrying out polymerization reactions in a homogeneous medium but control over the system is rather difficult since it is highly exothermic and possesses high activation energies. Due to the nature of the process, constant and rigorous stirring and reliable temperature control is essential, if not degradation, decolorization and broadening of the molecular weight distribution is ascertained. These problems can be annulled by conducting the polymerization in solution. Here, the solvent acts as a diluent, aids in both the stirring (as the viscosity of the reaction mixture is decreased) and in the transfer of the heat of polymerization, thus enhancing the conditions for polymerization. Also thermal control and stability is easily attained in solution than in bulk/mass polymerization systems. However this method has its own drawbacks, i.e., extra amount of care is necessary in choosing right solvents compatible with the system and the removal of the solvent from the polymeric material is a challenge [49].

1.3.4.2 Polymerization in Emulsion

This is one of the main types of the heterogeneous polymerization systems. On the application of this technique, polymer particles of size 50-500 nm can be produced. This type of process makes use of monomers (styrene, acrylates) which are meagerly soluble in water, surfactants both ionic and non ionic used above their critical micelles concentration (CMC) alongside water soluble initiators [50]. In research laboratories generally ionic surfactants are used, while in industry mixed systems (both ionic and non ionic) are needed in order to improve the colloidal stability of the system. The process of emulsion is as follows; the water soluble initiator upon heating begins to decompose and gives rise to radicals which are responsible for the propagation of the monomer in an aqueous phase. Upon adding small amounts of the monomer, the oligo-radicals become sufficiently hydrophobic and starts to enter the micelles thus initiating the polymerization reaction. Particle nucleation continues until all the micelles are nucleated or consumed by the growing particles and this carries on until all of the monomer is depleted. One advantage of this system is that the small radicals which arise from the chain transfer can exit the particles, thereby lowering the average number of radicals per particle, therefore near perfect system control can be achieved. This method has numerous industrial application i.e., manufacture of paints, adhesives etc., [50]. Figure 1.13 represents the emulsion process with the inclusion of nanocomposites.

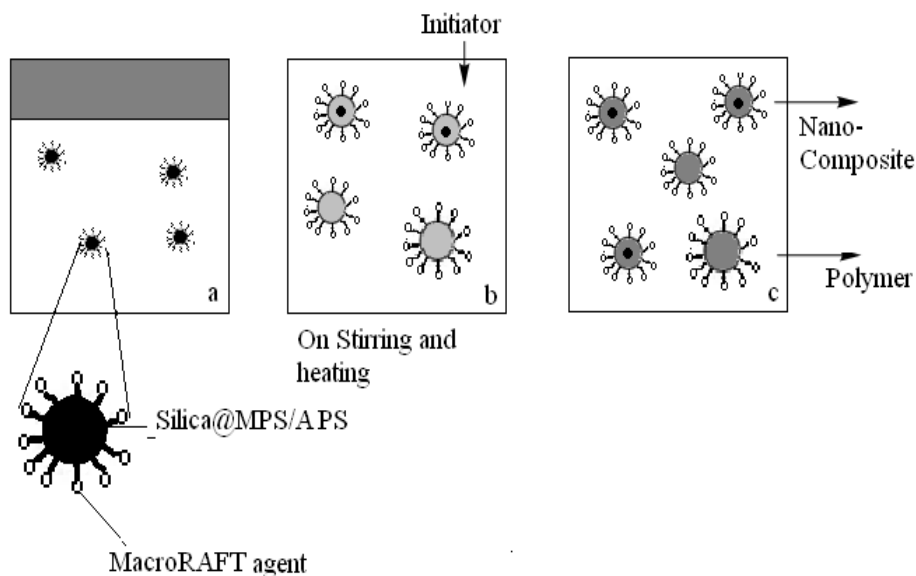


Figure: 1.13 Emulsion process adapted from [50, 51].

1.4 Nanocomposite Preparation Methodologies

There are many ways by which nanocomposite materials can be prepared, the three most common methodologies are shown in figure 1.14 [52, 53]. In the first method blending, the inorganic nanoparticles are mixed with the polymeric material using mechanical agitation. This is the most common method of preparing nanocomposite materials. The other two methods are in-situ in nature. In method (2), the inorganic precursors and the polymeric materials are taken and allowed to react under the set conditions and in method (3) the monomer is taken along with the inorganic nanoparticulates (and other necessary reagents) and are allowed to react, leading to the formation of a nanocomposite. In our probe we made use of the **in-situ method (3)** to prepare nanocomposites.

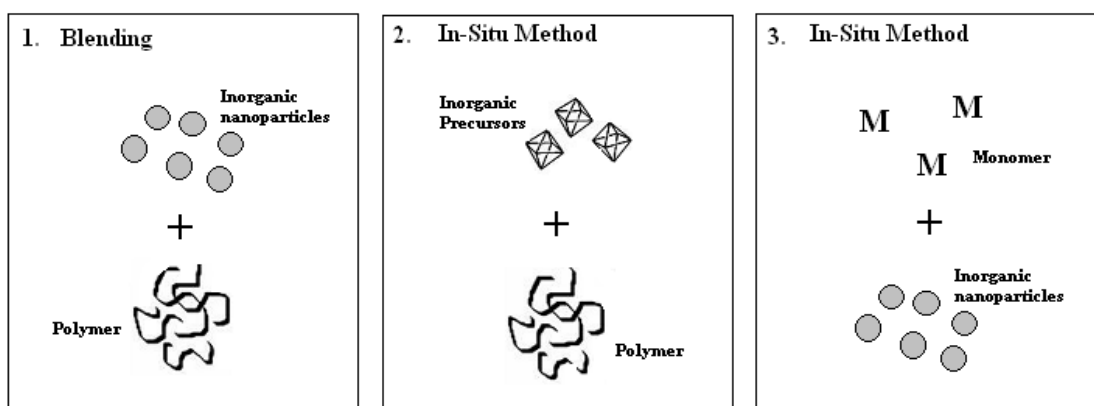


Figure: 1.14 Methods of Preparing Nanocomposites adapted from [52, 53].

1.5 Polymeric Encapsulation of Silica Nanoparticles

Polymer-encapsulated particles i.e., those particles which have an inorganic core covered by a polymeric shell have a lot of potential applications in the manufacture of cosmetics, paints and inks etc., where they are used to improve the compatibility between the filler and the binder. Encapsulation technologies have been designed so as to reduce the toxicity, mask odor, facilitate storage and greatly enhances the stability of the product. In the past, most of the encapsulation techniques were mechanical processes [54]. Bourgeat-Lami *et al.* in 1998-99 [54] prepared silica nanocomposites by using silica particles in a polymeric dispersion of styrene in an alcoholic/aqueous medium with poly (N-vinylpyrrolidone) (PVP) as a stabilizer. They observed that when unmodified silica was used, the silica bead has a tendency of covering the surface of the polystyrene particles thereby reducing encapsulation. In order to obtain better encapsulation, they modified the silica surface with 3-(trimethoxysilyl) propylmethacrylate (MPS) which introduces a hydrophobic character to the surface and facilitated its encapsulation with polystyrene. MPS also possesses a double bond which facilitates covalent bonding with the polymer matrix (true insertion). A large amount of research is available on the preparation of silica nanoparticles, surface modification of the particles by suitable coupling agents and nanocomposite formation as described in the review paper by Hua Zou, Shishan Wu *et al.* [55].

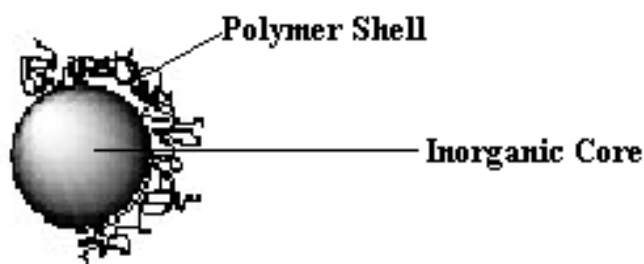


Figure: 1.15 Encapsulation of inorganic nanoparticles, adapted from [54].

In our attempts we utilized both the emulsion and solution conditions. In solution, a thick polymeric film developed around the nanofiller clusters, while in the case of emulsion beaded polymer particles of size (50-500nm) formed around the vicinity of the nanofillers. A schematic representation of the process is shown in figure 1.16.

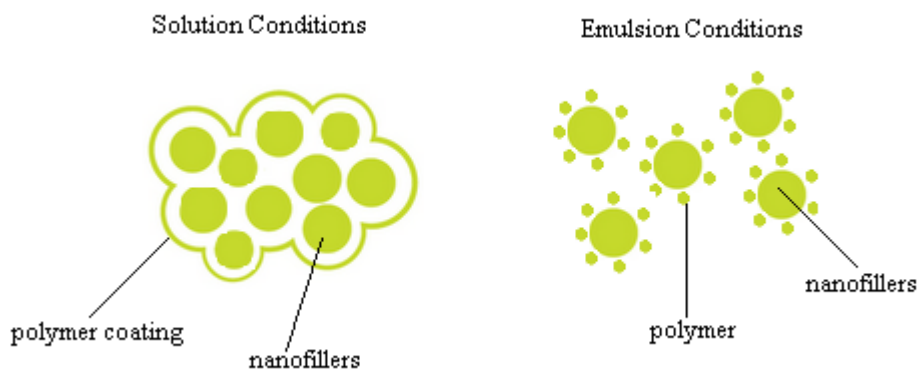


Figure 1.16 Nanocomposite formations in solution and emulsion conditions.

1.6 Anisotropic Nanocomposites (Polymer Encapsulated)

Anisotropy by definition is the property of being directionally dependent and is important as it enhances the mechanical and overall physical properties of the system. In the last three decades or so special interest has been taken in the preparation of anisotropic nanocomposites. However most of the research was focused on building anisotropic particles within metal matrices but very little has been done regarding the preparation of anisotropic particles within polymeric matrices until recently.

With the advent of controlled and living polymerization especially in multiphase systems a lot of advancement has been made and a direct route of preparing anisotropic nanocomposites was reported by Cooper and Rannard [56, 57] which relied on the combination of a hydrophilic mono-di or tri functional ATRP, PEG initiator in a solution of a hydrophobic monomer (n-butyl acrylate). They were able to form spherical and anisotropic dumbbell or “tripartite” clover-leaf anisotropic nanocomposites using different initiators and nanoparticles <100 nm [56, 57].

Ali *et al.* [26] were also able to synthesize anisotropic polymer-inorganic composite latexes with good control of the platelet orientation of Gibbsite nanoparticles with high encapsulation efficiency using emulsion based feed-monomer encapsulation techniques. They used di-benzyltrithiocarbonate as the RAFT agent, different combinations of acrylic acid and butyl acrylate systems and Gibbsite nanoparticles under starved feed emulsion polymerization conditions. They have demonstrated that, the control of the particle morphology highly influenced the orientation of the platelets during film formation, and that the monomer feed composition, chain length, and hydrophilic-lipophilic balance of the RAFT copolymer are found to be important factors responsible

for the overall efficiency of the encapsulation. In figure 1.17 the expected orientation of the platelets in the final films are seen for a) Spherical Particles b) Dumbbell Shaped Particles and c) Flat Particles [26].

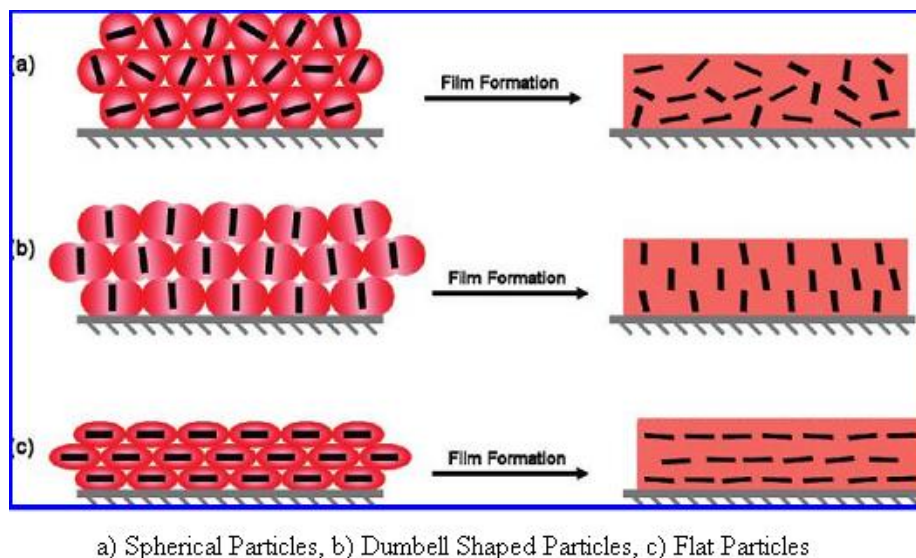


Figure: 1.17 Formation of Anisotropic Film Nanocomposite reproduced in its entirety from [26].

1.7 Deposition of Nanocomposites on glass

The formation of thin films on a substrate is relatively new, and there are different techniques available for film depositing onto a substrate or onto a previously deposited layer. The two main modes by which films are formed are **chemical deposition** or **physical deposition**. In the chemical deposition mode there are various advanced techniques involved like Chemical Vapour Deposition (CVD), Chemical Solution Deposition (CSD) etc., and in the physical deposition mode, Sputtering, Pulsed Laser Deposition, Cathodic Arc Deposition methods are available. In our series of experiments, only simple techniques like **spin coating** and **casting** methodologies were employed [58,59].

Further on, immobilization could be attempted following the work carried out by Kumar *et al.* [60] wherein they immobilization singled walled carbon nanotubes on a glass substrate (chemically functionalized). This could be used in bio sensory and bio-nanotechnology applications.

1.8 Thesis Breakup

The write up is divided into three major parts

1. A comprehensive study of the polymerization processes
2. The preparation and characterization of the inorganic nanofillers
3. Synthesis and characterization of nanocomposites

In the first part special emphasis has been given to the study of the Polymerization Process via RAFT. The strategy incorporated was bifocal (dual) in nature, the first describing the formation of the macroRAFT agent i.e., the homopolymerization of PAATTC the second being the copolymerization of the macroRAFT agent with butyl acrylate (P(AA-co-BuA)TTC). This was done to check the living and controlled characteristic of the copolymer formed which is an important parameter for encapsulation during the formation of nanocomposites. The second part focuses on the fabrication of inorganic nanofillers namely **a) Silica** and **b) Gd₂O₃:Eu³⁺@silica** wherein the wet process has been discussed with special emphasis on the material characterization. Also special attention was given on the surface modification with silane coupling agents to enhance their affinity with the polymer to obtain better encapsulation. Thirdly, in-situ nanocomposite preparation has been discussed alongside its characterization. A special mention is also made on the preparation of films in order to study the anisotropy of the nanocomposites prepared.

Work Chronology (duration in months)

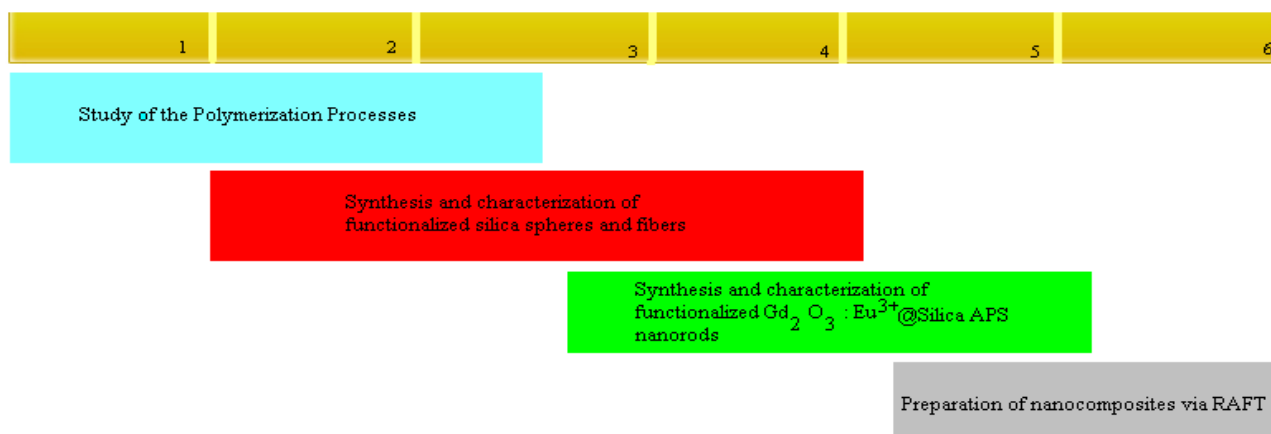


Figure: 1.18 Work Chronology.

1.9 Bibliography

1. Ajayan P.M, Schadler L.S, Braun P.V, “Nanocomposite science and technology”, Wiley, 2003, ISBN: 3527303596 .
2. Oriakhi C.O, “Polymer Nanocomposition Approach to Advanced Materials”, Journal of Chemical Education 2000, 77, 9, 1138-1146.
3. Esteves A.C, Timmons A.B, Trindade T, “Nanocompósitos de matriz polimérica: estratégias de síntese de materiais híbridos”, Química Nova 2004, 27, 5, 798-806.
4. Kickelbick G, “Concepts for the incorporation of inorganic building blocks into organic polymers on a nanoscale”, Progress in Polymer Science, 2003, 28, 83-114.
5. Sanchez C, Julián B, Belleville P, Popall M, “Applications of hybrid organic-inorganic nanocomposites”. Journal of Material Chemistry, 2005, 15, 3559-3592.
6. Bergaya F, Theng B.K.G, Lagaly G, “Handbook of Clay Science”, Elsevier, 2006.
7. Chivrac F, Pollet E, Avérous L, “Progress in Nano-Biocomposites Based on Polysaccharides and Nanoclays”, Materials Science & Engineering, 2009, 67,1-17.
8. Crosby A.J, Lee J.Y, “Polymer nanocomposites: the "nano" effect on mechanical properties”, Polymer Reviews 2007, 47, 217-229.
9. Sanchez C, Soller-Illia G. J, Ribot F, Lalot T, Mayer C, Cabuil V, “Designed hybrid organic-inorganic nanocomposites from functional nano building blocks”, Chemistry of Materials, 2001, 13, 10, 3061-3083.
10. Castro C, Ramos J, Millán A, González-Calbet J, Palacio F, “Production of magnetic nanoparticles in amine polymer matrixes”, Chemistry of Materials, 2000, 12, 12, 3681-3688.
11. Manias E, "Nanocomposites: Stiffer by design". Nature Materials, 2007 6: 9.
12. Image of Nanocomposite :
<http://www.fch.vutbr.cz/cs/laboratore/kompozity/nanocomposites.htm> -dated Sept 2010
13. Mai Y, Yu Z, “Polymer Nanocomposites”, Woodhead Publishing, 2007, ISBN 978-1-85573-969-7.
14. Bourgeat-Lami E. Lang J. “Encapsulation of inorganic particles by dispersion polymerization in polar media 1. Silica nanoparticles encapsulated by polystyrene”, Journal of Colloid and Interface Science, 1998, 192, 2, 293-308.
15. Pinto J.B, Marques P.A.A.P, Timmons A.B, Trindade T, Neto C, “SiO₂/cellulose nanocomposites obtained by in situ synthesis and via polyelectrolytes assembly”, Composites Science and Technology, 2008, 68, 1088-1093.

16. Lehocný M, Esteves A.C, Timmons A.B, Abreu V.L.G, Lapcik L, Trinidad T. and Coutinho J.A.P. "Silica Encapsulation via In Situ Emulsion Polymerization: Studies on surfaces Characteristics, Colloids and Surfaces A: Physicochemical and Engineering Aspects." (Unpublished).
17. Fang Y.P, Xu A.W, You L.P, Song R.Q, Yu J. C, Zhang H. X, Li Q, Liu H. Q, "Hydrothermal Synthesis of Rare Earth (Tb, Y) Hydroxide and Oxide Nanotubes", *Advanced Functional Materials* 2003, 13, 955.
18. Qun T, Jianmin S, Wenjia Z, Wu Z, Weichao Y, Yitai Q, "Preparation, characterization and optical properties of terbium oxide nanotubes", *Journal of Material Chemistry*, 2003, 13, 3103.
19. Yada M, Mihara M, Mouri S, Kuroki M, Kijima T, "Rare Earth (Er, Tm, Yb, Lu) Oxide Nanotubes Templated by Dodecylsulfate Assemblies", *Advanced Materials*, 2002, 14, 309.
20. Wong K.L, Law G. L, Murphy M. B, Tanner P. A, Wong W. T, Lam P. K. S, "Functionalized Europium Nanorods for In Vitro Imaging", *Inorganic Chemistry*, 2008, 47, 5190.
21. Söderlind F, Pedersen H, Petoral R. M, Käll P. O, Ovdal K, "Synthesis and characterisation of Gd₂O₃ nanocrystals functionalised by organic acids", *Journal of Colloid and Interface Science*, 2005, 288, 140 .
22. Information on lanthanides : <http://pubs.acs.org/cen/80th/lanthanides.html> - dated Sept 2010
23. Koen B, "Lanthanide-Based Luminescent Hybrid Materials", *Chemical Reviews*, 2009, 109, 4283–4374.
24. Henri B. K, "Introduction: Frontiers in Lanthanide Chemistry", *Chemical Reviews*, 2002, 102, 6, 1805–1806.
25. Yan B, "Sol–gel preparation and luminescence of silica/polymer hybrid material incorporated with terbium complex", *Materials Letters*, 2003, 57, 2535.
26. Ali S.I, Heuts J.P.A, Hawkett B.S, Herk A.M, "Polymer Encapsulated Gibbsite Nanoparticles: Efficient Preparation of Anisotropic Composite Latex Particles by RAFT-Based Starved Feed Emulsion Polymerization", *Langmuir*, 2009, 25, 18, 10523–10533.
27. Macedo A.G, Martins M.A, Fernandes S.E.M, Timmons A.B, Trindade T, Carlos L.D, Rocha J, "Luminescent SiO₂-coated Gd₂O₃:Eu³⁺ Nanorods /poly(styrene) nanocomposites by in situ polymerization", *Optical Materials*, 2010, 1622–1628.
28. Sperling H, "Introduction to Physical Polymer Sciences", Pgs 1-4, Fourth edition, Wiley Interscience, 2006.

29. Cunningham M.F. "Controlled/living radical polymerization in aqueous dispersed systems", *Progress in Polymer Science*, 2008, 33, 4, 365-398.
30. Matyjaszewski K, Spanswick J, "Controlled/Living Radical Polymerization", *Materials Today*, 2005, 3, 26-33.
31. Braunecker W.A, Matyjaszewski K, "Controlled/ living radical polymerization: Features, developments, and perspectives", *Progress in Polymer Science*, 2007, 32, 93–146.
32. Matyjaszewski K, Davis T.P, "Handbook of Radical Polymerization", Wiley Interscience, 2003.
33. Chiefari J, Chong Y.K, Ercole F, Krstina J, Jeffery J, Le T.P.T, Rosh, Mayadunne R.T.A, Meijs G.F, Moad C.L, Moad G, Rizzardo E, Thang S.H, "Living Free- Radical Polymerization by Reversible Addition–Fragmentation Chain Transfer: The RAFT Process", *Macromolecules*, 1998, 31, 16, 5559-5562.
34. Krstina J, Moad G, Rizzardo E, Winzor C.L, Berge C.T, Fryd M, "Narrow Polydispersity Block Copolymers by Free-Radical Polymerization in the Presence of Macromonomers", *Macromolecules*, 1995, 28, 5381.
35. Krstina J, Moad G, Rizzardo E, Moad C.L, Berge C.T, Fryd M, *Macromolecular Symposia*, 1996, 111, 13.
36. Rizzardo E, Harrison D.S, Laslett R.L, Meijs G.F, Morton T.C, Thang S.H, "Progressing Pacific Polymer Science", B.C. Anderson and Y. Imanishi, eds., Springer- Akademischer Verlag, Berlin, 1991, 77.
37. Thang S.H, Chong Y.K, Mayadunne R.T.A, Moad G, and Rizzardo E, "A novel synthesis of functional dithioesters, dithiocarbamates, xanthates and trithiocarbonates ", 1999, 40, 12, 19, 2435-2438.
38. Chiefari J, Mayadunne R.T.A, Moad G, Rizzardo E, Thang S.H, 1999, SH Patent WO9931144.
39. Chong Y.K, Le T.P, Moad G, Rizzardo E, Thang S.H, "A More Versatile Route to Block Copolymers and Other Polymers of Complex Architecture by Living Radical Polymerization: The RAFT Process", *Macromolecules*, 1999, 32, 2071.
40. Rizzardo E, Chiefari J, Chong Y.K, Ercole F, Krstina J, Jeffery J, Le T.P, Mayadunne R.T.A, Mei G.F, Moad C.L, Moad G, Thang S.H, *Macromolecular Symposia*, 1999, 143, 291.
41. Chong Y.K, Krstina J, Le T.P, Moad G, Postma A, Rizzardo E, Thang S.H, *Macromolecules* (inpress)

42. Moad G, Ercole F, Johnson C.H, Krstina J, Moad C.L, Rizzardo E, Spurling T.H, Fryd M, Anderson A.G, "Controlled-Growth Free-Radical Polymerization of Methacrylate Esters: Reversible Chain Transfer versus Reversible Termination", American Chemical Society Symposium Series, 1998, 685, 332.
43. Ganachaud F, Monteiro M.J, Gilbert R.J, Dourges M.A, Thang S.H, Rizzardo E, "Molecular Weight Characterization of Poly(N-isopropylacrylamide) Prepared by Living Free-Radical Polymerization", *Macromolecules*, 2000, 33, 6738.
44. Bozovic V, Manon J, Meuldijk H.T, Koning J, Klumperman C, "SAN-b-P4VP Block Copolymer Synthesis by Chain Extension from RAFT-Functional Poly(4-vinylpyridine) in Solution and in Emulsion", *Macromolecules*, 2007, 40, 7132–7139.
45. Prescott S. W, Ballard M. J, Rizzardo. E, Gilbert R.G, "Successful Use of RAFT Techniques in Seeded Emulsion Polymerization of Styrene: Living Character, RAFT Agent Transport, and Rate of Polymerization", *Macromolecules*, 2002, 35, 5417-5425.
46. Ferguson C.J, Hughes R.J, Pham B.T.T, Hawket B.S, Gilbert R.G, Serelis A.K, and Such C.H, "Effective *ab Initio* Emulsion Polymerization under RAFT Control", *Macromolecules*, 2002, 35, 25, 9243-9245.
47. Rieger J, Stoffelbach F, Bui C, Alaimo D, Jerme C, Charleux B, "Amphiphilic Poly(ethylene oxide) Macromolecular RAFT Agent as a Stabilizer and Control Agent in *ab Initio* Batch Emulsion Polymerization" *Macromolecules*, 2008, 41, 12, 4065-4068.
48. Leswin J.S.K, "Particle Formation in RAFT - mediated Emulsion Polymerization", PhD Thesis University of Eindhoven, 2007.
49. Odian G, "Principles of Polymerization", Wiley Interscience, 2004, Fourth Edition.
50. Antonietti M, Landfester K, "Polyreactions in miniemulsions", *Progress in Polymer Science*, 2002, 27, 689-757.
51. Oliveira F.C, "Preparation and Characterization of Novel Nanocomposites of inorganic/polysaccharide type", PhD Thesis, University of Aveiro-2010.
52. Mai Y.W, Yu Z.Z, "Polymer Nanocomposite", Woodhead publishing Limited, 2006, Cambridge England.
53. Hajji P, Gerard J. F, Pascault J.P, Vigier G, David L, "Synthesis, structure and morphology of polymer–silica hybrid nanocomposites based on hydroxyethyl methacrylate", *Journal of Polymer Science, PartB: Polymer Physics*, 1999, 37, 3172.
54. Bourgeat-Lami E, Lang J, "Encapsulation of Inorganic Particles by Dispersion

- Polymerization in Polar Media: 1. Silica Nanoparticles Encapsulated by Polystyrene”, *Journal of Colloid and Interface Science*, 1998, 197, 2, 293-308.
55. Zou H, Wu S, “Polymer/Silica Nanocomposites: Preparation, Characterization, Properties, and Applications”, *Chemical Reviews*, 2008, 108, 9, 3893-3957.
56. He T, Adams D.J, Butler M.F, Cooper A.I, Rannard S.P, “Polymer Nanoparticles: Shape-Directed Monomer-to-Particle Synthesis”, *Journal of the American Chemical Society*, 2009, 131, 1495–1501.
57. Sansona N, Rieger J, “Synthesis of nanogels/microgels by conventional and controlled radical crosslinking copolymerization”, *Polymer Chemistry*, 2010, 1, 965–97
58. Bunshah R.F (editor), "Handbook of Deposition Technologies for Films and Coatings", 1994, William Andrew Publishing/Noyes, second edition. Online version available at: http://knovel.com/web/portal/browse/display?_EXT_KNOVEL_DISPLAY_bookid=57&VerticalID=0 - dated sept 2010.
59. Bach H, Dieter K, "Thin Films on Glass", 2003, Springer- Akademischer Verlag, ISBN 3-540-58597-4.
60. Kumar S, Kumar R, Jindal V.K, Bharadwaj L.M, “Immobilization of single walled carbon nanotubes on glass surface”, *Materials Letters*, 2008, 62, 731–734.

Chapter 2

Polymerization Studies performed under RAFT

Preface:

This chapter is a compendium of all our polymerization attempts performed via RAFT (in an acrylate system) by making use of the bifocal strategy elaborated upon by Ferguson et al.[1] i.e., a) homopolymerization of the RAFT agent to form a macroRAFT agent and b) the copolymerization of the macroRAFT agent with a hydrophobic monomer. The polymer and copolymer obtained were characterized using ¹H NMR, FTIR-ATR, DSC, GPC and TGA. Also detailed discussions are provided with special attention to its control and living characteristics.

2.1 Introduction

The RAFT mechanism [2] allows the controlled polymerization of a variety of monomers at various temperature conditions and is the most viable mechanism among the other free radical polymerization strategies available. However, this is well formulated for homogeneous [3] systems and not for dispersion systems due to the transfer of the RAFT agent across the aqueous phase thus leading to low polymerization rates, low colloidal stability and broad molar mass distributions [1] (loss in system control). Attempts at preventing the transfer of the RAFT agent in a dispersion medium were first discussed by Prescott *et al.* [4], wherein they localized the RAFT agent in a seed particle before polymerization. Later techniques of unseeded emulsion polymerization (ab-initio) under RAFT in the absence of free surfactant were developed by Ferguson *et al.*[1,5,6] and Klumperman *et al.*[7]. They succeeded in controlling the molar mass of the chains by working under feed starved conditions by polymerizing hydrophilic macroRAFT agents, (2-(butylsulfanyl)-carbonothioyl-sulfanyl propanoic acid and 2-(dodecylsulfanyl)-carbonothioyl-sulfanyl propanoic acid) with hydrophobic monomers (butyl acrylate, methyl acrylate). Their strategy relied on the in-situ formation of an amphiphilic di-block reactive copolymer which self assembles into micelles [1] refer figure 1.12. The controlled feed of the monomer allows the polymerization to be carried out in the absence of monomer droplets (which is responsible for loss of control) thus in theory allowing good control of the polymeric system.

This work was further elaborated upon by Maud Save *et al.* [8], and they used the RAFT strategy to

prepare polyacrylate particle dispersions in an organic medium. The RAFT agent used was poly (2-ethylhexyl acrylate) containing either a dithiobenzoate reactive functional group or a trithiocarbonate one and was polymerized with the monomer, methyl acrylate in isododecane. The method produced stable colloidal particles with diameters below 100 nm. When trithiocarbonate functionality was employed the formation of mono-dispersed micelle aggregates of well-defined self-assembled block copolymers were obtained and when dithiobenzoate functionality was employed strong rate retardation and poor control over the polymer chains were observed. This technique was further expanded by Jutta Rieger *et al.* [9] and they proved that PEOTTC (macroRAFT agent) can behave as both a particle stabilizer and as a control agent in the ab-initio batch emulsion polymerization of styrene and butyl acrylate.

Based on the strategy reported by Ferguson *et al.* [1,5,6] and further work developed by Jutta Rieger *et al.* [9], a similar bifocal strategy was deployed in our polymerization processes performed via RAFT i.e., (i) the homopolymerization of PAATTC (preparation of the macroRAFT agent) followed by (ii) the preparation of a block copolymer (P(AAcoBuA)TTC)

2.2 Preparation of the Macro-RAFT agent PAA-TTC

In the preparation of core/shell nanoparticles the best suited RAFT agents used to obtain good control of the particle size are those based on amphiphilic trithiocarbonates. 2-(Dodecylthiocarbonothioylthio)-2-methyl propanoic acid (TTCA) [9,10] is a widely employed trithiocarbonatethio RAFT agent, that is known for efficiently controlling the polymerization of a large variety of mono substituted monomers in homogeneous and heterogeneous systems [9,10].

The homopolymerization reaction was deployed under solution conditions. According to the synthetic path shown in figure 2.1, acrylic acid (monomer), DMF (solvent), initiator (4, 4- azobis (4- cyanopentanoic acid)) and the RAFT agent TTCA were allowed to react based on kinetic studies performed by the team Barros Timmons - Charleaux in UPMC, Paris [11] for 135 minutes corresponding to 100% conversion (α) and this is illustrated in figure 2.2. The reaction was carried out in the absence of air, and periodically samples were withdrawn to monitor the particle size and monomer conversion by $^1\text{H-NMR}$ and gravimetry. After drying the number average molar mass (M_n) was determined by GPC.

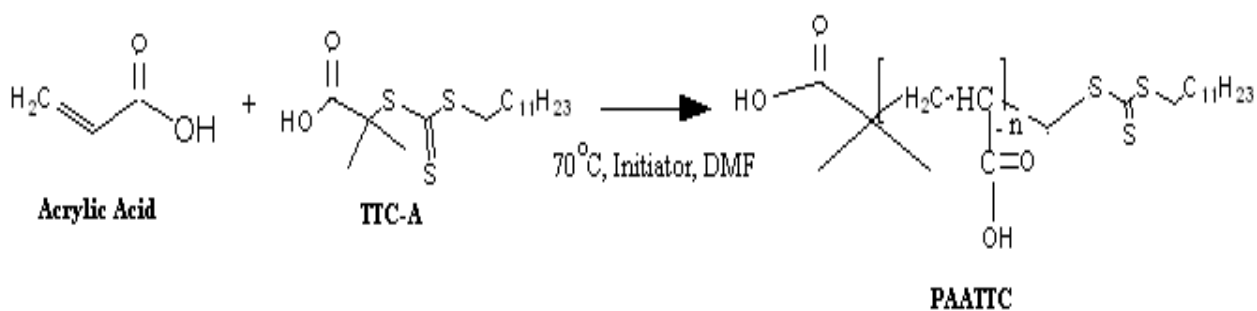


Figure 2.1 The synthesis of PAATTC.

The reaction contents were purified by precipitation with n-hexane to remove traces of the unreacted monomer and the solvent DMF. The complete preparatory details of PAATTC can be found in §5.3.1.1.

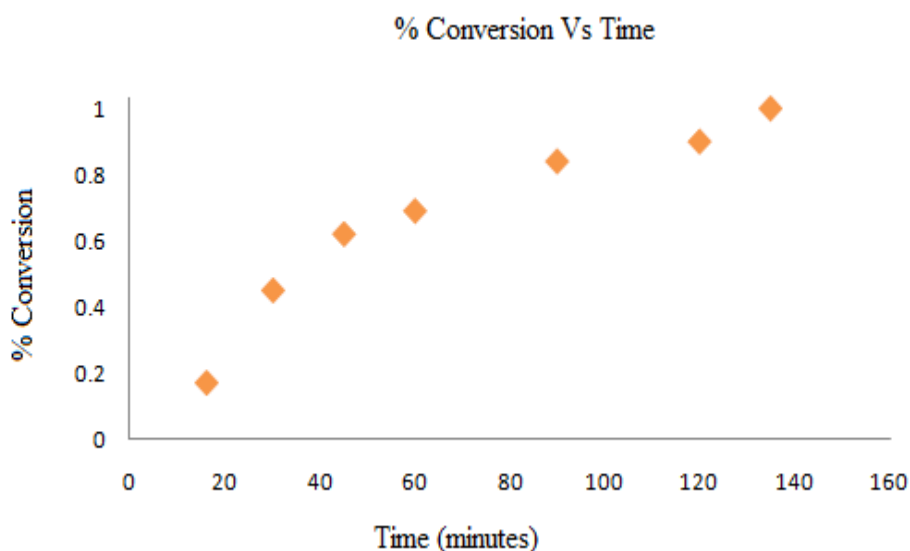


Figure 2:2 Kinetic Studies performed on PAATTC.

According to the previous kinetic studies [11] the experimental Mn of the sample obtained was 4747 g/mol at 135 minutes. This corresponds to the theoretical molecular weight of the sample at 100% conversion. Based on this information, data extrapolation was performed and the values obtained are shown in the tabular column 2.1 and these formed the starting point of our experimentation.

Tabular Column 2.1: % Conversion as a function of time.

% Conversion	Time (minutes)
20	17
50	40
70	63
80	83
100	135

The theoretical molecular weights were calculated using the equation shown below.

$$M_{n, th} = \frac{[M]_0}{[RAFT]_0} xm_0 + M_{RAFT}$$

Equation 2.1: Theoretical molecular weight formula.

Where $[M]_0$ and $[RAFT]_0$ are the initial concentrations of monomer and RAFT agent, x refers to the overall monomer conversion and, m_0 and M_{RAFT} are the molecular weights of the monomer and RAFT agent respectively.

However, preliminary attempts and subsequent co-polymerization with hydrophobic monomers (butyl acrylate, styrene, methyl acrylate) in mini-emulsion and solution conditions were uneventful and could be attributed to the fact that macroRAFT agents polymerized to 100% conversion jeopardizes the living characteristics of the system. In fact, it is known that at slightly lower conversion rates (50-80%) the system may possess both living and controlled behavioral characteristics. Hence we resolved to work at low conversions in our series of experiments. The five different conversion values worked upon were, a) 20% conversion, b) 50% conversion, c) 70% conversion, d) 80% conversion and e) 100% conversion. The % conversion as a factor of time are shown in the tabular column 2.1

2.2.1 Characterization of the RAFT and the macroRAFT agent

The $^1\text{H-NMR}$ and FTIR -ATR were performed on TTC-A and the newly formed macroRAFT agent PAATTC. The resulting spectra obtained can be found in Annex 1 (a,b) and Annex 2 (a).

The macroRAFT agents were then analyzed by GPC. PAATTC (100% conversion) was first purified by precipitation with n hexane in order to remove any traces of unreacted monomer and methylated as described in §5.7.1. A typical GPC chromatogram is shown in figure 2.3

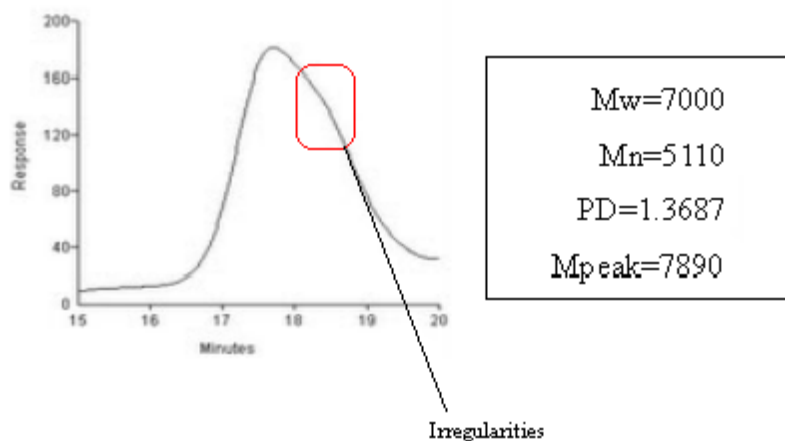


Figure 2.3 GPC chromatogram of PAA-TTC (100% conversion).

Using DMA as eluant, the GPC chromatogram was obtained, however the presence of a secondary peak was well evident. This could be due to the possibility of conventional radical polymerization occurring alongside RAFT polymerization. This could also be due to the poor compatibility between the eluant (DMA) and the polymeric system and/or the presence of impurities. The measurements were repeated with THF as the eluant and these irregularities were suppressed. Other systems of lower conversion were tested viz., PAA-TTC (80% conversion), PAA-TTC (50% conversion), PAA-TTC (20% conversion) and PAA-TTC (70% conversion) refer figure 2.4. Molecular weight ranging from 2000-8000 g/mol were witnessed. The theoretical and experimental molecular weights as well as the PDI obtained are summarized in table 2.2.

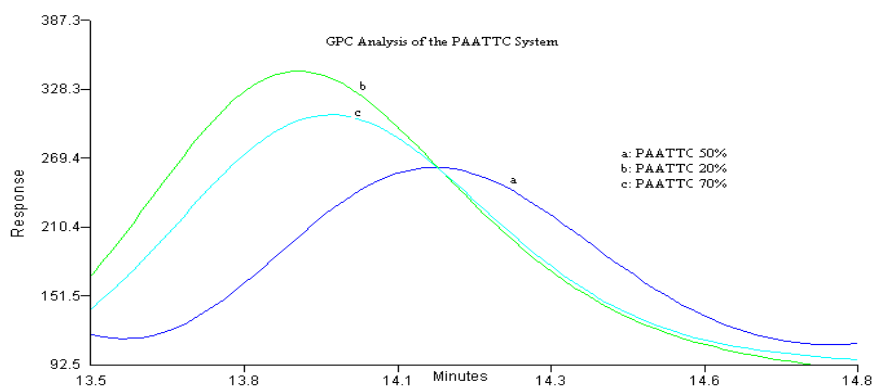


Figure 2.4: GPC chromatogram of PAA-TTC (20%, 50% and 70% systems).

From size exclusion chromatography (SEC) or GPC, we are cognizant of the fact that higher molecular weight compounds exit the system faster than lower molecular weight compounds. However in our case, a converse demeanor was observed refer figure 2.4 (a, b, c) where the chromatogram for 70% conversion (higher molecular weight) eluted much slower than the 50% and at the same time as the 20% conversion. This could be due to various factors viz. different flow rates, different experimental runs, strong methylating agents which could destroy the RAFT agent, different chromatogram widths and heights etc. This abnormality needs to be further investigated.

Tabular Column 2.2: Poly dispersities, theoretical and experimental molecular weights of the PAA-TTC system at various % conversion determined by GPC analysis.

% Conversion (α)	Theoretical Molecular Weight (Mn)	Obtained Molecular Weight (Mn)	Poly dispersity Index (Mw/Mn)
20	1237	5981	1.1
50	2547	5827	1.06
70	3420	7727	1.11
80	3857	7718	1.16
100	4730	7530	1.15

From table 2.2, significant dissimilarities between the theoretical and experimental molecular weights are witnessed, however polydispersity indices which fit within the acceptable criteria (i.e., <1.2) were obtained. Although narrow PDIs were observed, to further check on the controlled behavioral characteristics of the system, complete system kinetics needs to be performed for the experimental conditions and facilities available in Aveiro. To assert the living behavior, the copolymerization with butyl acrylate monomer was carried out and monitored by GPC, to detect any increments in the molecular weight refer §Table 2.5 and 2.6.

DSC Analysis was carried out for the different samples. The samples were prepared by drying them overnight in an oven at 60°C and placing them in a desiccation unit until analysis. The melting point of pure TTC-A (as obtained) was 63.86°C. The T_g values of samples prepared with different conversions of PAA-TTC are recorded in tabular column 2.3.

Tabular Column 2.3 T_g values by DSC, attempt 1.

Sample	T _g (°C)
PAATTC-100%	-24.38
PAATTC-80%	-12.33
PAATTC-70%	-13.93
PAATTC-50%	-21.32
PAATTC-20%	-19.73

The PAA-TTC (20%-100%) samples were tested and T_g values ranging from -24.38°C to -12.33°C were obtained. This behavior is abnormal as the T_g of PAA is found to be around +105°C [12]. Upon further investigations, we noticed that better sample preparation was required to completely eradicate moisture from the system, as trace water could act as a plasticizer and could alter the values of the T_gs obtained.

In our second attempt, the samples, PAA-TTC (100% conversion) and PAA-TTC (80% conversion) were dried thoroughly by keeping them in an oven overnight at 110°C to remove any traces of moisture and leaving them in a desiccator until analysis. T_gs were obtained at -7°C and -10°C (refer Annex 3 a) thus providing clear evidence that water acts as a plasticizers and affects the system.

Another important parameter that was not taken into account was the thermal-mechanical history of the system. This was detected by small variations of the T_g value on the thermogram. In order to account for the thermo-mechanical history, the T_g values were once again determined upon cycles of heating and cooling of PAA-TTC (80% conversion). A wide variety of T_gs were observed with variations from -10.12 to +2.2°C (refer Annex 3 a). Further attempts to obtain accurate values of T_g are currently being processed, yet these results highlight the difficulties of determining the T_g for these type of polymers.

2.3 Formation of Block Copolymers

In order to test the living and the controlled nature of the macroRAFT agent, block copolymerization was performed using the macroRAFT agent and a hydrophobic monomer (butyl acrylate). This was proceeded by using two different process techniques namely **a) solution** and **b) emulsion**.

2.3.1 Block Copolymerization in Solution and Emulsion

With regard to co-polymerization in solution, the macroRAFT agent was dissolved in ethanol and suitable quantities of a water soluble initiator (4, 4- azobis (4-cyanopentanoic acid) and purified butyl acrylate monomer were appended. The contents were allowed to react for a time corresponding to 100% conversion and the contents were purified and consecutively analyzed by $^1\text{H-NMR}$, FTIR-ATR, DSC, GPC and TGA. Conversely in emulsion instead of ethanol, ultra pure water was used and NaHCO_3 was added which makes the system a polyelectrolyte by adding an electrolyte group to the repeating units of the polymer [13]. For the complete synthetic procedure refer segment § 5.3.1.2.

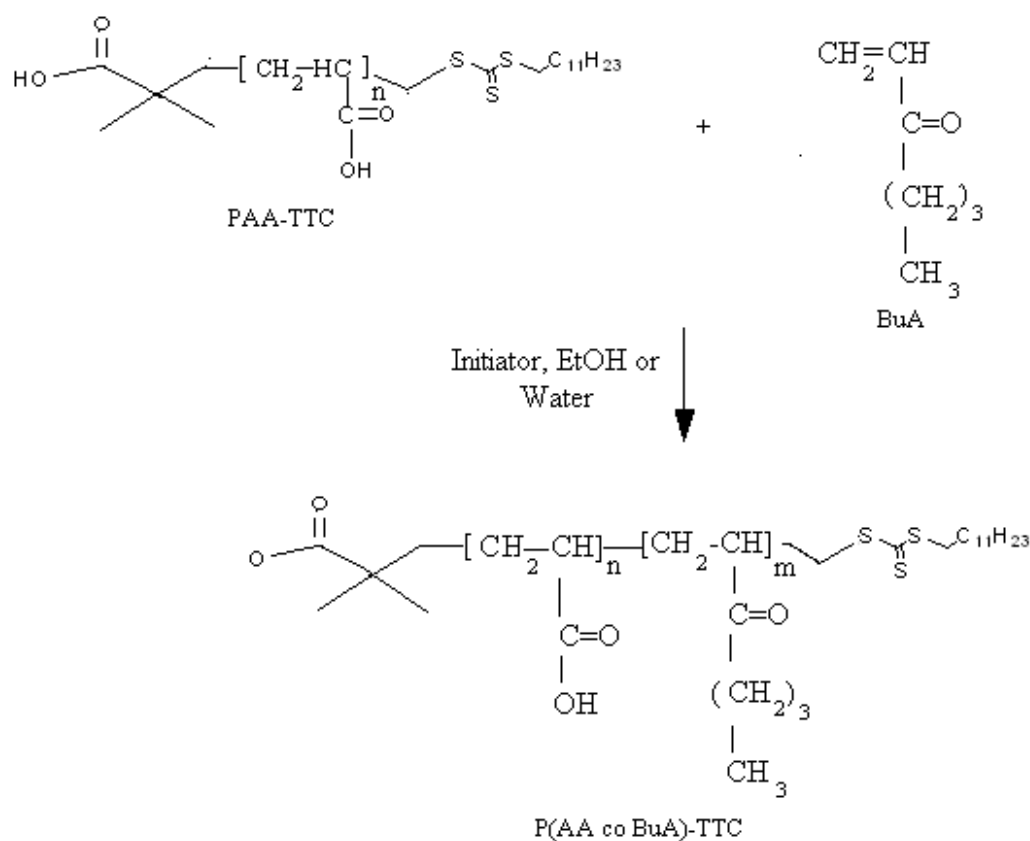


Figure 2.5 Synthetic Approach to the preparation of P(AAcoBuA)-TTC.

In our series of experiments, we made use of different % conversions of PAA-TTC and copolymerized them with butyl acrylate in both solution and emulsion conditions. However for most emulsion reactions, colloidal instability lead to immediate phase separation of the product obtained, while in the case of solution stable systems were obtained. A snapshot of the end products of co-polymerization (80% conversion), in both solution and emulsion are shown in figure 2.6.

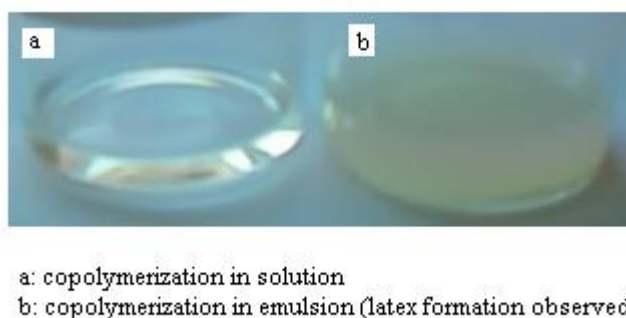


Figure 2.6 Snapshot of copolymers P(AAcoBuA)TTC obtained in (a) solution and (b) emulsion conditions (80% conversion)

2.3.2 Characterization of P(AA co BuA)-TTC

The copolymer was characterized by FTIR-ATR and ¹H-NMR. And the spectra along with relevant band information are provided in the Annex. (1(c) and 2(b)). The thermogravimetric studies (TGA) studies were carried out on P(AA co BuA) TTC (80% conversion).

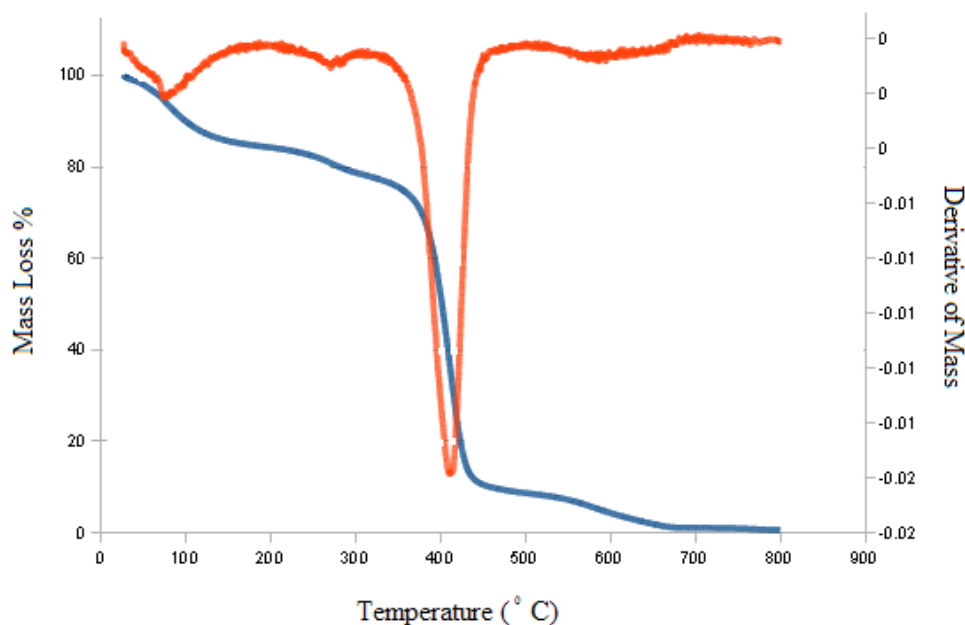


Figure 2.7 TGA of P(AAcoBuA)TTC-80% conversion

From the figure 2.7 we observe that the first decomposition of the copolymer occurs at 278-280°C, followed by the decomposition at 415-420°C and a subsequent decomposition at 630°C (due to the

disintegration of the molecular structure). From literature, we are aware that PBuA in the presence of a water soluble initiator degrades at 292°C due to the ester decomposition caused by the radical attack on the nearby carbonyl groups [14]. A schematic representation of this decomposition is shown in figure 2.8.

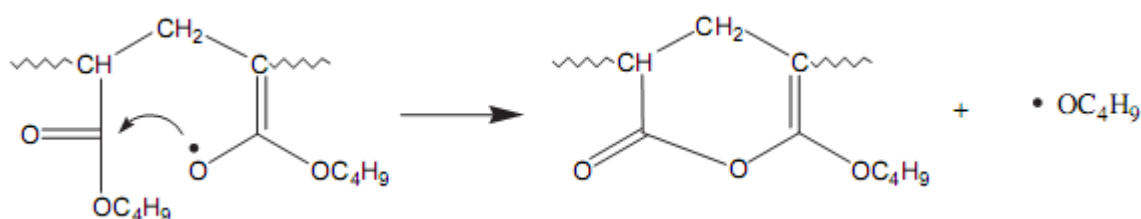


Figure 2.8 Systematic degradation of PBuA at 292°C reproduced from [18].

The degradation of PAA is observed above 250°C accompanied by the release of water, CO and CO₂ [15]. The TGA analysis of TTC-A (as obtained) has not yet been performed hence no comparative data is available to analyze the disintegration of the TTC compound. (**Note:** the mass loss observed at 80-110°C may correspond to the loss of water within the system and eventually TTC).

The Differential Scanning Calorimetric (DSC) Analysis were carried out on the P(AAcoBuA) TTC samples prepared with different % conversion of the macroRAFT agent. Since block copolymeric materials were analyzed, two T_g values were expected, one corresponding to the poly (acrylic acid) block at around +105°C [12] and the other to the poly (butyl acrylate) at -50 °C [16]. The results obtained are shown in the tabular column 2.4.

Tabular Column 2.4: DSC studies of P(AAcoBuA) TTC, Analysis 1

Sample Analyzed	T _{g1} (°C)	T _{g2} (°C)
P(AAcoBuA) TTC(100%)	-46.46	33.19
P(AAcoBuA) TTC (80%)	-51.46	25.98
P(AAcoBuA) TTC (50%)	-48.7	40.8

From the results obtained no striking trend in data could be observed. Also as mentioned previously, water could act as a plasticizer hence extreme care should be taken while preparing the samples for

DSC. The experiments were repeated to confirm the original values however this time for P(AAcoBuA)TTC(100%) two T_gs were witnessed, with T_{g2} at -3.06. In the case of P(AAcoBuA)TTC (80%) and P(AAcoBuA)TTC (50%) only one T_g value was obtained i.e., T_{g1} refer Annex 3 (b). This could be due to a wide variety of factors i.e., exposure to moisture (water acts as a plasticizer), decomposition of the polymer, blending of the aliphatic chain of the TTC with the poly(butyl acrylate) block and the destabilization of the poly(acrylic acid) block, the thermal mechanical history of the system under study and the presence of impurities. These results are further being looked into. It should also be noted that DSC was performed on nanocomposites and two T_gs were obtained (with the exception of modified silica fibers) refer Table 4.2 and 4.3.

GPC or SEC analysis were performed on the P(AAcoBuA) TTC copolymer (20-100% conversion) upon methylation and the results obtained are tabulated in Table:2.5, alongside the theoretical and experimental results of the corresponding macroRAFT agent.

Tabular Column 2.5 GPC studies of the P(AAcoBuA)TTC copolymer compared with the GPC results of the macroRAFT agent (PAATTC).

System	Mn, th PAATTC Theoretical (g/mol)	Mn, exp PAATTC Theoretical (g/mol)	Mn, th of P(AAcoBuA) TTC (g/mol)	Mn, exp P(AAcoBuA) TTC in solution (g/mol)	Mn, exp P(AAcoBuA) TTC in emulsion (g/mol)
P(AAcoBuA) TTC-100%	4730	7530	19803	10856	-
P(AAcoBuA) TTC-80%	3857	7718	18930	15920	-
P(AAcoBuA) TTC -70%	3420	7727	18493	23407	-
P(AAcoBuA) TTC-50%	2547	5827	17620	11690	78334
P(AAcoBuA) TTC -20%	1237	5981	15693	-	42670

Again, large variations between the theoretical and experimental molecular weights were witnessed. However from the figures 2.9 and 2.10 we can confirm that the system was living due to the presence of one peak, but no control was obtained as the PDIs were higher than 1.2.

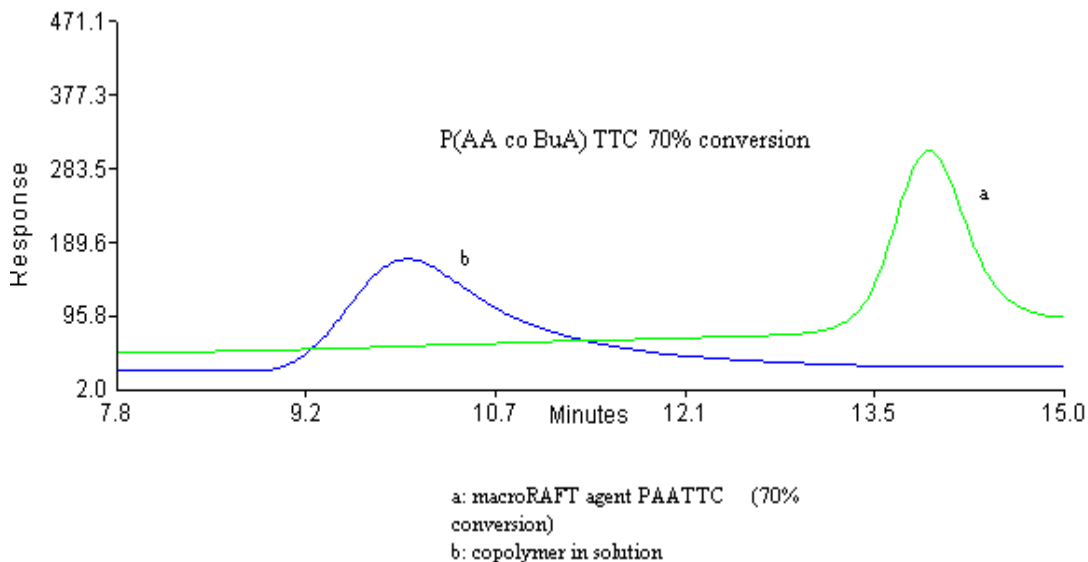


Figure 2.9 GPC studies of the P(AAcoBuA)/TTC copolymer.

In the tabular column 2.8 some spaces are left blank this is due to the fact that the system either destabilized or showed multiples peaks on the chromatogram, hence these results were ignored. Some more examples of GPC data are shown in figure 2.10.

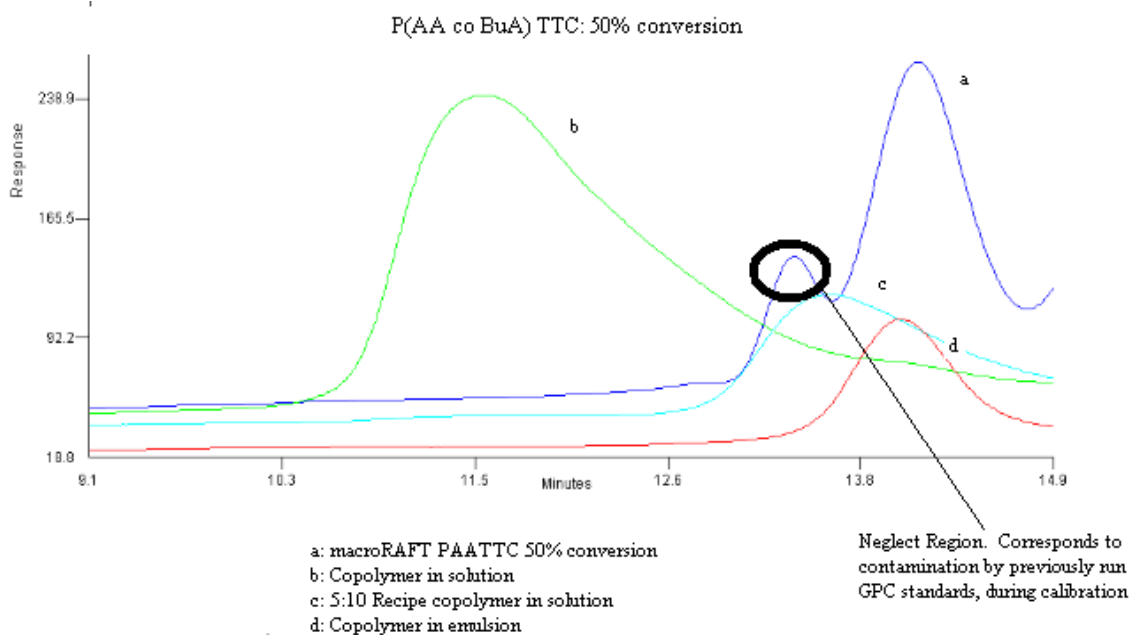


Figure 2.10 GPC studies of the P(AAcoBuA) TTC: 50% conversion.

Figure 2.10 is a clear indication of the living nature due to the presence of one peak and also due to the fact that figure 2.10 (b, d) possess molecular weights greater than the macroRAFT agent (a). However, loss of control (PDIs >1.2) was observed. This system needs to be further optimized in order to obtain narrow Mn distributions i.e., better poly dispersity values.

For most of the emulsion systems the polydispersities were in the range of 1.4-1.9 (uncontrolled) and for solution systems between 1.3-1.8. i.e., unacceptable PDIs. A comparative study of the polydispersity indices were done (refer tabular column 2.6). A wide variation in polydispersity indices between the macroRAFT agent (PAATTC) and the copolymeric system existed. In this regard, further study needs to be performed in order to obtain optimized results.

Tabular Column 2.6 PDI studies of P(AAcoBuA)TTC system compared with results of the macroRAFT agent PAATTC.

System	PDIs of PAATTC	PDIs of P(AAcoBuA)TTC in solution	PDIs of P(AAcoBuA)TTC in emulsion
P(AAcoBuA)TTC- (100%)	1.14	1.35	-
P(AAcoBuA)TTC- (80%)	1.16	1.54	-
P(AAcoBuA)TTC- (70%)	1.11	-	-
P(AAcoBuA)TTC- (50%)	1.06	1.74	-
P(AAcoBuA)TTC- (20%)	1.1	-	1.54

2.4. Preparation of P (AAcoBuA) TTC (5:10 ratio)

Following the instructions provided by Ali *et al.*[17] with minor adjustments, attempts at preparing copolymers with the ratio of 5:10 were carried out i.e., 5 BuA units and 10 AA units, making use of PAATTC-50% conversion as starting material. For a complete description on the synthetic process refer segment § 5.3.1.3. In order to prepare anisotropic nanocomposites and to foster encapsulation another method is detailed wherein the macroRAFT copolymer i.e., P(AA co BuA)TTC 5:10 was further polymerized via starved feed emulsion polymerization with MMA/BuA at a ratio of 7:3. A snapshot of the end product obtained is shown in figure 2.11. Due to the lack of time and an

unoptimized process condition further attempts were abandoned and focus was given only to the bifocal technique elaborated upon by Ferguson *et al.* [1].

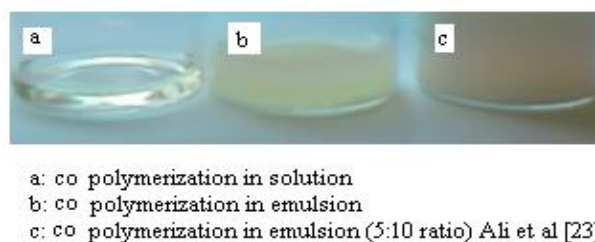


Figure 2.11 Copolymerization in solution, emulsion and emulsion (5:10).

2.5 General Remarks, Conclusions and Future Work

- The characterization of the RAFT agent TTC-A by $^1\text{H-NMR}$, FTIR-ATR, DSC etc., was performed.
- MacroRAFT agents were synthesized by the homopolymerization of TTC-A with acrylic acid based on previous kinetics studies conducted by Barros Timmons-Charleux [11]. Different conversions of the macroRAFT viz., PAA-TTC 20% conversion, PAA-TTC-50% conversion, PAA-TTC-70 % conversion, PAA-TTC-80% conversion and PAA-TTC 100% were prepared and characterized by $^1\text{H-NMR}$, FTIR-ATR, GPC, DSC etc. From the results obtained, we can safely conclude that the homopolymers had a narrow molecular weight distribution and low polydispersity indices, proving that the system was controlled.
- The copolymerization of PAA-TTC with butyl acrylate was carried out for different conversions of PAA-TTC (from 20-100%) in both solution and emulsion conditions. In solution conditions, evidence of living behavior was obtained but the M_n obtained were very different from the theoretical values, also polydispersity indices >1.3 were obtained thus proving loss of control within the system. In the case of emulsion broad molecular weight distributions were observed, almost three times the theoretical values and extremely high polydispersity indices (1.9) were obtained proving loss of control.
- Solution system conditions proved to be more favorable than emulsion systems, as the emulsion systems showed a loss of colloidal stability which led to phase separation within a matter of hours.
- A complete kinetic study, based on the experimental setup available in Aveiro, needs to be performed on both the homopolymerization and copolymerization reactions in order to obtain optimized process conditions.

- Further on, attempts at obtaining block copolymers should be investigated, by the slow and controlled addition of the hydrophobic monomer (BuA), in order to obtain copolymers of desired chain lengths i.e., monomer under starved feed conditions.
- The procedure detailed by Ali *et al.* [17] should be further investigated upon and optimized.

2.6 Bibliography

1. Ferguson C. J, Hughes R. J, Pham B. T. T, Hawkett B. S, Gilbert G, Serelis A. K, Such C. H, “Effective ab Initio Emulsion Polymerization under RAFT Control”, *Macromolecules* 2002, 35, 9243– 9245.
2. Chiefari J, Chong Y.K, Ercole F, Krstina J, Jeffery J, Le T.P.T, Mayadunne R.T.A, Meijs G.F, Moad C.L, Moad G, Rizzardo E, Thang S.H, “Living Free-Radical Polymerization by Reversible Addition–Fragmentation Chain Transfer: The RAFT Process” *Macromolecules*, 1998, 31, 16, 5559-5562.
3. Barner K, C. Ed. “Handbook of RAFT Polymerization” Wiley-VCH: Weinheim, 2008.
4. Prescott S. W, Ballard M. J, Rizzardo E, Gilbert R. G, “Successful use of RAFT techniques in seeded emulsion polymerization of styrene: Living character, RAFT agent transport and rate of polymerization”, *Macromolecules*, 2002, 35, 5417–5425.
5. Ferguson C. J, Hughes R. J, Nguyen D, Pham B. T. T, Gilbert R. G, Serelis A. K, Such C. H, Hawkett B. S, “Ab Initio Emulsion Polymerization by RAFT-Controlled Self-Assembly”, *Macromolecules*, 2005, 38, 2191–2204.
6. Sprong E, Leswin J. S. K, Lamb D. J, Ferguson C. J, Hawkett B. S, Pham, B. T. T Nguyen, Such D, Serelis C.H, Gilbert R.G, “Molecular Watchmaking: ab initio Emulsion Polymerization by RAFT-controlled Self-assembly”, *Macromolecular Symposia*, 2006, 231, 84–93.
7. Bozovic V, Manon H.T, Meuldijk J, Koning C, Klumperman B, “SAN-b-P4VP Block Copolymer Synthesis by Chain Extension from RAFT-Functional Poly (4-vinyl pyridine) in Solution and in Emulsion”, *Macromolecules*, 2007, 40,7132–7139.
8. Houillot L, Bui C, Save M, Charleux B, Farcet C, Moire C, Raust J.A, Rodriguez I, “Synthesis of Well-Defined Polyacrylate Particle Dispersions in Organic Medium Using Simultaneous RAFT Polymerization and Self-Assembly of Block Copolymers. A Strong Influence of the Selected Thiocarbonylthio Chain Transfer Agent” *Macromolecules*, 2007, 40, 6500-6509.
9. Rieger J, Stoffelbach F, Bui C, Alaimo D, Jerme C, Charleux B, “Amphiphilic Poly (ethylene oxide) Macromolecular RAFT Agent as a Stabilizer and Control Agent in ab-Initio Batch Emulsion Polymerization” *Macromolecules*, 2008, 41,12, 4065-4068.
10. Lai J.T, Filla D, Shea R, “Functional Polymers from Novel Carboxyl-Terminated Trithiocarbonates as Highly Efficient RAFT Agents”, *Macromolecules*, 2002, 35, 6754–

6756.

11. Timmons A.B, Charleaux B in UPMC, Paris, [unpublished data].
12. Maurer J.J, Eustace D.J, Ratcliffe C.T, “Thermal characterization of poly (acrylic acid)”, *Macromolecules*, 1987, 20, 1, 196–202.
13. Sperling L.H, “Introduction to Physical Polymer Sciences” Pg 51, Fourth edition, Wiley Interscience, 2006, ISBN: 978-0-471-70606-9.
14. Hu Y.H, Chen C.Y, Wang C.C, “Thermal degradation kinetics of poly (n-butyl acrylate) initiated by lactams and thiols”, *Polymer Degradation and Stability*, 2004, 84, 505-514.
15. Dubinsky S, Grader G.S, Shter G.E, Silverstein M.S, “Thermal degradation of poly (acrylic acid) containing copper nitrate”, *Polymer Degradation and Stability*, 2004, 86, 171-178.
16. PBUA Tg Values: <http://www.polymerprocessing.com/polymers/PBA.html>. -dated Sept 2010
17. Ali S.I, Heuts J.P.A, Hawkett B.S, Herk A.M, “Polymer Encapsulated Gibbsite Nanoparticles: Efficient Preparation of Anisotropic Composite Latex Particles by RAFT-Based Starved Feed Emulsion Polymerization” *Langmuir*, 2009, 25, 18, 10523–10533.

Chapter 3

Inorganic Nanofillers

Preface:

This chapter will dwell on the importance of inorganic nanofillers, the wet processes involved in their formation and the characterization of these particles. The two filler materials probed into were a) Silica and b) Gd₂O₃:Eu³⁺@Silica nanorods/fibres. Though our attention was focussed on Gd₂O₃:Eu³⁺@Silica nanorods/fibres, silica nanoparticles were prepared solely to be used as models and their results were further expanded upon and used on Gd₂O₃:Eu³⁺@Silica nanorods/fibres. The first half of this chapter is devoted to the preparation of silica nanoparticles (both spheres and fibres) by the sol-gel process. The surface modification with suitable silane coupling agents was performed to enhance its compatibility with the organic phase, followed by its characterisation. The latter half of this chapter is ascribed to the formation of Gd₂O₃:Eu³⁺ nanorods/fibres, its encapsulation within a silica coat and finally its functionalization with relevant coupling agents. Also the characterisation, especially photoluminescence (PL) is detailed.

3.1 Silica Nanoparticles

3.1.1 Introduction

The sol-gel methodology has been widely studied as a method of preparing ceramic precursors and inorganic glasses at relatively low temperatures for quiet some time now. Ebelman [1, 2] was the first to observe in the mid 1800s that the hydrolysis of tetraethylorthosilicate (TEOS, Si(OC₂H₅)₄) under acidic conditions yielded SiO₂, and since then several researchers have implemented and ameliorated upon his research, in order to study and optimize the preparation of SiO₂ spherical nanoparticles with adept dimension and shape control [3,4].

Out of the scores of synthetic routes available, Stöber *et al.* [5] proposed a simple method for preparing spherical silica nanoparticles. The main processes involved are **a) hydrolysis of a metal alkoxide** and **b) poly condensation reactions**. Silica fibres can also be prepared by making use of the sol-gel technique, by abiding by the directions delineated by Nakamura and Matsui [6] with minor alterations i.e., preparation at room temperature by the hydrolysis of a metal alkoxide in the presence of ammonia, tartaric acid and ethanol.

The use of silica particles as filler materials is not new but dates back to the beginning of the 19th

century [7], where the examination of the blending of organic and inorganic material were taking place. Over time as research progressed, the inorganic particles were chemically modified in order to enhance their compatibility with the materials. In the case of silica, surface modification was carried out by employing silane coupling agents [8]. Now the inorganic particle, possessed the ability to attach itself to the polymeric material thereby forming new polymer matrix nanocomposites with enhanced properties viz. improved thermal, electrical properties, mechanical properties etc. [9]

3.1.2 Spherical Silica Nanoparticles

The most prolific method to prepare silica nanoparticles is the sol-gel technique modified and developed by Stöber *et al.* [2]. Upon usage of this method spherical silica particles with good size, shape and dimensional control can be prepared. This method with minor modifications was employed in our attempts to prepare spherical silica nanoparticles. The alkoxide used in our case was TEOS or tetraethylorthosilicate, which was preferred over the others, due to its slow and controllable rate of reaction [10]. The other requisite reagents were absolute ethanol, water (ultra pure) and NH₃ (catalyst). Tetraethylorthosilicate (TEOS) is appended to a mixture of water, ethanol and ammonia. The hydrolysis of TEOS is shown in figure 3.1.

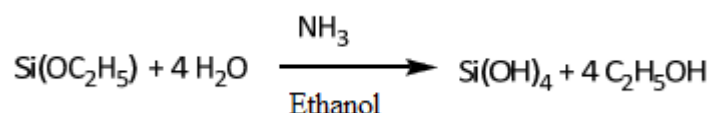


Figure 3.1 The hydrolysis of TEOS reproduced from [11].

The hydrolysis of TEOS is a relatively slow process; hence the catalyst NH₃ was deployed. NH₃ possesses a dual role and acts as both, a catalyst and a stabilizer thereby helping in the stabilization of the newly formed nanoparticle. The condensation of this product leads to the formation of silica spheres. Refer figure 3.2.

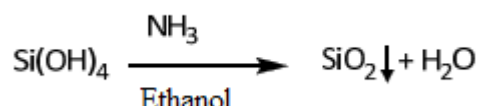


Figure 3.2: Formation of silica reproduced from [11].

The silica nanoparticle formed is stabilized by the electrostatic repulsion of the ions in the ammonia solution as shown in figure 3.3

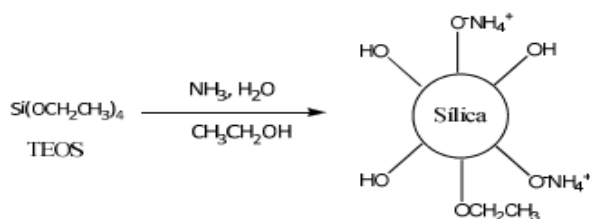


Figure 3.3: Stabilization of silica nano particles reproduced from [11].

Special care should be taken while preparing spherical silica nanoparticles, as it is stated in literature that variations in size can occur with venial changes in reaction conditions like temperature, amount of ammonia (NH₄OH) present and also the ratio of the concentrations of H₂O and TEOS [12]. Pinto *et al.*[13] were able to further optimize Stöber method and were able to obtain monodispersed spherical nano silica particles by varying the amounts of NH₄OH added, and finally verified that the size of the nanoparticles is related to the amount and concentration of NH₄OH present. In this study, emphasis was focussed only on the preparation of 300 nm silica particles hence from their investigation approximately 0.5 mol/dm³ of NH₄OH was used.

Table 1
Diameter of SiO₂ particles prepared in ethanol using [TEOS] = 0.2 mol dm⁻³ and [H₂O] = 5 mol dm⁻³, for distinct amounts of NH₄OH

[NH ₄ OH] (mol dm ⁻³)	D (nm) ± σ (%)
0.2	127 ± 10
0.3	197 ± 7
0.5	299 ± 7
1.0	381 ± 7
2.0	486 ± 4

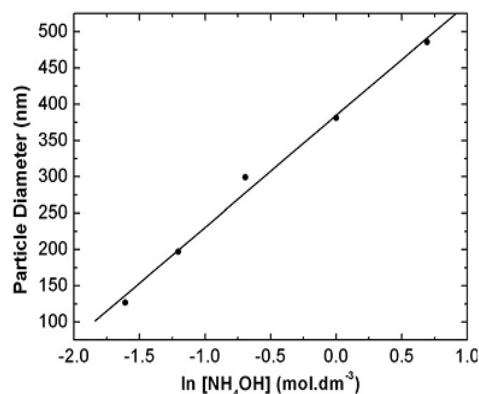


Figure 3.4 Particle diameter as a function of ln [NH₄OH] reproduced from [13].

After the synthesis of the particles, it is essential to thermally activate them by first heating them in an oven at 60 °C overnight to remove traces of moisture, and then by calcination at 700 °C. The particle dispersion and the size of the nanoparticles were obtained by DLS.

3.1.3 SiO₂ nanofibers (hollow)

Like spherical silica nanoparticles, a lot of research has been carried out in this arena, primarily due to their inherent properties like large surface area, chemical stability, easy surface modification [1,6]

etc. The hackneyed procedure for preparing silica fibres is the sol-gel technique as it permits the fabrication of silica fibres with good size control, relatively good distribution and morphology. The technique used in this report is similar to the technique described by Nakamura and Matsui [6] with minor alterations.

Nakamura and Matsui [6] prepared fibres by initially hydrolysing TEOS in a medium of ethanol, water, NH_4OH and tartaric acid. The addition of NH_4OH fosters the precipitation of ammonium tartarate crystals and later on silica fibres. The following manoeuvre is the separation of the silica fibres from the ammonium tartarate crystals, by washing the precipitate with large quantities of distilled water as it is well established from literature that [6] ammonium tartarate crystals are insoluble in alcoholic mediums while the converse is true in aqueous mediums. Upon washing, hollow silica fibres of lengths 300-400 microns, and widths 200-800 nm were obtained, thus conforming with literature [6].

3.1.4 Modification of SiO_2 nanoparticles

It is common knowledge that silica nanoparticles can enhance the properties of composite materials. However by default, silica possesses a negative surface charge [8], which reduces its affinity to the matrix which predominantly possesses a negative charge as well. In order to subdue this barrier, chemical alterations to the surface of the silica nanoparticles have been performed using suitable reagents like silane coupling agents, to enhance the compatibility between the nanoparticles and the polymer matrix. This is done, by building additional hydrogen bridges, covalent bonds or by electrostatic interactions [8, 14]. Besides enhancing its compatibility it can also facilitates the addition of functional groups like amine, epoxy, acrylate etc., on the silica surface [4, 9, 15]. The two silane coupling agents used to modify the silica nanoparticles which were chosen on the basis of their applications were

- a) methacryloxypropyltrimethoxysilane (MPS)
- b) 3-aminopropyltrimethoxysilane (APS)

Both silane coupling agents used were bi functional in nature, i.e., they contained two types of reactive functional groups attached to one Si atom.

3.1.4.1 Surface Modification with MPS

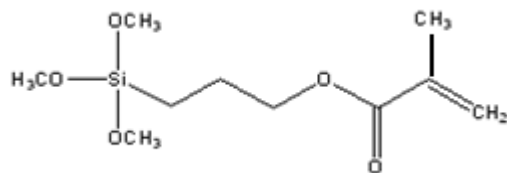


Figure 3.5: methacryloxypropyltrimethoxysilane (MPS)-chemical formula.

The figure 3.5 gives the chemical formula for MPS. When MPS is added to silica in an aqueous medium, the three methoxy groups of the silane coupling agent were initially hydrolysed and then they condense with the silanol on the silica surface to form -Si-O-Si- bonds. The second functional group, methacrylate allows the formation of covalent bonds with the polymer, thus enhancing the compatibility [8, 16]. A diagrammatic representation of the process is shown below in figure 3.6.

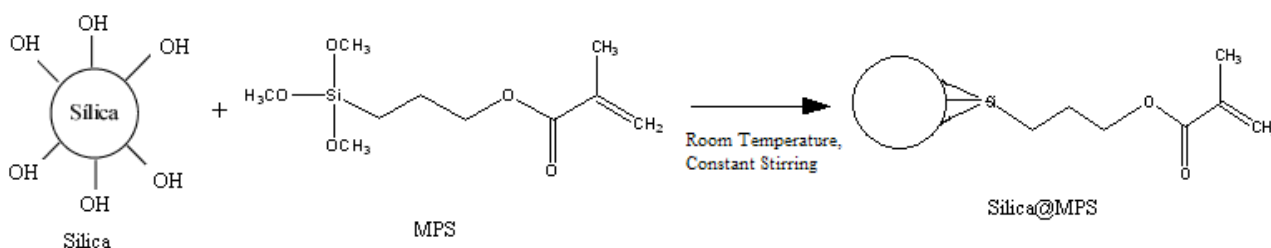


Figure 3.6: Surface modification of silica with methacryloxypropyltrimethoxysilane (MPS).

3.1.4.2 Surface Modification with APS

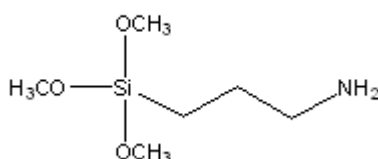


Figure 3.7: 3-aminopropyltrimethoxysilane (APS)-chemical formula.

The figure 3.7 gives the chemical formula for APS. When APS is added to silica in a toluene medium, it is adsorbed onto the silica surface via hydrogen bonds formed between the amine groups and the silanol on the silica particles, and an amine-down position is adopted. At a much later stage, a flip in the APS molecule is observed and an amine-up position is witnessed. This also plays the role of a catalyst during the condensation reaction that occurs between the silane moiety of the adjacent APS and the silanol moiety of the silica surface thus forming siloxane bonds in the

presence of toluene [17]. The amino group of the APS molecule is found to change the electrical double layer present in the medium and as a result better electrostatic interactions between the positive and negative charges of the polymer matrix are expected, which in turn leads to better stability within the system. A diagrammatic representation of this process is shown in figure 3.8.

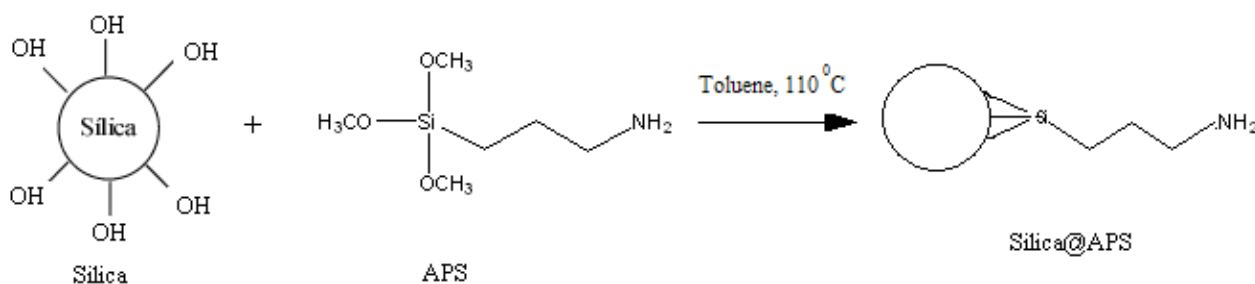


Figure 3.8: Surface modification of silica with 3-aminopropyltrimethoxysilane (APS).

3.1.5 Characterization of SiO₂ particles (unmodified)

DLS (dynamic light scattering) was used, in order to obtain the size and particle distribution of the silica spheres. Initially, getting spheres of a size of 300 nm proved to be quite cumbersome but after critically reviewing the work of Pinto *et al.*[13] and using the right amounts of NH₄OH i.e., 0.5 mol/dm³, spherical silica particles of the desired size were obtained. The results fitted within the acceptable quality range as shown in figure 3.9. However a major limitation with this technique is that the distribution of only spherical silica can be analysed by DLS and not fibres.

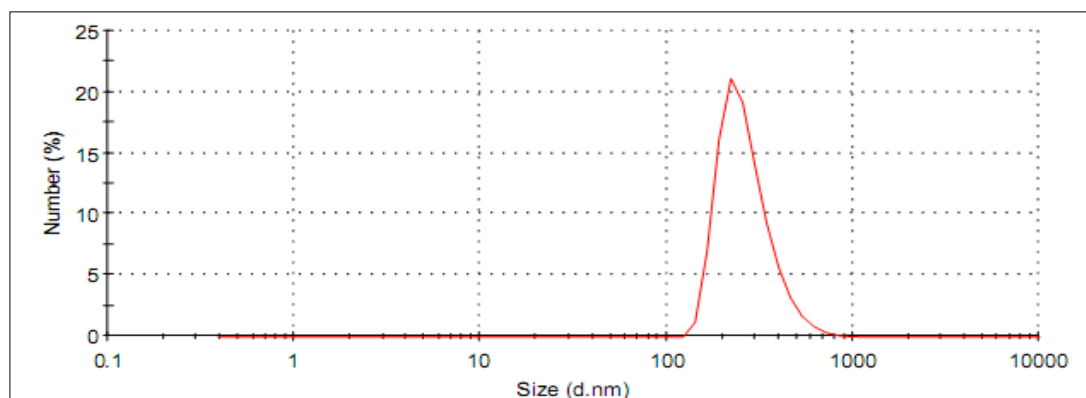


Figure 3.9: DLS result for Si-300 nm spherical particles.

To study the surface morphology of the silica particles SEM analysis was performed on both the silica 300nm spherical particles and silica fibres.

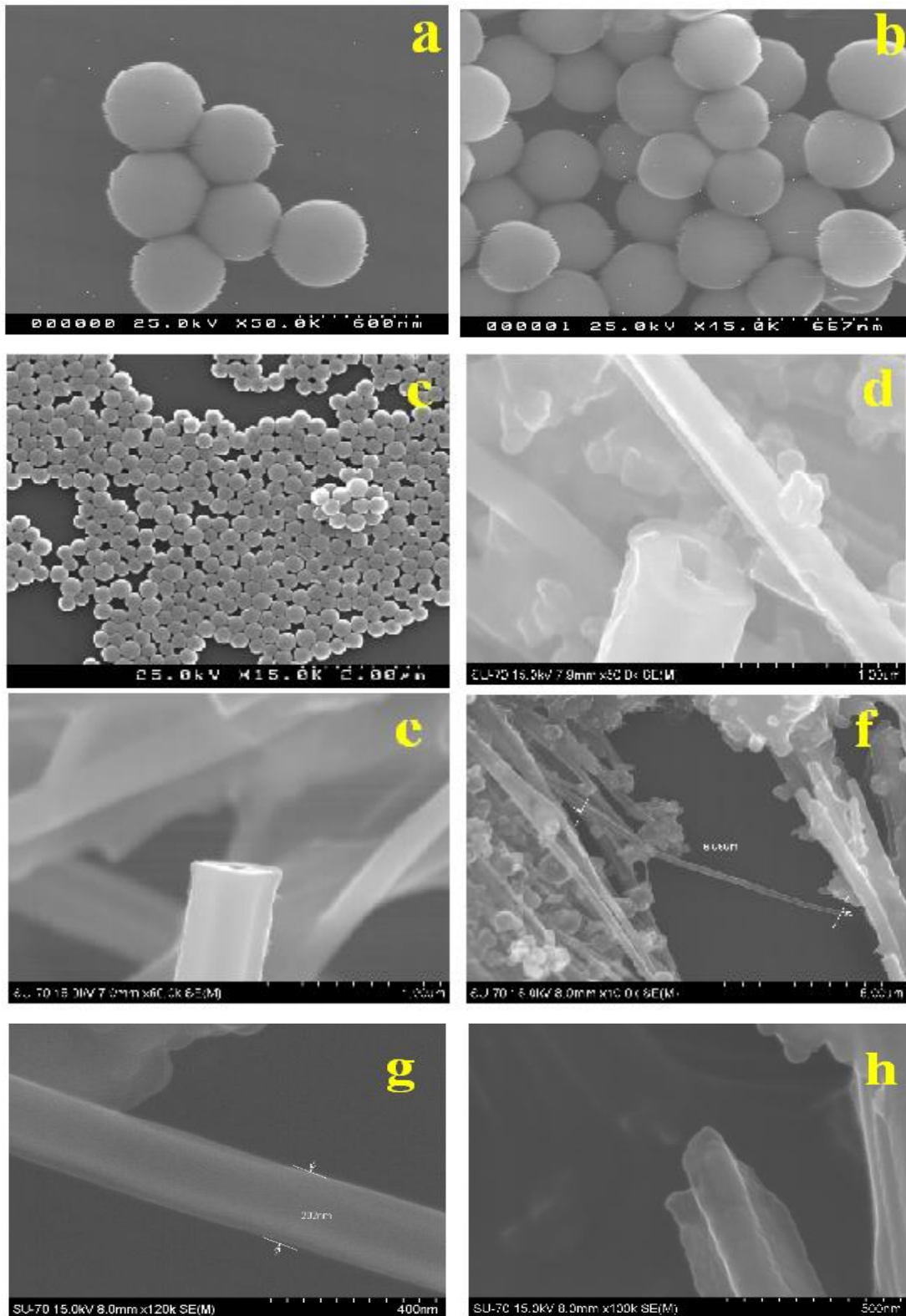


Figure 3.10: SEM images of SiO_2 particles: a, b, c -silica spheres d, e, f, g, h -silica fibres.

In figure 3.10 the images (a), (b) and (c) correspond to silica 300 nm spherical particles and from

them we notice a narrow particle size distribution of silica spheres (approx 300 nm) thus conforming with literature. Figure 3.10 (d), (e), (f), (g), (h), are images of silica fibres. From the figure 3.10. (d) we witness the presence of silica fibres alongside small spheres, which could be either silica spheres or minute quantities of unwashed ammonium tartarate [20]. From figure 3.10 (d) and (e) we affirm that the fibres obtained were hollow in nature and possessed diameters ranging from 200-350 nm and lengths of 8-10 microns, thus again conforming with literature. The last image 3.10 (f) bears witness to the edges of the silica fibres and some of the edges are ruptured, which could be due to its innate delicate nature.

Silica particles both spheres and fibers were characterised by FTIR-ATR spectroscopy. The typical vibration bands of amorphous spherical SiO₂ particles and hollow SiO₂ fibres were easily identified for all samples and are summarised in table 3.1.

Tabular Column 3.1: FTIR-ATR bands of Silica Spheres and Fibres.

Attribution	Experimental Wavenumber (cm⁻¹) of 300 nm Silica Spheres	Literature Wavenumber (cm⁻¹) of Silica Fibers	Literature Wavenumber (cm⁻¹)
v OH	3250	3300	3700-3200 [18,19]
v Si-O	1110	1130	1110-1000 [6,19]
v Si-OH	845	Not observed	910-830 [6,20]
δ Si-O-Si	Not observed as readings were taken from 600-5000 cm ⁻¹		460 [21]

v - Stretching δ - Bending

In the case of silica fibres additional bands were encountered at 1600 and 2360 cm⁻¹, which were characterized by Matsui *et al.* [6] as the adsorption bands of tartaric acid, and is a clear indication that the fibers were not properly rinsed with water. Hence additional rinsing attempts were performed, wherein the freshly formed fibers were subjected to large amounts of distilled water and were later centrifuged. However the newly formed particles were extremely delicate and this method further disintegrated the particles, hence an alternate method needs to be sought after.

A study was also performed along with Fabiane Oliveira *et al.* [22] in order to find out the effect of thermal treatment on the surface of silica. The silica spheres (300 nm) were calcined to 700°C for 4:00 hours and SEM microscopy was used to study the surface morphology of the particles before and after calcination. The results obtained are shown in figure 3.11.

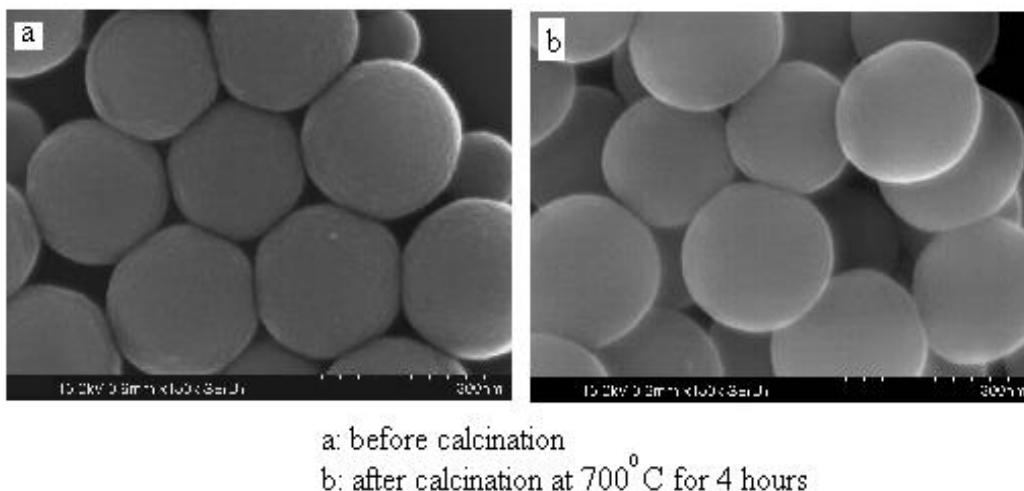


Figure 3.11: SEM images of SiO₂ spheres (300 nm) before and after calcination.

It is well documented in literature that thermal treatment is essential as it assists in the functionalization step, this is due to the increase of the hydroxyl surface groups which can promote the formation of Si-OR bonds (R denotes functional group). From SEM analysis, no clear indication of the surface alteration was obtained, refer figure 3.11 (a), (b) however from FTIR-ATR analysis, a significant decrease in the absorption band of the hydroxyl group (at approx 2600cm⁻¹) was observed, refer figure 3.12.

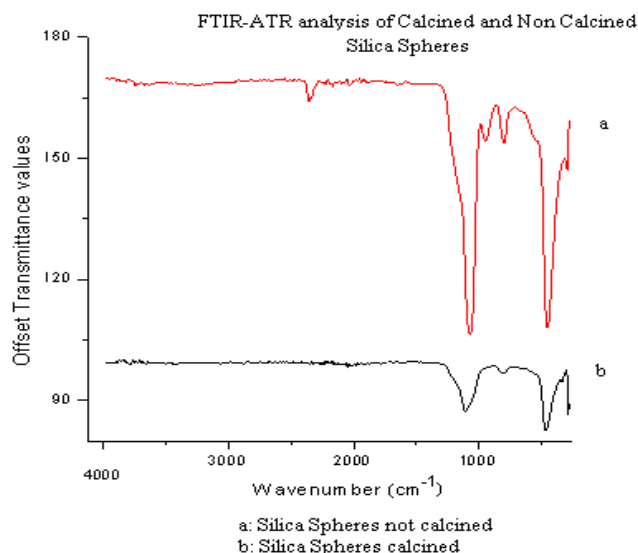


Figure 3.12: FTIR-ATR analysis of SiO₂ spheres (300nm) before and after calcination.

Since the SEM results were inconclusive, BET surface area measurements were carried out on both silica spheres (calcined and non calcined) and silica fibres. From the data obtained only a minor

increase in the surface area was observed, refer tabular column 3.2.

Tabular Column 3.2: BET surface areas of Silica Samples.

Sample	BET Surface Area Measurements (m²/g)
Silica Spheres non calcined	17.4
Silica Spheres calcined	21.3
Silica Fibers	8.71

3.1.6 Characterization of surface modified SiO₂ particles

Silica@MPS spheres (300 nm), were characterized by FTIR-ATR spectroscopy. From literature the most important band corresponding to the anchorage of MPS to the silica surface, is found between 1713-2840 cm⁻¹. Upon high magnification of the spectrum, we can conclude that the band at 1730 cm⁻¹ corresponds to C=O stretching, 1634 cm⁻¹ corresponds to the stretching of the C=C bond and the band at 2931 cm⁻¹ corresponds to the asymmetric stretching of the C-H bonds. Bands of colloidal silica were also observed at 1110 cm⁻¹ corresponding to the Si-O-Si bond stretching and deformation [20, 21]. Refer Annex 2 c.

The FTIR-ATR studies of silica@APS (300nm) spheres were also performed and upon magnification of the curve we can confirm the presence of the successful attachment of APS to the silica particles due to the presence of a band situated at 1432 cm⁻¹ corresponding to the bending of Si-CH₂ bond, and of the band at 807 cm⁻¹ which corresponds to the bending (δ) of N-H. From the spectrum, the bands corresponding to the stretching of both C-H at 2690 cm⁻¹ and N-H at 3000 cm⁻¹ were not observed due to the overlap with the O-H stretching band at 2600 cm⁻¹ [17, 20]. Refer Annex 2 d.

Zeta Potential Measurements were carried out for bear silica, silica@MPS and silica@APS.

Tabular Column 3.3 Zeta Potential Measurements.

Samples Analyzed	Zeta Potential (mV)
Silica (un modified)	-30
Silica@ MPS	-24
Silica @APS	15

As expected at neutral pH, bare silica and silica@MPS possessed a negative charge while silica@APS possessed a positive charge due to the presence of an amine group. This amine group as mentioned earlier, changes the electrical double layer in the medium thereby enhancing the interactions between the positive charge of the modified silica particle and the predominantly negative polymer matrix, thereby enhancing system stability [17, 22]. Thus silica@APS was preferred over silica@MPS in the preparation of nanocomposites.

3.2 Gd₂O₃:Eu³⁺@silica Nanorods/Fibres Preparation

3.2.1 Inorganic Lanthanide (Ln³⁺) Series Introduction

Recently, keen interest has been taken in the study of inorganic lanthanides (Ln³⁺) [23-26] especially in the preparation of Ln³⁺ rods and fibres due to its applications in the biomedical and optics domain [27, 38]. The idea expounded upon by research [27, 29] was the presupposition that functionalizing the Ln³⁺ surface with a suitable coupling agent would enhance its affinity with the polymeric matrix.

Another important strategy investigated upon was nano-encapsulation with silica [27, 29]. Encapsulation technologies as discussed in the introductory chapter were designed so as to reduce the toxicity, mask odour, facilitates storage and to greatly enhance the stability of the inorganic filler material. We know from literature that inorganic lanthanides (Ln³⁺) are highly reactive on exposure to moisture, hence adept encapsulation is needed.

Documented studies, conducted by the K. L. Wong *et al.* [27] have demonstrated that encapsulating (Ln³⁺) nanoparticles with silica enhances its photoluminescence ability due to the reduction of the number of surface Ln-OH bonds. Another attempt of preparing Gd₂O₃:Eu³⁺ nanorods/fibre was demonstrated by Macedo *et al.* [29], where they prepared Gd₂O₃:Eu³⁺ nanorods/fibre via hydrothermal synthesis, encapsulated them with silica and functionalized the surface with the silane coupling agent MPS. They embedded the nanofillers by making use of the in-situ radical polymerization technique of styrene under mini-emulsion and suspension conditions and were eventually able to produce polymer based nanocomposites but with reduced signal intensities (optical properties).

In our attempt to prepare nanocomposites we utilized a similar strategy as prescribed by Macedo *et*

al. [29]. We encapsulated the obtained inorganic particle with silica and further modified the surface with the silane coupling agent APS. Polymer nanocomposites were prepared via in-situ polymerization under solution conditions via the RAFT mechanism using PAATTC as the macroRAFT agent in an acrylate (acrylic acid, butyl acrylate) system. The entire process is detailed in Chapter 4. In this segment the formation, silica encapsulation, functionalization and the characterization of $\text{Gd}_2\text{O}_3:\text{Eu}^{3+}$ @silica nanorods/fibres are elaborate upon.

3.2.2 $\text{Gd}_2\text{O}_3:\text{Eu}^{3+}$ Nanorods/Fibers Preparation

The $\text{Gd}_2\text{O}_3:\text{Eu}^{3+}$ nanorods/fibers were prepared by J. Rocha and his team utilizing the hydrothermal synthetic technique described by L.Q. Lin *et al.* [30]. The nanorods were calcined and then coated with SiO_2 as described in literature [29]. They were then dried, and thermally treated to activate the surface. For in-depth preparatory methods refer section §.5.4.2.

3.2.2.1 Surface modification of SiO_2 coated $\text{Gd}_2\text{O}_3:\text{Eu}^{3+}$ with coupling agents

Our initial proposition was to perform the surface modification with both APS and MPS coupling agents however due to time restrictions, only the modification with APS was considered. APS (as mentioned earlier) possesses an amine functional end group which enhances the electrostatic interaction and thereby making the nanofillers more compatible with the polymeric matrix [17, 22].

Figure 3.13 is the schematic procedure involved in this process.

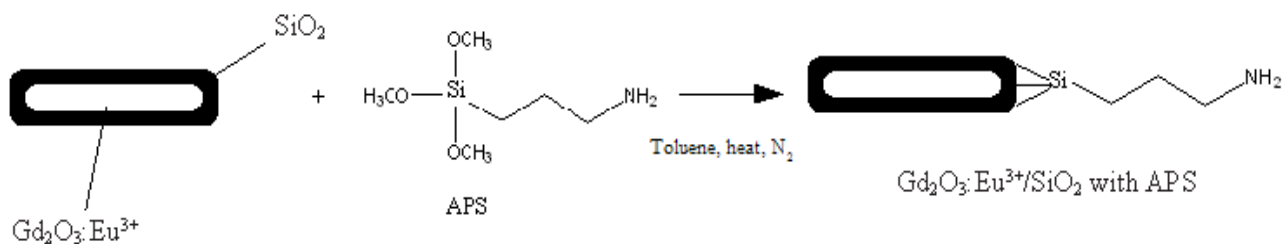


Figure 3.13: The surface modification of $\text{Gd}_2\text{O}_3:\text{Eu}^{3+}$ @ SiO_2 with APS.

The surface modification formulation is very similar to the silica@APS and is described in detail in segments § 5.4.1.3.2.

3.2.3 Characterization of the $\text{Gd}_2\text{O}_3:\text{Eu}^{3+}$ particles

The $\text{Gd}_2\text{O}_3:\text{Eu}^{3+}$ particles were pre-prepared and briefly characterized by Prof J. Rocha *et al.* and some of their results are shown here, refer figure 3.14 (a),(b).

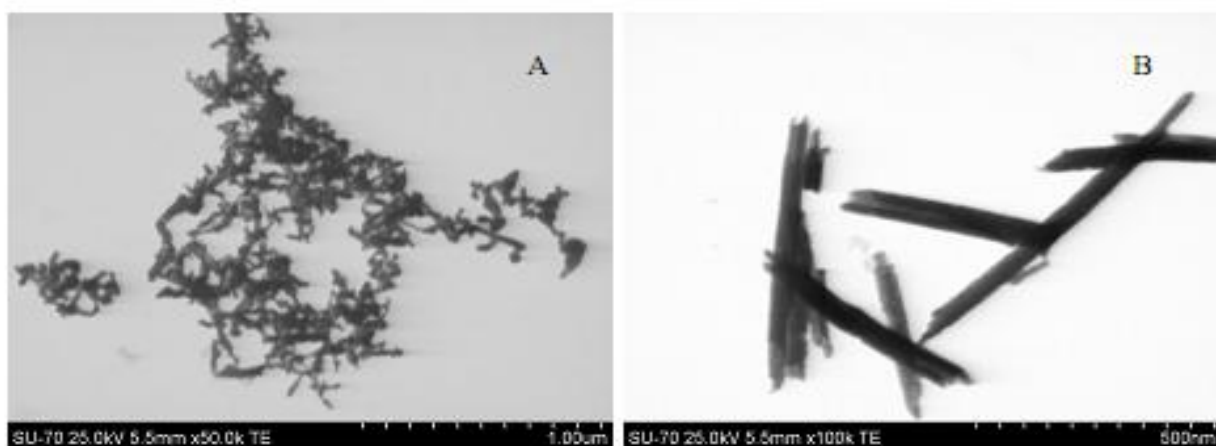


Figure 3.14 (a,b): S-TEM images of Gd₂O₃:Eu³⁺ nanofillers.

S-TEM was performed and rods with dimension i.e., 10-60 nm in diameter (external), 100-500 nm in length and 5-12.5 nm thick were obtained. From figure 3.14 (b) the rough and cracked edges of the nanofibers are noticed which bears witness to its fragile trait, hence extra precaution should be taken during the wet process of silica encapsulation to ensure no further rupture of the nanorods. The BET surface area studies were conducted on these nanofibers and S_{bet} 28 m²/g was obtained for N₂ adsorption at 77 K. Knowing the surface area made it easier to speculate upon the quantity of APS necessary for the functionalization of the Gd₂O₃:Eu³⁺@silica surface as prescribed by literature [17].

The Gd₂O₃:Eu³⁺ particles were then coated with silica and were again analysed by S-TEM refer figure 3.15. From the figure 3.15 (a), (b) and (d) a distinct silica coat is witnessed around the nano particle however in the case of (c) a non uniform coating is observed. This could be due to varying factors like unequal stirring, not enough time to react etc. K. L. Wong *et al.* [27] have shown that by encapsulating Ln³⁺ particles with silica, enhancement in the optical properties were witnessed due to the reduction of the Ln-OH bonds, however unequal silica encapsulation could intensify the formation of the Ln-OH bonds which in turn could hinder the PL/optical properties.

From the S-TEM results, a visual attestation to the encapsulation of silica over the nanoparticles can be ascertained however to reassert the claim EDS (method of chemical analysis) was employed.



Figure 3.15 (a,b,c,d): S-TEM images of $Gd_2O_3:Eu^{3+}@SiO_2$.

From the spectra obtained refer figure 3.16 a clear indication of Gd is observed alongside the presence of Si, thereby actuating our claim. The remaining elements witnessed were from the sample holder (Sn, Al) and TEM grating (Cu). However the presence of europium could not be detected by EDS. This could be due to a number of factors **a) the EDS is not sensitive to small amounts of europium (in S-TEM mode)** and **b) during the wet process of silica encapsulation the europium was leached**. This should be further looked into, by performing elemental analysis like ICP, Atomic Flame Atomization etc.

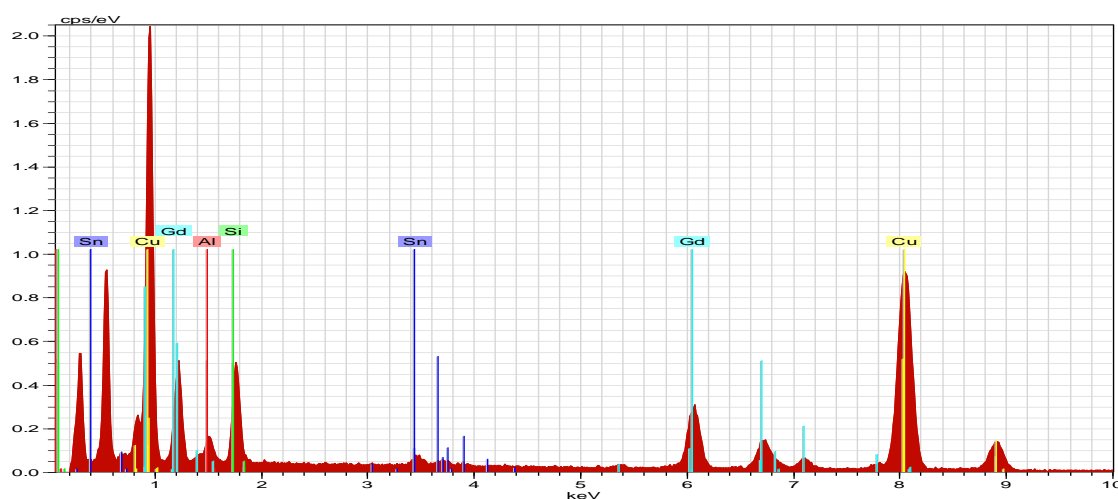


Figure 3.16: Chemical Analysis of the sample by EDS.

In order to study the optical properties of the sample, the photoluminescence studies were carried out. The excitation spectra of the modified and unmodified nanorods are shown in Fig. 3.17.

On doping Gd₂O₃ with Eu³⁺ ions, the latter was found in two distinct crystallographic sites, with two symmetries namely C₂ and S [33, 34]. From this data the excitation spectra was monitored from 200 nm to 650 nm. For the Gd₂O₃:Eu³⁺ (a) calcined, at around 255 nm a broad band transition occurs i.e., Eu³⁺ ⁵D₀→⁷F₂ (C₂) due to the O²⁺→Eu³⁺ ligand-to-metal charge transfer (LMCT). For the Gd₂O₃:Eu³⁺@Silica (b) a similar process occurs at 253 nm and for Gd₂O₃:Eu³⁺@silicaAPS this transition occurs at 250nm [29]. In the case of (a) and (b) a similar signal intensity was observed however upon functionalization (c) a significant decrease in signal intensity was witnessed.

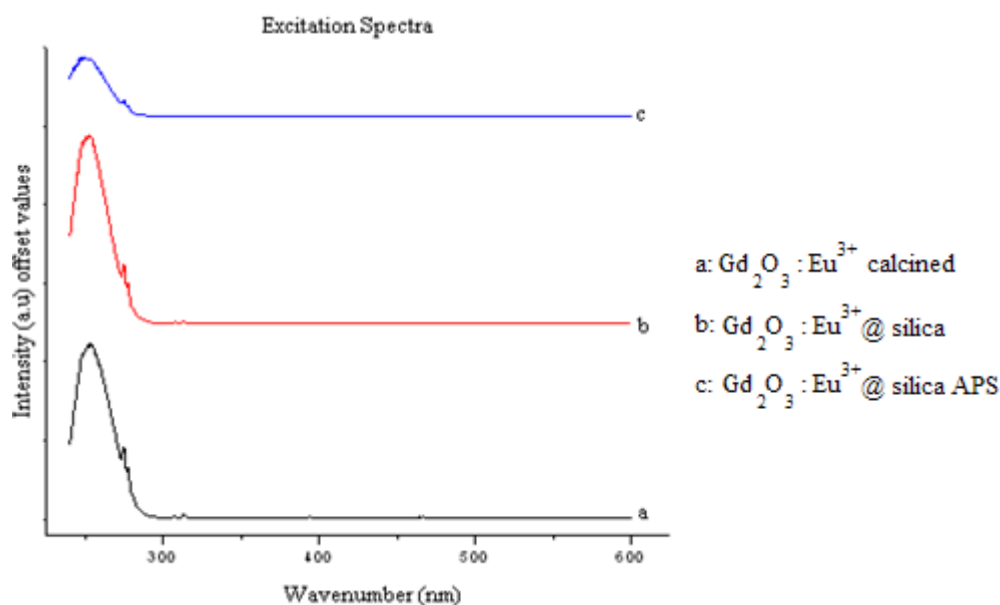


Figure 3.17: Excitation Spectra of Gd₂O₃:Eu³⁺, Gd₂O₃:Eu³⁺@SiO₂ and Gd₂O₃:Eu³⁺@SiO₂APS.

The same Eu³⁺ emission lines were observed in the spectra (refer figure 3.18) of Gd₂O₃:Eu³⁺ (a), Gd₂O₃:Eu³⁺@SiO₂ (b) and Gd₂O₃:Eu³⁺@SiO₂ APS (c) however, in (c) a reduction in signal was observed while (b) showed a slight enhancement in the signal intensity. The emission spectra exhibits the ⁵D₀→⁷F₀₋₄ transitions of the C₂ Eu³⁺ ions (no inversion centre) and the low-intensity magnetically allowed ⁵D₀→⁷F₁ transition, ascribed to the S₆ Eu³⁺ ions (with inversion centre, selection rules $\Delta J = 0, \pm 1$, thus $J=0 \rightarrow J=C$ is forbidden) [29].

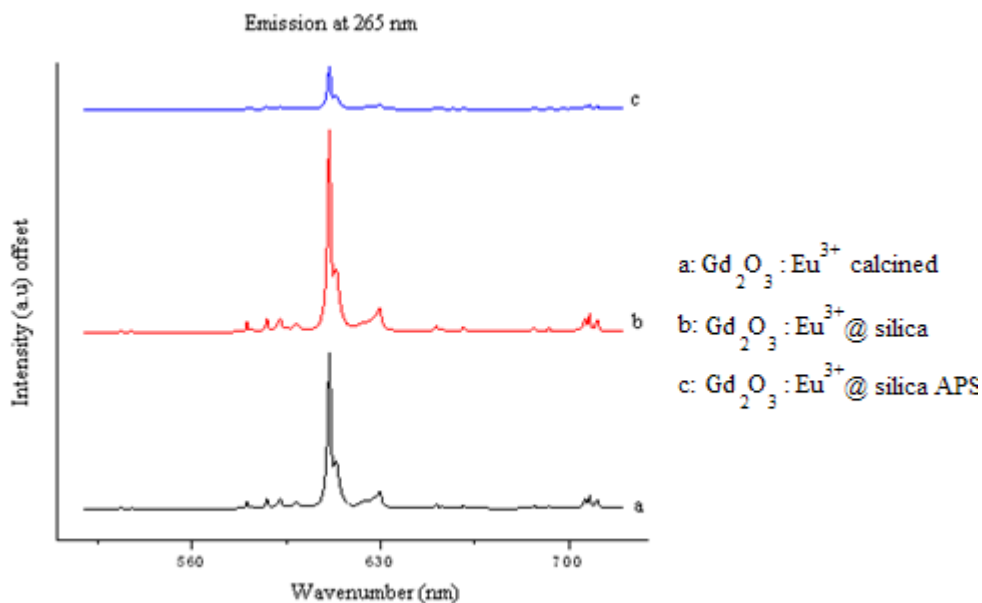


Figure 3.18: Emission Spectra of $Gd_2O_3:Eu^{3+}$, $Gd_2O_3:Eu^{3+} @SiO_2$ and $Gd_2O_3:Eu^{3+} @SiO_2APS$.

For the emission spectra at 300nm, upon closer observation an additional peak was observed at 630 nm for $Gd_2O_3:Eu^{3+} @SiO_2$ (b) and $Gd_2O_3:Eu^{3+} @SiO_2 APS$ (c). This could be due to a change in phase, resulting due to the wet process of silica encapsulation. This was further checked by XRD. Also a major decrease in signal intensity was witnessed for (b) and (c).

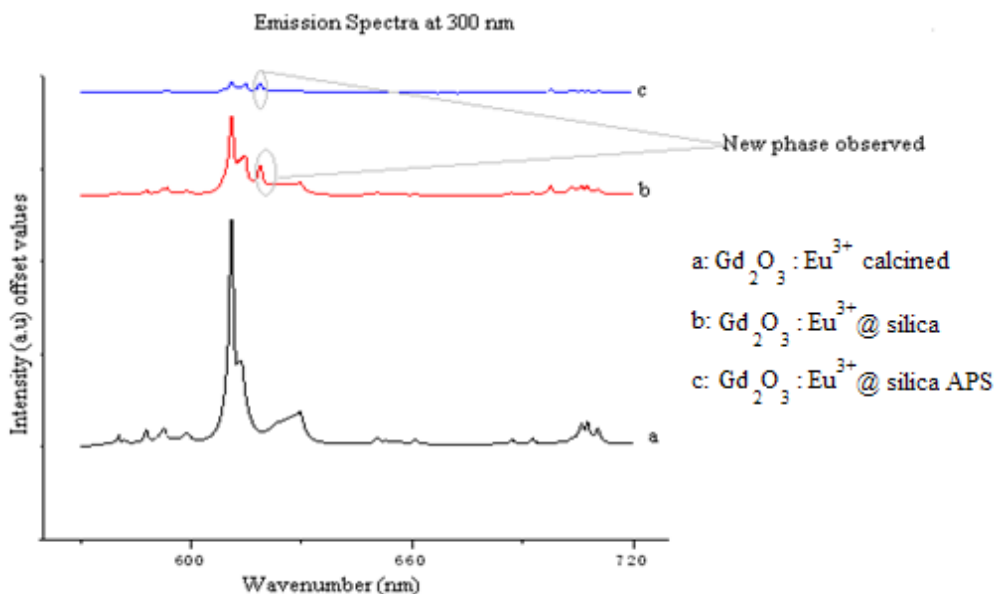


Figure 3.19: Emission Spectra of $Gd_2O_3:Eu^{3+}$, $Gd_2O_3:Eu^{3+} @SiO_2$ and $Gd_2O_3:Eu^{3+} @SiO_2APS$.

The XRD analysis was carried out on both Gd₂O₃:Eu³⁺ and Gd₂O₃:Eu³⁺@silica samples and the results obtained are shown in figure 3.20. From the diffractogram other than at position 2θ=43 no other characteristic change was observed. The variation at 2θ=43 is till unknown and should be looked into, however this does not prove any evidence of adequate phase change which could further shed light onto the reduction in signal intensity. Further investigation needs to be performed before drawing further conclusions.

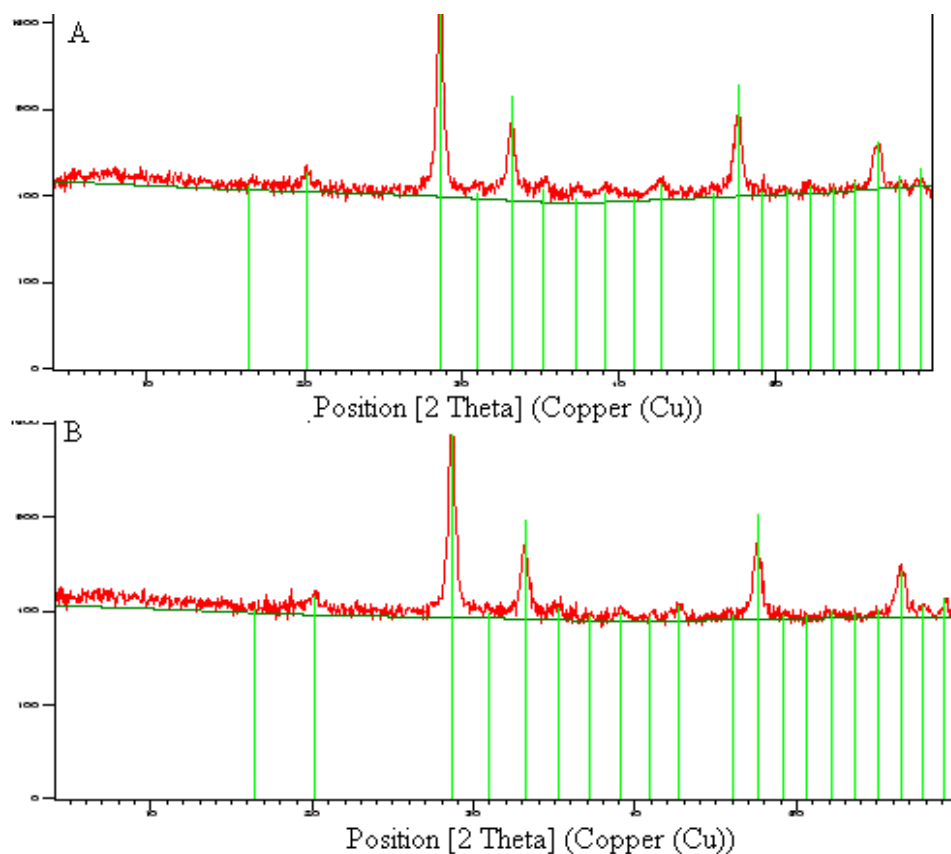


Figure 3.20(a,b): XRD analysis of of Gd₂O₃:Eu³⁺ (A) and Gd₂O₃:Eu³⁺@Silica (B).

The FTIR-ATR spectra for Gd₂O₃:Eu³⁺ (a), Gd₂O₃:Eu³⁺ calcined (b), Gd₂O₃:Eu³⁺@SiO₂ (c) and Gd₂O₃:Eu³⁺@SiO₂ APS (d) are shown in figure 3.21. All four spectra confirm the presence of Gd₂O₃:Eu³⁺ due to the bands at 336, 386 and 431 cm⁻¹ respectively. For the samples Gd₂O₃:Eu³⁺@SiO₂ (c) and Gd₂O₃:Eu³⁺@SiO₂ APS (d) the characteristic bands of silica were witnessed at 1110, 845 and 460 cm⁻¹. Upon magnification of the spectra (d) the band corresponding to the bending of N-H and Si-CH₂ bonds of APS were witnessed at 807 cm⁻¹ and at 1432 cm⁻¹. However bands corresponding to the stretching of N-H at 2600 cm⁻¹ were not observed and could be due to the overlap with the O-H stretching band at 2600 cm⁻¹ [17, 20, 21, 32].

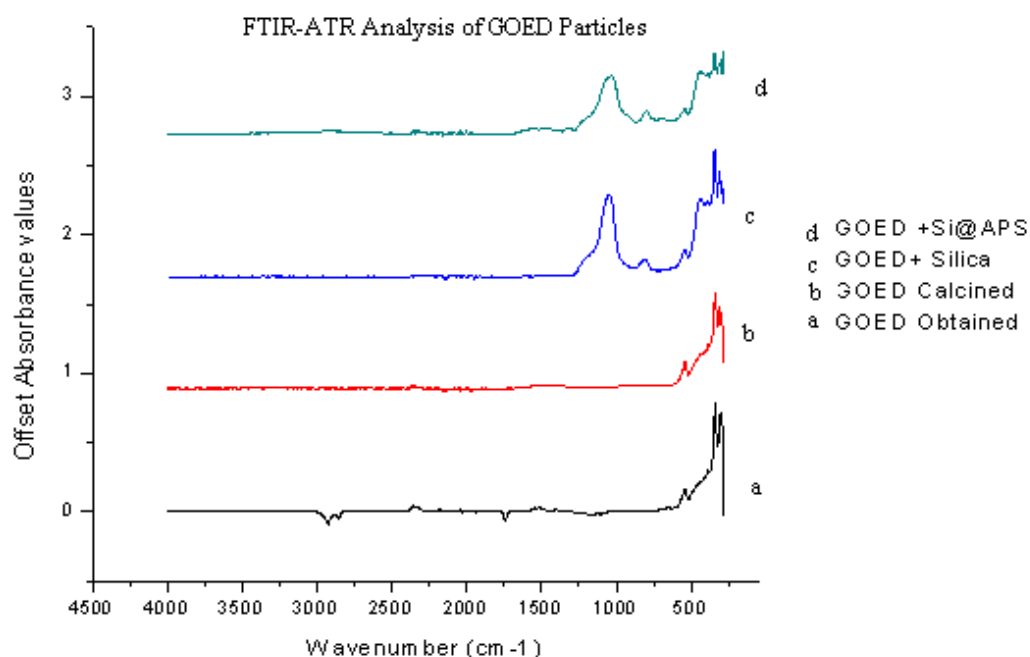


Figure 3.21: FTIR-ATR analysis of $\text{Gd}_2\text{O}_3:\text{Eu}^{3+}$, $\text{Gd}_2\text{O}_3:\text{Eu}^{3+}$ calcined, $\text{Gd}_2\text{O}_3:\text{Eu}^{3+}$ @Silica and $\text{Gd}_2\text{O}_3:\text{Eu}^{3+}$ @Silica APS.

Also solid state NMR could have been done in order to confirm the presence of APS but was neglected due to time constraints.

3.3 General Remarks and Conclusions

- Silica nanofillers both spheres (300 nm) and fibres were studied as models for the $\text{Gd}_2\text{O}_3:\text{Eu}^{3+}$ @silicaAPS nanocomposite formation.
- Major difficulties were incurred, during the preparation of Silica spheres 300nm particles, however upon incorporating the work of Pinto *et al.* [13], silica nanoparticles of the required dimensions were obtained. Silica fibres proved to be an even harder task, as the fibres obtained were delicate and ruptured upon touch. Also the complete removal of ammonium tartarate from the fibres was difficult.
- Surface modification of the silica nanoparticles with suitable silane coupling agents was performed to enhance its incorporation within the polymeric matrix.
- A study was performed in order to deduce the influence of thermal treatment on the silica surface, using techniques like SEM, FTIR-ATR and BET analysis, and we can concur that small changes did occur.

- Gd₂O₃:Eu³⁺ nanofillers obtained, were coated with silica and further functionalized with APS and this was confirmed by FTIR-ATR, PL and S-TEM. However, in some cases an uneven silica coating was observed, which could reduce the optical properties due to the presence of excess Gd-OH bonds (on the surface) [27]. Hence the silica encapsulation process needs to be further optimized.
- In the case of PL studies, for Gd₂O₃:Eu³⁺@silica small increments in the signal intensity was observed, however on functionalization with APS major reduction in the signal intensity was ascertained.
- Quantum yield studies need to be performed in order to find out the emission efficiency of the Gd₂O₃:Eu³⁺@silica (modified and unmodified) nanofillers.

3.4 Bibliography

1. Ebelmen, M., "Sur les combinaisons des acides borique et silicique avec les ethers". *Annales des Chimie et des Physique*, 1846, 16, 129.
2. Ebelmen, M., "Sur l'hyalite artificielle et l'hydrophane". *Les Comptes rendus de l'Académie des sciences*, 1847, 25, 854.
3. Leite C.A.P, Souza E.F, Galembeck F, "Core-and-Shell Nature of Stöber Silica Particles", *Journal Of The Brazilian Chemical Society*, 2001, 12.
4. Van Blaaderen A, Vrij A, "Synthesis and Characterization of Monodisperse Colloidal Organo-silica Spheres". *Journal of Colloid and Interface Science*, 1993, 156, 1, 1-18.
5. Stöber, W, Fink A, Bohn E, "Controlled growth of monodisperse silica spheres in the micron size range", *Journal of Colloid and Interface Science*, 1968, 26, 62-69.
6. Nakamura H, Matsui Y, "Silica Gel Nanotubes Obtained by the Sol-Gel Method", *Journal of the American Chemical Society*, 1995, 117, 9, 2651-2652.
7. Sanchez C, Soler-Illia G.J.A.A, Ribot F, Grosso D, "Design of functional nano-structured materials through the use of controlled hybrid organic-inorganic interfaces", *Comptes Rendus Chimie*, 2003, 6, 8-10, 1131-1151.
8. Chen H, Gu G, Wu L, "Study on modification and dispersion of nano-silica", *Journal of dispersion science and technology* 2005, 26, 27-37.
9. Zou H, Wu S, Shen J, "Polymer/Silica Nanocomposites: Preparation, Characterization, Properties, and Applications", *Chemical Reviews*, 2008, 108, 9, 3893-3957.
10. Mark J.E, Allcock H.R, West R, "Inorganic polymers", New York: Oxford University Press, 2005.
11. Nozawa K, Gailhanou H, Raison L, Panizza P, Ushiki H, Sellier E, Delville J. P , Delville M. H, "Smart Control of Monodisperse Stober Silica Particles: Effect of Reactan Addition Rate on Growth Process", *Langmuir*, 2004, 21, 4, 1516-1523.
12. Park S.K, Kim K.D, Kim H.T, "Preparation of silica nanoparticles: determination of the optimal synthesis conditions for small and uniform particles. *Colloids and Surfaces A*", *Physicochemical and Engineering Aspects*, 2002, 197, 1-3, 7-17.
13. Pinto J.B, Marques P.A.A.P, Timmons A.B, Trindade T, Neto C, "SiO₂/cellulose nanocomposites obtained by in situ synthesis and via polyelectrolytes assembly", *Composites Science and Technology*, 2008, 68, 1088-1093.
14. Esteves A.C.C, Timmons A.B, Trindade T, "Nanocompósitos de matriz polimérica:

- estratégias de síntese de materiais híbridos”, *Química Nova*, 2004, 27, 798-806.
15. Iler, R.K., “The Chemistry of Silica: Solubility, Polymerization, Colloid and Surface Properties and Biochemistry”. 1979, New York: Chichester: John Wiley. & Sons.
 16. Özcan M, Matinlinna J.P, Vallittu P.K, Huysmans M.C, “Effect of drying time of 3-methacryloxypropyltrimethoxysilane on the shear bond strength of a composite resin to silica-coated base/noble alloys”, *Dental Materials*, 2004, 20, 6, 586-590.
 17. Vrancken K.C, Possemiers K, Van Der Voort P, Vasanth E, “Surface Modification of silica gels with amino-organo silanes”, *Colloids and Surfaces A: A Physicochemical and Engineering Aspect*, 1995, 10, 492-499.
 18. Miyaji F, Davis S.A, Charmant J.P.H, Mann S, “Organic Crystal Templating of Hollow Silica Fibers”, *Chemistry of Materials*, 1999, 11, 11, 3021-3024.
 19. Silverstein R.M, G.C.B., “Spectrometric Identification of Organic Compounds”, 2 ed. 1967 New York-London-Sydney: John Wiley and Sons.
 20. Foschiera J.L, Pizzolato T.M, Benvenuti E.V, “FTIR Thermal Analysis on Organofunctionalized Silica Gel”, *Journal of the Brazilian Chemical Society*, 2001, 12, 159-164.
 21. Bourgeat-Lami E, Lang J, “Encapsulation of Inorganic Particles by Dispersion Polymerization in Polar Media: Silica Nanoparticles Encapsulated by Polystyrene”, *Journal of Colloid and Interface Science*, 1998, 197, 2, 293-308.
 22. Olivera F.C, PhD Thesis “Preparation and Characterization of Novel Nanocomposites of Inorganic/Polysaccharide Type”, University of Aveiro, Department of Chemistry July, 2010.
 23. Fang Y.P, Xu A.W, You L.P, Song R.Q, Yu J. C, Zhang H. X, Li Q, Liu H. Q, “Hydrothermal Synthesis of Rare Earth (Tb, Y) Hydroxide and Oxide Nanotubes”, *Advanced Functional Materials*, 2003, 13, 955.
 24. Qun T, Jianmin S, Wenjia Z, Wu Z, Weichao Y, Yitai Q, “Preparation, characterization and optical properties of terbium oxide nanotubes”, *Journal of Material Chemistry*, 2003, 13, 3103.
 25. Yada M, Mihara M, Mouri S, Kuroki M, Kijima T, “Rare Earth (Er, Tm, Yb, Lu) Oxide Nanotubes Templated by Dodecylsulfate Assemblies”, *Advanced Materials*, 2002, 14, 309.
 26. Yada M, Taniguchi C, Torikai T, Watari T, Furuta S, Katsuki H, “Hierarchical Two- and Three-Dimensional Microstructures Composed of Rare-Earth Compound Nanotubes”, *Advanced Materials*, 2004, 16, 1448.

27. Wong K.L, Law G.L, Murphy M.B, Tanner P.A, Wong W.T, Lam P.S.K, "Functionalized Europium Nanorods for In Vitro Imaging", *Inorganic Chemistry*, 2008, 47, 5190.
28. Söderlind F, Pedersen H, Petoral R.M, Käll P.O, Ovdal, "Synthesis and characterisation of Gd₂O₃ nanocrystals functionalised by organic acids", *Journal of Colloid and Interface Science*, 2005, 288, 140 .
29. Macedo A.G, Martins M.A, Fernandes S.E.M, Timmons A.B, Trindade T, Rocha J, "Luminescent SiO₂-coated Gd₂O₃:Eu³⁺ nanorods /poly (styrene) nanocomposites by in situ polymerization", *Optical Materials*, 2010, 32, 1622–1628.
30. Liu L, Ma E, Li R, Liu G, Chen X, "Effects of phonon confinement on the luminescence dynamics of Eu³⁺ in Gd₂O₃ nanotubes", *Nanotech*, 2007, 18, 015403.
31. Buijs M, Meyerink A, Blasse G, "Energy transfer between Eu³⁺ ions in a lattice with two different crystallographic sites: Y₂O₃:Eu³⁺, Gd₂O₃:Eu³⁺ and Eu₂O₃", *Journal of Luminescence*, 1987, 37, 9.
32. Hunt R.B, Pappalardo R.G, "Fast excited-state relaxation of Eu-Eu pairs in commercial Y₂O₃: Eu³⁺ phosphors", *Journal of Luminescence*, 1985, 34, 133.

Chapter 4

Synthesis and Characterization of Nanocomposites

Preface:

The formation and the characterization efforts undertaken for both silica and Gd₂O₃: Eu³⁺@silica nanocomposites are reported here. The bifocal polymerization method was further expanded in the preparation of nanocomposites (as mentioned previously) and both solution and emulsion process conditions were deployed. The nanocomposites formed were characterized by FTIR-ATR, SEM, S-TEM, PL, and DSC analysis. From SEM and FTIR-ATR we can affirm the successful synthesis of nanocomposites. The PL studies of the Gd₂O₃:Eu³⁺@silica APS nanocomposite, showed a huge drop in the signal intensity.

4.1 General Introduction

As mentioned antecedently, the availability of different types of nanocomposite materials is numerous but in this chapter the organic-inorganic type nanocomposites are discussed [1,2]. These materials are typecasted as one which contains both an inorganic and an organic phase, wherein one of the phases constitutes a nanometric dimension. They possess, the properties of both the inorganic and organic parts i.e., rigidity, thermal stability ascertained from the inorganic segment while flexibility, ductility, processability from the organic part [2]. When nanocomposites are prepared via in-situ polymerization, an increase in the interfacial area is observed which conversely results in the formation of significant amounts of interfacial polymer whose properties are distinct from the bulk. The inorganic fillers could be semiconductors viz., PbS, Cds, metals viz., Au, Ag, metal oxide viz., SiO₂, TiO₂ etc [2]. Nevertheless the most influential filler material which has amassed the attention of both academia and industry is SiO₂ nanoparticles [2,3].

In 1989, attempts at encapsulating inorganic nanofillers with polymers were carried out in emulsion by Caris *et al.* [4-7], where they studied the encapsulation of TiO₂ with methyl methacrylate (MMA). Their research, proved useful in the paint industry where the uniform distribution of pigment in the matrix is a necessity. Other fillers materials viz., talc, mica, barytes have been investigated by Yamaguchi *et al.* [8,9], Hasegawa *et al.* [10,11] and Haga *et al.*[12,13] and they employed the surfactant free emulsion polymerization process mode. The early encapsulation of functionalized silica was carried out by Hergeth *et al.* [14,15] and Furusawa *et al.* [16] and the

composites formed displayed noteworthy increases in the mechanical properties when the polymer was covalently bounded to the silica using silane coupling agents. These experiments were elaborated upon by Bourgeat-Lami *et al.* [3] who encapsulated silica particles using the dispersion polymerization of styrene in an aqueous ethanol medium with poly (N vinyl pyrrolidone) as a stabilizer, and they were able to obtain nanocomposites with good size distribution and morphology. Since then (1988-present day) many researchers have tried to synthesize silica nanocomposites making use of mini-emulsion and emulsion process conditions via Living and Controlled polymerization mechanisms, however most of these techniques employ surfactants to help in the stabilization of the nanocomposites formed, but which is detrimental to the formation of thin films as they play a role in phase separation.

To overcome this difficulty Ali *et al.*[17] synthesized anisotropic polymer-inorganic composite latexes with good control of the platelet orientation of Gibbsite nanoparticles with high encapsulation efficiency using emulsion based feed-monomer encapsulation techniques via RAFT. Also lately RAFT polymerization utilized in the formation of core-shell hybrid formation was delineated by Daigle *et al.* [18] wherein a bifocal method was utilized, firstly the inorganic nanofiller was dispersed in poly (acrylic acid) (PAA) via RAFT polymerization and then radically copolymerized using a hydrophobic monomer (BuA) in emulsion conditions. They employed a wide range of filler materials like metal oxides (alumina, barium, copper oxide etc), metals (zinc, molybdenum) and inorganic nitrides.

In this study, the works of Daigle *et al.* [18], Ali *et al.* [17] and Bourgeat-Lami *et al.* [3] were furthered and we sought to synthesize nanocomposites in an acrylate system (PAA-PBuA) via the RAFT process incorporating both solution and emulsion process conditions. Initial attempts were carried out on silica spheres and then expanded to include silica fibres as they closely resembled the surface morphology of the $Gd_2O_3:Eu^{3+}$ nanofillers. Finally an attempt at preparing $Gd_2O_3:Eu^{3+}$ @silica nanofillers were performed and the results were documented. The nanocomposites formed were characterized using standard techniques like FTIR-ATR, SEM, S-TEM, PL and DSC analysis. Films were prepared by spin coating to better study the surface morphology, anisotropy and the interface (inorganic/inorganic) characteristics.

There are different synthetic routes that can be pursued while preparing nanocomposites, some

more advantageous than the rest. When silica nanocomposites are concerned the three general approaches are

- sol-gel
- blending
- in situ polymerization

These strategies can be used separately or could be combined as shown in the figure 4.1

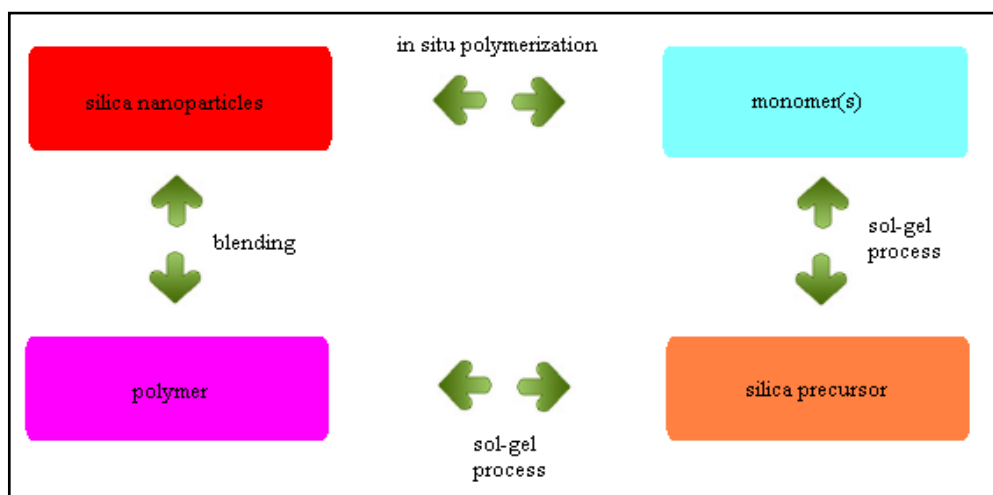


Figure 4.1 Methods of Producing Silica Nanocomposites reproduced from [2].

For the sake of simplicity, in this chapter silica nanocomposites (models) will first be accounted for followed by Gd₂O₃:Eu³⁺ @silica nanocomposites.

4.2 Silica Nanocomposites Preparation

In our studies, we applied the **sol-gel** and **in situ polymerization** methods. The silica nanoparticles both spheres and fibres were synthesized using an extension of the sol-gel technique [19,20] as described in Chapter 3, making use of TEOS as precursor. Furthermore, additional efforts were taken to functionalize the surface of the silica nanofillers, with suitable coupling agents like MPS and APS. Initially on a purely experimental basis, silica nanospheres functionalized with MPS were employed in the preparation of nanocomposites, however adept affinity between the filler surface and polymer matrix was unavailable and loss in colloidal stability were observed. Thus MPS was disregarded and attempts with APS were considered as they showed better affinity due to the presence of the amine group. In our series of experiments both bear and APS surface modified silica were used in-order to reaffirm and build a case for surface functionalization.

Silica nanofillers (5g/kg of initial monomer), macroRAFT agent (80% conversion), ethanol (or water) and initiator were allowed to react in both emulsion and solution conditions as delineated in Chapter 2. For experiments performed in solution evidence of stability was incurred while those performed under emulsion demonstrated a loss in colloidal stability and phase separated within a matter of hours. A list, of the attempts assayed is detailed in the tabular column 4.1.

Tabular Column 4.1: Silica nanocomposite formation attempts

Sample	Process Conditions	Functionalization	MacroRAFT agent	Hydrophobic Monomer	Status
Spheres	Solution	bear	PAATTC (80%)	BuA	success
		APS	PAATTC (80%)	BuA	success
	Emulsion	bear	PAATTC (80%)	BuA	Not performed
		APS	PAATTC (80%)	BuA	success
Fibers	Solution	bear	PAATTC (80%)	BuA	success
		APS	PAATTC (80%)	BuA	success
	Emulsion	bear	PAATTC (80%)	BuA	Not performed
		APS	PAATTC (80%)	BuA	Not performed

Emulsion attempts both with bear and APS modified silica fibers were not carried out due to time constraints and due to the unavailability of an optimized process condition.

4.2.1 Silica Nanocomposites Characterization

Blank silica trials as well as silica@APS trials were carried out in an acrylate system i.e., P(AA co BuA) TTC-(80%). When blank or unmodified silica was used, it was noticed that the silica was not thoroughly incorporated within the matrix. This is due to the fact that unmodified silica possesses a negative charge while the matrix also possesses a negative charge hence very weak electrostatic repulsion was observed. However, when the silica particles were modified with suitable coupling agents i.e., APS a positive surface charge was observed and consequently better affinity between the polymeric system and silica filler was noticed refer figure 4.2.

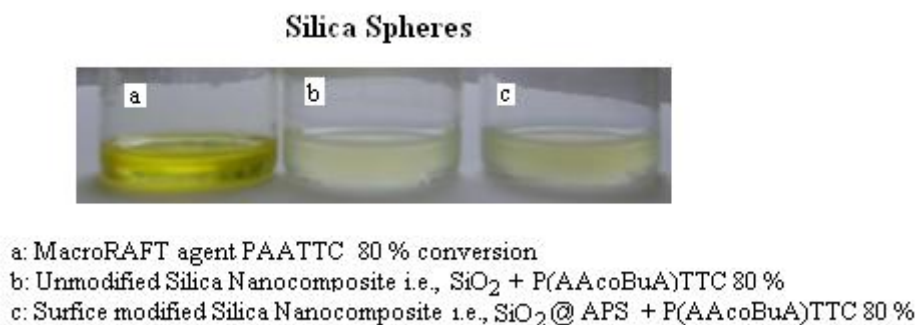
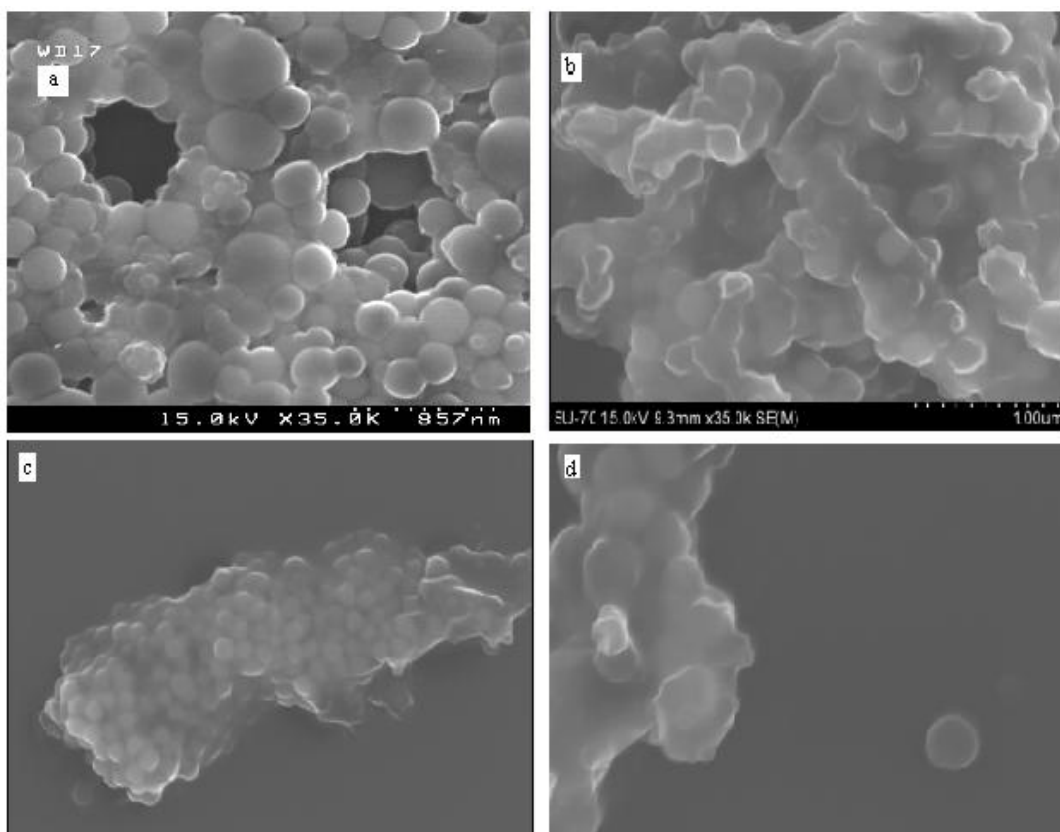


Figure 4.2: Snapshot of Silica (spheres) nanocomposites in a solution of ethanol.

From figure 4.2 (b) we notice that the unmodified silica nanocomposites solution appear to be visually opaque, which affirms that the nanoparticles were not well dispersed within the matrix. If the system is left untouched the unmodified silica begins to settle down at the bottom of the glass vile instantaneously. In the case of modified silica particles (c) the system appears to be more clear and transparent (almost similar to (a)) which proves that an even dispersion of silica particles within the polymer matrix is obtained. However as the nanocomposite was prepared via the solution technique precipitation did occur after 3-4 hours.

These modified silica spheres (300 nm) nanocomposite samples were analyzed by SEM, refer figure 4.3. The nanocomposites prepared in both emulsion and solution conditions were analyzed. The experiment performed in emulsion conditions is represented in figure 4.3 (a) and this shows 300 nm silica filler completely surrounded by spherical polymeric particles of sizes 50-500 nm, thereby proving that that spherical nanocomposites were prepared in an acrylate polymeric medium but system control was not attained due to the presence of free polymer. Figure 4.3 (b, c, d) are images of a nanocomposite prepared under solution conditions. Figure 4.3 (b) is a magnified image of the silica (si-300 nm) nanocomposite, figure 4.3 (c) is an overview of the nanocomposite, wherein silica clusters surrounded by a polymer coat can be witnessed, and figure 4.3 (d) is an image of an isolated silica particle within the polymeric matrix , thereby suggesting that further improvements are required to improve the adsorption of PAATTC on the surface of the filler before the copolymerization with BuA, in order to have better affinity with the polymeric matrix.



a: Silica/APS @ P(AAcoBuA)TTC 80 % in emulsion (Silica particles surrounded by spherical polymer)
 b: Silica/APS @ P(AAcoBuA)TTC 80 % in solution (Overview)
 c: Silica/APS @ P(AAcoBuA)TTC 80 % in solution (Nanoparticle cluster coated with polymer)
 d: Silica/APS @ P(AAcoBuA)TTC 80 % in solution (lone silica particle disjoint from matrix)

Figure 4.3: SEM Imagery of Silica (300nm spheres) Nanocomposites in solution and emulsion.

The ensuing nanocomposite was characterized by FTIR-ATR and the corresponding spectrum was obtained refer fig 4.4.

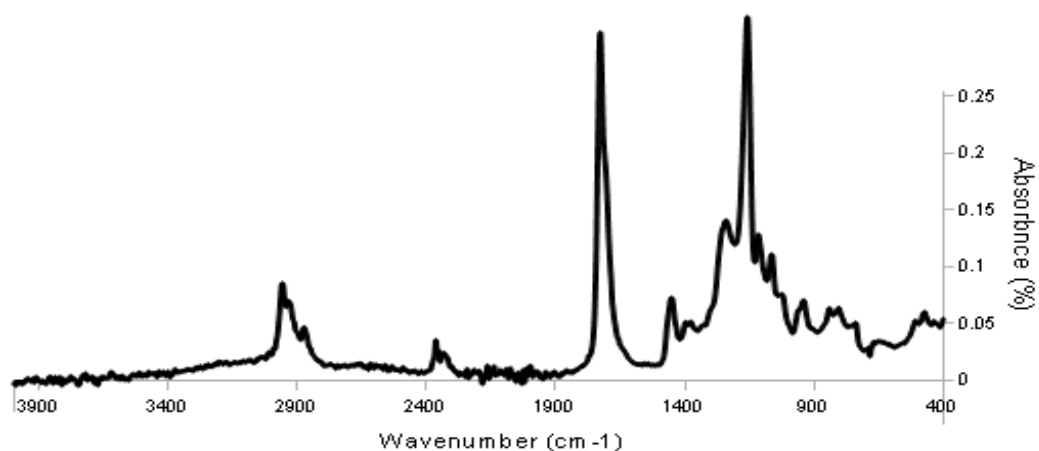


Figure 4.4: FTIR-ATR spectra of silica@APS nanocomposites (spheres).

The absorption band corresponding to the C=O stretching was noticed at 1700 cm⁻¹. Bands at 1238 cm⁻¹ and 1167 cm⁻¹ correspond to the C-O stretching. The band at 3000-3500 cm⁻¹ is attributed to the O-H stretching vibration of the PAA dimers which is a characteristic of carboxylic acids; the stretching vibration of the C-H band is witnessed at 2900 cm⁻¹. The band at 2961 cm⁻¹ corresponds to the aliphatic chain of poly butyl acrylate and the low frequency bands at 1466 and 1375 cm⁻¹ are characteristic of the methyl group present in butyl acrylate. The band at 1432 cm⁻¹ corresponds to the Si-CH₂ bending and the bands at 807 cm⁻¹ corresponds to the bending (δ) of N-H. From the spectrum the bands corresponding to the elongation of the C-H bond in CH₃ and the N-H bond in NH₂ were not observed (at 2600 cm⁻¹ and 3000cm⁻¹), this could be due to the overlap with the bandwidth corresponding to the enormous stretching band of the hydroxyl group. The remaining bands are attributed to TTC-A and the silica.

DSC analysis was performed on our nanocomposite and these results were compared to the original polymerization results, refer tabular column 4.2.

Tabular Column 4:2 DSC results of silica spheres nanocomposites.

Sample	T _{g1} (°C)	T _{g2} (°C)
P(AA co BuA) (80%)	-51.46	25.98
P(AAcoBuA) 80% + silica@APS spheres nanocomposite (trial 2)	-50.79	62.23

From the results obtained we conclude that T_{g1} values for both the samples were almost similar while T_{g2} values showed differences of up to 40°C or so. This could be due to a variety of reasons like presence of moisture and/or impurities; thermal-mechanical history of the system was not taken into notice etc.

DMA analysis was also considered and nanocomposite films were prepared by two different methods **a) Film casting** and **b) Spin Coating** on a glass slide. A complete description of both these methods is detailed in §5.6. The films obtained were too thin and gluey and ruptured easily upon peeling. Taking this into account DMA was not performed at this time.

The films formed were analyzed via SEM and from figure 4.5(a) silica nanofiller clusters encapsulated within a polymeric matrix were witnessed. The figure 4.5(b) is a magnified image of the nanocomposites and the figure 4.5 (c) shows the general distribution of the nanofillers within

the matrix. From 4.5 (c), we notice that an uneven particle distribution is prevalent and some regions have a higher filler density than the others.

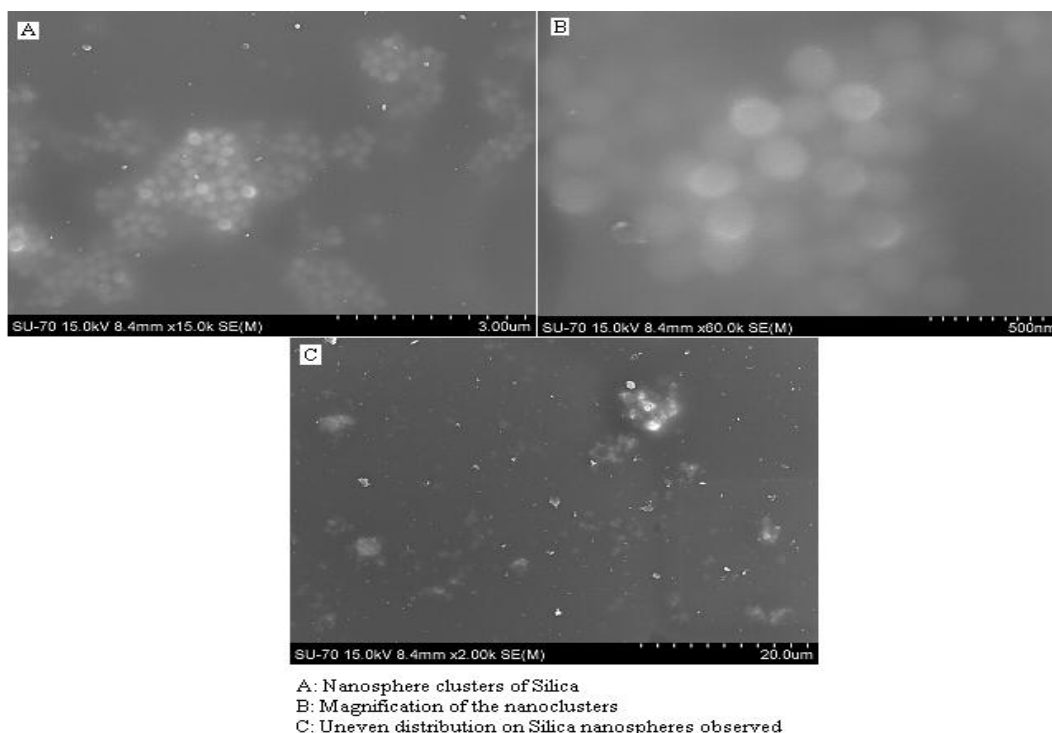


Figure 4.5: SEM Imagery of Silica@APS Nanocomposites (spheres) thin films.

Silica fibre nanocomposites were prepared as they closely resemble $Gd_2O_3:Eu^{3+}$ @silica nanofillers. When modified and unmodified silica fiber nanocomposites were visually compared it was noticed that the unmodified silica nanocomposites were more optically opaque than the one with functionality. This goes to show that functionality enhances the affinity between the polymeric matrix and the filler material. Also better dispersion is observed in the case of modified silica (hence the relative transparent characteristic). This is shown in figure 4.6.

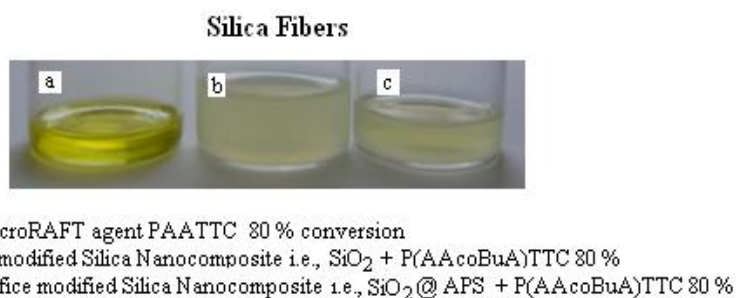


Figure 4.6: Snapshot of Silica (fibres) nanocomposites in solution.

SEM analysis was performed on the modified silica fibre nanocomposite.

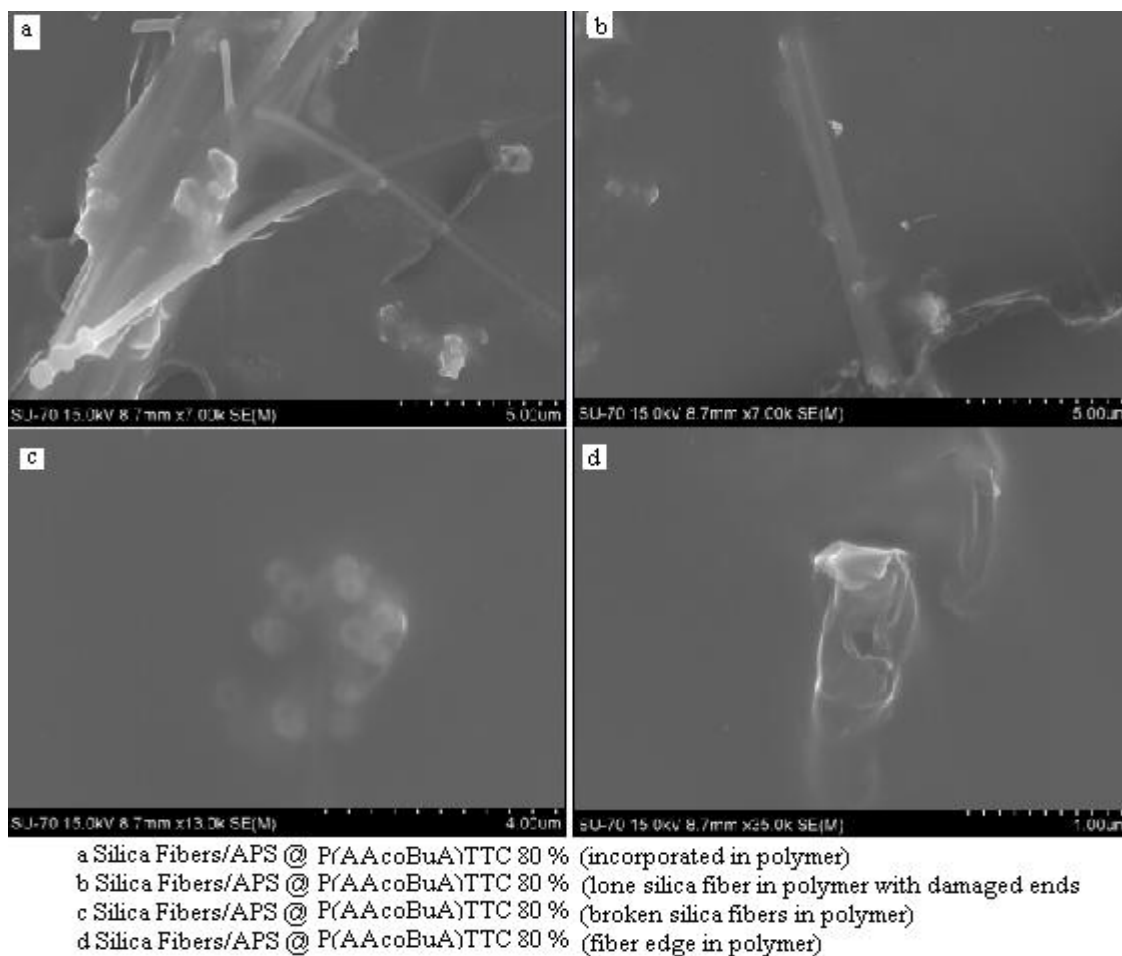


Figure 4.7: SEM Imagery of Silica@APS Nanocomposites (fibres).

From figure 4.7 (a) we can notice a cluster of fibers within a polymer matrix. However most of the fibres did not retain their original lengths, this could be due to the mechanical agitation that was used during the preparation of nanocomposites, and hence an alternate method of stirring needs to be sought after and deployed. Figure 4.7 (a, b, c) shows broken silica fibers within a polymer matrix, which possessed lengths of 50 nm and these were analyzed by EDS refer figure 4.8 to affirm the presence of silica, and a strong signal was detected. However, this could affect the anisotropy of our nanocomposites, as the silica fibers now possess unequal lengths and dimensions and which could affect the mechanical properties, hence DMA needs to be performed in order to draw out more conclusions. Figure 4.7 (d) shows an edge of the silica fiber embedded in the polymer.

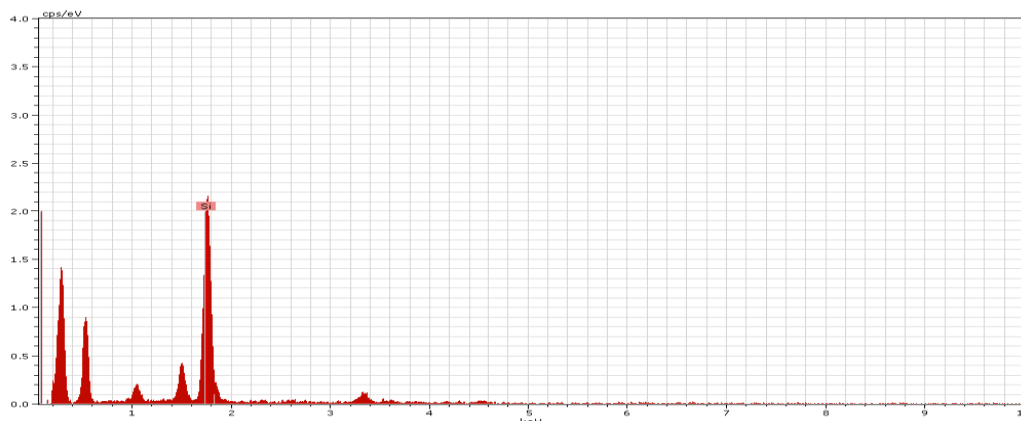


Figure 4.8: EDS of silica fibre nanocomposites in solution.

DSC analysis was carried out in this case for both bear and silica @ APS fibre nanocomposites, and the results were compared to the original polymer.

Tabular Column 4:3 DSC results of silica fibre nanocomposites.

Sample	Tg ₁ (°C)	Tg ₂ (°C)
P(AAcoBuA) TTC (80%)	-51.46	25.98
P(AAcoBuA) TTC (80%) + silica fibers nanocomposite	-51.71	61.43
P(AAcoBuA) TTC (80%) + silica@APS fiber nanocomposite	-	33.63

For the modified fibre nanocomposites, only one Tg was observed while for unmodified nanocomposites the presence of two Tgs were witnessed thereby deviating from the conventional behavior. The reason behind this phenomenon is still unknown and further investigative probes are being carried out. DMA was also considered, but was not performed due to the disintegration of the film.

FTIR-ATR analyses were performed and the results are shown in Annex 2e as they are almost similar to the silica spheres with minor exceptions.

Thin films were prepared by spin coating and these were analyzed by SEM to assert whether any preferential orientation of the fibers was obtained. From the figure 4.9 (a, b, c) we can confirm the presence of fillers within a polymeric matrix. However the silica fibres were further reduced in lengths and due to the spin maneuver, cluster of the spherical particles and broken fiber pieces were observed. Some fibres which retained their original length coated in polymer were also witnessed. From the above results we can prove that silica nanocomposites were formed but to know more

about them further analysis like TEM, AFM, DMA and TGA needs to be performed.

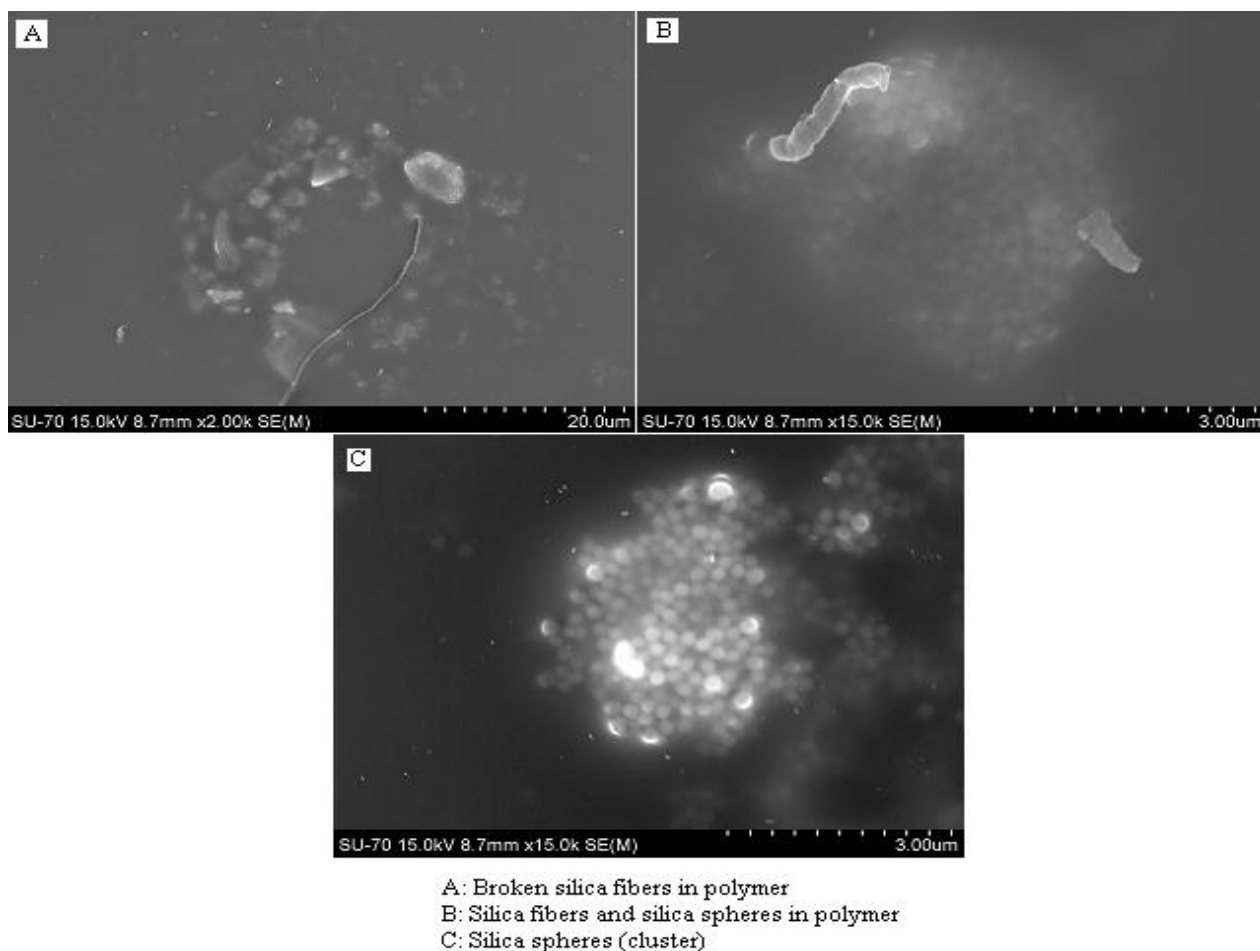


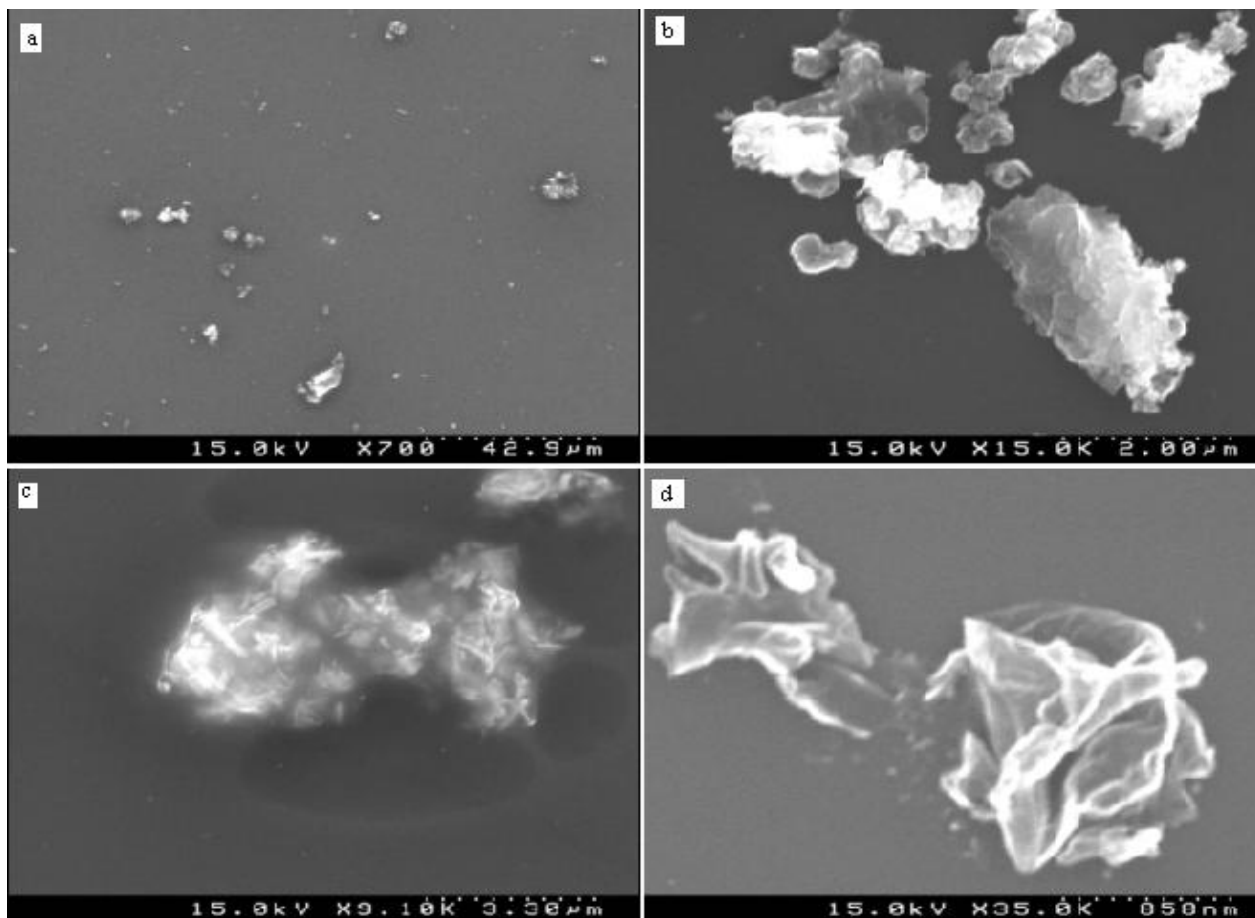
Figure 4.9: SEM imagery of silica@APS nanocomposites (fibres) thin films.

4.3 Gd₂O₃:Eu³⁺@ Silica Nanocomposites Preparation and Characterization

Following a similar procedure used in the preparation of silica sphere/fibre nanocomposites, Gd₂O₃:Eu³⁺@Silica nanocomposites were obtained. For the complete synthetic route refer § 5.5.

The sample obtained was analyzed by SEM. The results are shown in figure 4.10 (a, b, c, d). From the figure 4.10 (a) an uneven distribution of filler material within the matrix was witnessed. From figure 4.10 (b) Gd₂O₃:Eu³⁺@silicaAPS nanofibers coated with polymer was witnessed thereby confirming the formation of the nanocomposite. The image 4.10 (c) shows the orientation of the nanorods within the polymeric matrix. From the results we notice that anisotropic nanocomposites

were not obtained as the rods are embedded within the matrix randomly. Figure 4.10 (d) is a magnification of the nanocomposites formed.



a: Overall distribution of GOED @silicaAPS nanocomposites
b: GOED@silicaAPS nanocomposites
c: Non uniform orientation of GOED@silicaAPS rods/fibers within the matrix
d: Magnification of the GOED@silicaAPS rods/fibers within the matrix

Figure 4.10 SEM images of $Gd_2O_3:Eu^{3+}@silica$ nanocomposites.

The FTIR-ATR studies were performed on the sample and the results are detailed in Annex 2 f

DSC analyses were performed on the sample and the results were compared to the results of the silica fibre nanocomposites both modified, bear and the original polymer results as seen in tabular column 4.4.

Tabular column 4.4 DSC analysis of Gd₂O₃:Eu³⁺@silica APS nanocomposites.

Sample	Tg 1 °C	Tg 2 °C
P (AAcoBuA)TTC (80%)	-51.46	25.98
P (AAcoBuA)TTC (80%) + silica fibers nanocomposite	-51.71	61.43
P (AAcoBuA)TTC (80%) + silica@APS fibers nanocomposite	-	33.63
P (AAcoBuA)TTC (80%) + Gd ₂ O ₃ :Eu ³⁺ @silica APS nanocomposites	-50.39	59.45

The results obtained were similar to the copolymer and the non functionalized silica fibre nanocomposites (as they possessed two Tg values) rather than the functionalized silica fibre nanocomposites. The reason for this is still unknown and further investigation is needed to better understand this behavior.

Films were prepared via spin coating and SEM was performed on the sample, refer figure 4.11

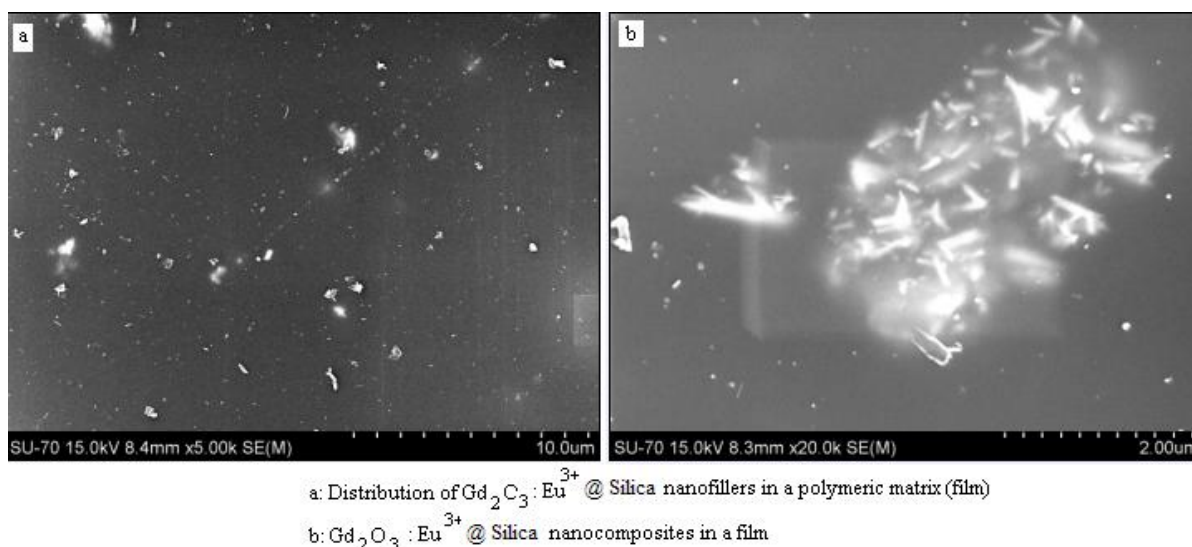


Figure 4.11 SEM images of Gd₂O₃:Eu³⁺@silica nanocomposites (thin films).

Figure 4.11 (a) gives the distribution of the fillers within the matrix and an uneven deposition of fillers (within the matrix) was observed. Figure 4.11 (b) is a magnification of the nanocomposite formed. From this the direction of the orientation of the fibres can be ascertained. Since the films were prepared by spin coating, optimum results were not obtained and further methods like capillary extrusion should be considered to prepare anisotropic particles.

The PL studies were also performed on the sample and the emission spectra at both 265 nm and 300

nm were obtained as in [21, 22]. The figure 4.12 is the emission spectrum of the $Gd_2O_3:Eu^{3+}@silicaAPS$ nanocomposites at 300 nm. When compared with the spectra obtained for the filler material alone, a decrease in the intensity of the peak was observed.

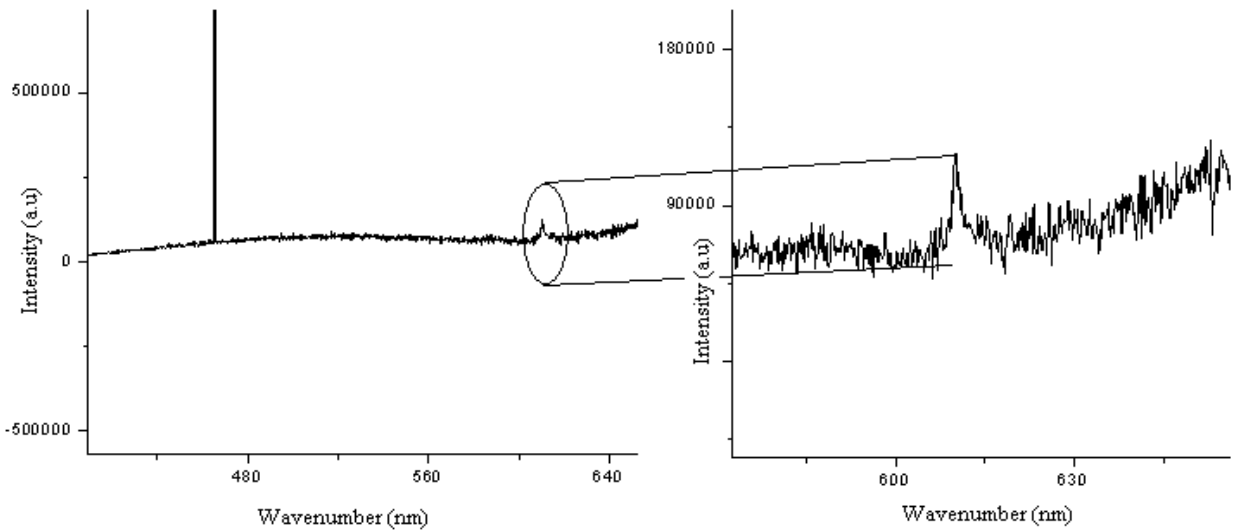


Figure 4.12 Emission spectrum of $Gd_2O_3:Eu^{3+}@silicaAPS$ nanocomposites at 300 nm.

The emission spectrum at 265 nm is shown in figure 4.13

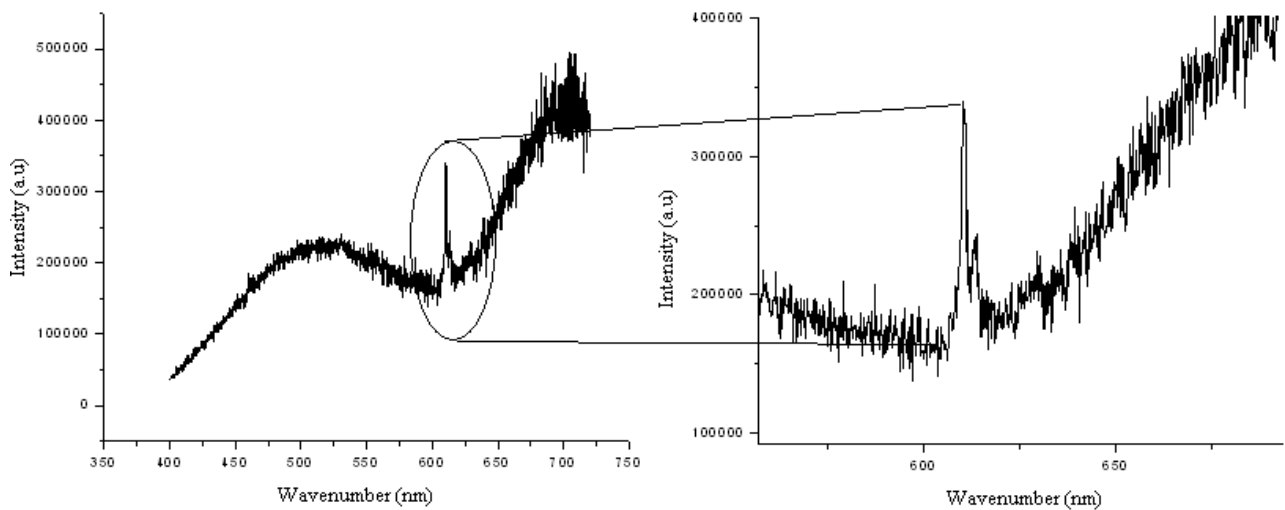


Figure 4.13 Emission spectrum of $Gd_2O_3:Eu^{3+}@silicaAPS$ nanocomposites at 265 nm.

Signals were observed but with a decrease in intensity, which could be due to a lot of factors i.e., leaching of europium, small concentration of fillers within the nanocomposite, extremely thin film,

quenching etc. The excitation spectra could not be obtained due to low intensities. Quantum Yield studies needs to be performed in order to find the emission efficiency at 256 and 300 nm respectively and compare it with that of the fillers.

4.4 General Remarks and Conclusions

- Silica nanocomposites (both spheres (300 nm) and fibres) and Gd₂O₃:Eu³⁺@silica nanocomposites were prepared successfully as deduced by SEM and FTIR-ATR analysis.
- Despite adequate surface modification with APS unequal distribution of filler material within the matrix was observed in all three cases. These results highlight the need for further efforts mainly in the polymerization processes. The results of Silica (300 nm) nanocomposites in emulsion were promising and the process needs to be explored further.
- The film preparation also needs to be optimized and other methods like extrusion etc., needs to be considered in order to obtain directionally dependent nanocomposites.
- DSC results were carried out and the T_g values were obtained. In the case of silica@APS fibres an abnormality was observed i.e., the presence of one T_g instead of two. The reason for this is still unknown and the experiment needs to be repeated.
- In the case of Gd₂O₃:Eu³⁺@ silica nanocomposites, the PL studies show a further reduction in signal intensity. This could be due to inadequate sample preparation, hence the nanocomposite and PL sample formation method needs to be optimized before any further hypotheses are ascertained.
- Quantum Yield studies need to be performed.

4.5 Bibliography

1. Mai Y.W, Yu Z.Z, "Polymer Nanocomposite", Woodhead publishing Limited, 2007, ISBN 978-1-85573-969-7.
2. Zou H, Wu S, "Polymer/Silica Nanocomposites: Preparation, Characterization, Properties, and Applications", Chemical Review, 2008, 108, 9, 3893-3957.
3. Bourgeat-Lami E, Lang J, "Encapsulation of Inorganic Particles by Dispersion Polymerization in Polar Media: 1. Silica Nanoparticles Encapsulated by Polystyrene", Journal of Colloid and Interface Science, 1998, 197, 2, 293-308.
4. Caris C.H.M, van Herk A.M, German A.L, in "XXth Fatipec, Conference Book", 1990, 325.
5. Caris C.H.M, van Elven L.P.M, van Herk A.M, German A.L., in "XIXth Fatipec Conference Book", 1988, 3, 341.
6. Caris, C.H.M, Kuijpers R.P.M, van Herk A.M, German A.L, "Kinetics of (co) polymerization at the surface of inorganic submicron particles in emulsion-like systems", Die Makromolekulare Chemie, Macromolecular Symposia, 1990, 35/36, 535.
7. Caris C.H.M., van Elven L.P.M., van Herk A.M, German A.L, "Polymerization of MMA at the surface of inorganic submicron particles", British Polymer Journal, 1989, 21, 133.
8. Yamaguchi T, Ono T, Ito H, "Polymerization of vinyl monomers in the presence of inorganic substances", Makromolekulare Chemie, 1973, 32,177.
9. Yamaguchi T, Ono T, Saito Y, Ohara S, "Polymerization of methyl methacrylate in the presence of graphite", Makromolekulare Chemie, 1976, 53, 65.
10. Hasegawa M, Arai K, Saito S, "Uniform encapsulation of fine inorganic powder with soapless emulsion polymerization", Journal of Polymer Science Part A: Polymer Chemistry, 1987, 25, 3117.
11. Hasegawa M, Arai K, Saito S, "Selective adsorption of polymer on freshly ground solid surfaces in soapless emulsion polymerization", Journal of Applied Polymer Science, 1987, 33, 411.
12. Haga Y, Watanabe R, Angew Y.R, "Photoconductive properties of cadmium sulfide encapsulated in polymers", Makromolekulare Chemie, 1987, 153, 71.
13. Haga Y, Inoue S, Sato T, Angew Y.R, "Photoconductivity properties of zinc oxide encapsulated in polymers", Makromolekulare Chemie, 1986, 139, 49.

14. Hergeth W.D, Starre P, Schmutzler K, Wartewig S, “Polymerizations in the presence of seeds: 3. Emulsion polymerization of vinyl acetate in the presence of quartz powder”, *Polymer*, 1988, 29, 1323.
15. Hergeth W. D, Steinau U, Bittrich H. J, Simon G, Schmutzler K, “Polymerization in the presence of seeds. Part IV: Emulsion polymers containing inorganic filler particles”, *Polymer*, 1989, 30, 254.
16. Furusawa K, Kimura Y, Tagawa T, “Syntheses of composite polystyrene latices with silica particles in the core”, *Journal of Colloid and Interface Science*, 1986, 109, 69.
17. Ali S.I, Heuts J.P.A, Hawkett B.S, van Herk A.M, “Polymer Encapsulated Gibbsite Nanoparticles: Efficient Preparation of Anisotropic Composite Latex Particles by RAFT-Based Starved Feed Emulsion Polymerization”, *Langmuir* 2009, 25, 18, 10523–10533.
18. Daigle J.C, Claverie J.P, “A Simple Method for Forming Hybrid Core-Shell Nanoparticles Suspended in Water”, *Journal of Nanomaterials*, 2008, 609184, 8.
19. Stöber W, Fink A, Bohn E, “Controlled growth of monodisperse silica spheres in the micron size range”, *Journal of Colloid and Interface Science*, 1968. 26, 1, 62-69.
20. Leite C.A.P, Souza E.F, Galembeck F, “Core-and-Shell Nature of Stöber Silica Particles”, *Journal of the Brazilian Chemical Society*, 2001, 12.
21. Macedo A.G, Martins M.A, Fernandes S.E.M, Timmons A.B, Trindade T, Rocha J, “Luminescent SiO₂-coated Gd₂O₃:Eu³⁺ nanorods /poly (styrene) nanocomposites by in situ polymerization”, *Optical Materials*, 2010, 32, 1622–1628.
22. Liu L, Ma E, Li R, Liu G, Chen X, “Effects of phonon confinement on the luminescence dynamics of Eu³⁺ in Gd₂O₃ nanotubes”, *Nanotech*, 2007, 18, 015403.

Chapter 5

Laboratory Experimentation

Preface:

In this chapter the synthetic strategies are brought to light. The synthetic routes for the preparation of the macroRAFT agent (PAA-TTC), the co-polymer (P(AAcoBuA)TTC), inorganic nanofillers (silica and Gd₂O₃:Eu³⁺@silica particles), and the preparation of nanocomposites are detailed. A brief note on the numerous analytical instrumentation techniques used along with a list of the various chemical reagents utilized are provided here. Sample preparation methodologies for various analytical techniques are also elucidated.

5.1 Instrumentation

- Particle size and zeta potential measurements were determined using a Malvern zeta-potential analyser.
- Thermal properties (TGA) were studied on a Shimadzu TGA-50 analyser from 25 up to 700°C under N₂ flow and a heating rate of 10 °C/ minute.
- The absorption spectra were recorded using a Jasco V- 560 UV-Vis spectrophotometer.
- Attenuated total reflection Fourier transformed infra-red spectroscopy (ATR-FTIR) spectra were recorded on a Matson 7000 FTIR spectrometer in absorbance mode.
- Scanning Electron Microscopy (SEM) images were obtained using a FEG-SEM Hitachi S4100 field emission microscope. Transmission Electron Microscopy (TEM) images were obtained using a Hitachi H-9000 Electron Microscope.
- The active surface area (S_{bet}) was determined by nitrogen adsorption on a Micromeritics Gemini equipment.
- Proton NMR Broker Avance/300 with frequency 300 MHz and solvents CDCl₃ and DMSO were used for ¹H-NMR.
- Room temperature emission and excitation spectra were recorded on a Fluorolog Ò -3 Model FL3–2T with a double excitation spectrometer (Triax 320).
- Water was purified using a Sation 8000/ Sation 9000 purification unit

5.2 Reagents Used

Tetraethylorthosilicate (TEOS, Sigma-Aldrich) 98%, 3-methacryloxypropyltrimethoxysilane (MPS, Sigma-Aldrich), 3-aminopropyltrimethoxysilane (APS, Fluka), DL-tartaric acid (Aldrich-Sigma), dimethyl sulfoxide (Merck), ammonia aqueous solution 25% NH₄OH (Merck), ethanol (Fluka), 4,4 azobis (4 cyanopentanoic acid) (Azobiz, Sigma-Aldrich), acrylic acid or propenoic acid (99%, Sigma Aldrich), TTC-A (2-(dodecylthiocarbonothioylthio)-2-methyl propanoic acid) was synthesized by Barros Timmons-Charleux, N,N-Dimethylformamide ACS reagent, ≥99.8% (Sigma aldrich), tert butyl acrylate (98%, Sigma aldrich), acetone (99.5%) (Panreac), chloroform (98%) (Panreac), methanol (99.8%) (Panreac).

Note: All these reagents were deployed in their innate form unless mentioned. Butyl acrylate monomer was purified by passing it through an alumina column under vacuum.

5.3 Laboratory Synthesis

5.3.1 Polymerization Processes

The polymerization process employed was actuated on the work carried out by Ferguson *et al.* [1] which is bifocal in nature i.e.

- The homo-polymerization of PAATTC
- The co-polymerization of P(AAcoBuA)TTC

5.3.1.1 Homo-Polymerization of Acrylic Acid (PAA-TTC)

Based on former kinetic studies the monomer (acrylic acid, 0.045090 mol, 3.5733 g) and RAFT agent (TTCA, 0.000744 mol, 0.2708 g) were taken in a 25 ml round bottom flask and were dissolved in the solvent (DMF, 0.200205 mol, 15.5 ml). The contents were well stirred using a magnetic stirrer until complete dissolution of the macroRAFT agent was noticed. Just before the start of the reaction the thermally active initiator (4, 4 azobis (4 cyanopentanoic acid), 0.000078 mol, 0.02186 g) was added and the round bottom flask was sealed with a rubber stopper and the system was stirred in an ice bath while simultaneously being degassed by bubbling nitrogen for 20 minutes. The contents were permitted to react for 135 minutes (100% conversion, based on previous kinetic studies [2]) at 80°C and the reaction was terminated by immersing the reaction vessel in an ice bath and exposing the contents to air. The contents were purified by precipitation with n-hexane to remove traces of unreacted monomer and solvent DMF. This was dried by using a vacuum pump

for 4-5 hours and collected and stored in a desiccator until further use. The polymer obtained was characterized by FTIR-ATR, NMR, GPC and DSC.

Note: In order to obtain macroRAFT agents, the [Monomer]/[RAFT] ratio taken was 61 and the [RAFT]/[Initiator] ratio taken was 9.48 [2].

5.3.1.2 Co-Polymerization of Acrylic Acid (PAA-TTC) with Butyl Acrylate (BuA)

The copolymerization was carried out using two different process methodologies **a) in solution** and **b) in emulsion** [2]

5.3.1.2.1 Co-Polymerization in Solution

In a round bottom flask (25ml), macroRAFT agent (PAATTC, 0.0000103 mol, 0.5 g), ethanol (0.729444 mol, 13 ml) and the thermally active initiator (4,4 azobis (4 cyanopentanoic acid), 0.0000257 mol, 0.0072 g) was added and the contents were allowed to stir until all of the macroRAFT agent was dissolved in the alcoholic medium. Butyl acrylate (0.0152mol, 2.00 g) was added to our initial contents and the reaction vessel was sealed with a rubber stopper and the contents were stirred in an icebath while being degassed by bubbling nitrogen gas for 20 minutes. The contents were allowed to react for 5:00 hours at a temperature of 70°C and the reaction was terminated by immersing the reaction vessel in an ice bath while simultaneously exposing the contents to air. The copolymer obtained was characterized by FTIR-ATR, NMR, GPC and DSC.

5.3.1.2.2 Co-Polymerization in Emulsion

This is similar to the procedure described in section 5.3.1.2.1 with certain exceptions. In a 25 ml round bottom flask the macroRAFT agent (PAATTC-A, 0.0000103 mol, 0.5 g) was taken and ultra pure water (0.729444 mol, 13 ml), the thermally active initiator (4,4 azobis (4 cyanopentanoic acid), 0.0000257 mol, 0.0072 g) and NaHCO₃ (0.000090 mol, 0.0078 g) were added sequentially and the contents were stirred until the complete dissolution of the macroRAFT agent was observed. The monomer (butyl acrylate, 0.0152mol, 2.00 g) was added to the above mixture and the reaction vessel was sealed with a rubber stopper and the contents were stirred and simultaneously degassed by bubbling nitrogen gas for 20 minutes. The reaction was carried out at 80°C for 4:00 hours. On

completion, the reaction was terminated by plunging the reaction vessel into an icebath while simultaneously exposing its contents to air. The copolymer obtained was characterized by FTIR-ATR, NMR, GPC and DSC.

5.3.1.3 Copolymerization in Emulsion (5:10 ratios)

This was based on the strategy proposed by Ali *et al.* [3]. RAFT copolymers containing on average 5 BA units and 10 AA units, abbreviated as BA5-co-AA10, were synthesized as follows: 9.67 g (76 mmol) of BuA, 10.9 g (151 mmol) of PAATTC-50%, and 0.22 g (1.34 mmol) of 4,4 azobis (4 cyanopentanoic acid) were mixed in a round bottom flask until complete dissolution of PAA-TTC in ethanol was witnessed. The mixture was degassed by bubbling nitrogen gas for 20 minutes and the reaction was heated and stirred at 70°C for 5:00 hours. The reaction was terminated by immersing the reaction vessel in an ice bath and by exposing the contents to air. The sample obtained was purified by precipitation with n hexane to remove traces of the unreacted monomer.

5.4 Inorganic Nanofillers

5.4.1 Silica Nanofillers

5.4.1.1 Preparation of Spherical Silica Nanoparticles

In order to prepared spherical silica nanoparticles the Stöber method [4] was employed. In an Erlenmeyer flask ethanol (42.30 ml), ultra pure water (4.5 ml) and the catalyst (NH₄OH, 1.15 ml) were added and the contents were stirred with a magnetic stirrer for 5-10 minutes before the addition of the metalalkoxide (TEOS, 2.3 g). Upon sealing the flask the mixture was allowed to stir for 24 hours (uninterrupted) at room temperature. The silica particles formed were collected and centrifuged at 12,000 rpm for 20 minutes and then purified by consecutive redispersion /centrifugation cycles using ethanol and distilled water. The precipitate obtained Si-300 nm was collected in a petri dish and dried in a ventilated oven at 60°C for 24 hours.

Si-300 nm was used in the preparation of the nanocomposites after calcination at 700°C for 4:00 hours. Silica particles were characterized by FTIR spectroscopy, zeta potential, dynamic light scattering (DLS) and the morphology was analyzed by scanning electron microscopy (SEM).

5.4.1.2 Preparation of hollow SiO₂ fibres

The method reported by Miyaji *et al.* [5] for the preparation of hollow SiO₂ fibers was used. In this method the metalalkoxide (TEOS, 0.73 g), ethanol (5ml), dl-tartaric acid (0.02 g) and deionized-ultra pure water (0.06 g) were taken in a Erlenmeyer flask (50ml), agitated and left to stand for 30 minutes (molar ratio, TEOS: H₂O: C₂H₅OH: dl-tartaric acid = 1:1:24.3:0.038). The catalyst (NH₄OH, 28% wt. 2 mL) was added to the mixture and it was allowed to stand for another 25-30 minutes. Stirring was avoided as this could lead to the rupture of the newly formed silica hollow fibres. The white precipitate obtained was washed with substantial amounts of distilled water to remove traces of ammonium tartarate and sieved through a brass mesh (400 Mesh-0.038 mm) to remove colloidal aggregates. The fibres were collected and left in a desiccation unit, overnight and then dried in a ventilated oven at 60°C for 24 hours to remove moisture. In order to activate the surface the sample was calcined at 700 °C for 4:00 hours in a calcination unit. They were characterized by FTIR-ATR, SEM and BET.

5.4.1.3 Surface Modification of Silica

5.4.1.3.1 Surface Modification of Silica with MPS

In order to modify the surface of the spherical silica particles MPS (3-methacryloxy propyl trimethoxy silane) was used. The procedure used was similar to the one prescribed by Bourgeat Lami *et al.* [6] with certain exceptions. Silica (0.5g) was taken into a Erlenmeyer flask and ultra pure water (50ml) was added. The contents were sonicated in a sonication bath for a duration of 5-10 minutes to remove aggregates and a good dispersion of silica was obtained. The pH was measured and was kept constant (near neutral) to prevent the homocondensation of MPS which affects the stability of the system. The amount of MPS needed can be found out by calculating the surface area of silica as a function of its diameter and density. According to Bourgeat Lami *et al.* [6] MPS coupling agent per square meter of Silica corresponds to 2.5 times of silanol surface concentration. On calculating, for 1g of silica 0.0528 mL of MPS was added. In our case to the original contents, MPS (0.0264 mL) was added and was left to stir for four days. The next task was to remove the free MPS from the system. This was done by dialysis wherein a cellulose membrane (Polylabo) was used. The membrane was activated by boiling it in distilled water for 3 hours and then the mixture was placed within the membrane and was then tightly sealed by some clamps and was immersed in ultrapure water (3000mL) under constant agitation for a week. Every 24 hours or so the water was changed and was analyzed for free MPS by UV spectroscopy at 203nm

(corresponding to the absorption band of MPS). This was carried out until a very low value of absorbance was observed, which occurred after 4-5 days [6, 7, 8]. The contents were characterized by FTIR-ATR and Uv-Vis analysis and their zeta potential value was obtained via the zetasizer.

5.4.1.3.2 Surface Modification of Silica with APS

In a 50 ml, double necked round bottom flask silica particles (0.5 g) were dispersed in toluene (30 ml) and were sonicated for 30 minutes to ensure good dispersion of the silica particles. Then APS (140 μ L, 0.802 μ mol) was added and the mixture was stirred under reflux conditions for 24 hours at 110°C under nitrogen atmosphere. The silica obtained was filtered under vacuum using a polyamide membrane (NL16, 100 STUCK, 0,2 μ m and ϕ 50 mm) and washed with excess toluene in order to remove free APS. The contents obtained were placed in a desiccation unit under vacuum and were characterized by FTIR-ATR analysis and their zeta potential value was obtained by the zetasizer [9, 10].



Figure 5.1: Lab setup for the preparation of Silica@APS.

5.4.2 Gd₂O₃:Eu³⁺@Silica APS nanorods/fibres Nanocomposites

5.4.2.1 Gd(OH)₃:Eu³⁺ Nanorod/fibres Preparation

Gd(OH)₃:Eu³⁺ was prepared by J. Roach and his team following the hydrothermal methodology reported by L.Q. Lin *et al.*[11]. A mixture of Eu(NO₃)₃·5H₂O (0.19 mmol) and Gd(NO₃)₃·6H₂O (4,2 mmol) was prepared and was stirred for an hour during which the pH was kept constant at 13. The contents were placed in a pre-heated autoclave at 120°C for 15:00 hours. The precipitate obtained was filtered, washed and dried at 60°C for 24 hours. In order to obtain Gd₂O₃:Eu³⁺ the sample was calcined at 700 °C for 4:00 hours. The sample was then characterised by FTIR, S-TEM and BET.

5.4.2.2 Gd₂O₃:Eu³⁺@silica Nanorods Preparation

Immediately after the calcination, Gd₂O₃:Eu³⁺ (380 mg) nanorods were taken in a 100 ml round bottom flask and ethanol (50ml) was added and it was placed in an ultrasonic bath for 10 minutes to remove any aggregation. To this suspension, NH₄OH (30 ml) and the metalalkoxide (TEOS, 1 ml) were added and the contents were mixed by using an ultrasonic probe for 2:00 hours in an ice bath. The final product was purified by three successive centrifugation/ redispersion cycles using absolute ethanol and dried in a ventilated oven at 60°C, for 12:00 hours. The white precipitate obtained was calcined at 700°C for 4:00 hours to thermally activate the surface and this was then characterized by FTIR, S-TEM and photoluminescence (PL) [12].

5.4.2.3 Gd₂O₃:Eu³⁺@SiO₂ APS preparation

This method is similar to the method described in section 5.4.1.3.2. However in this case as only 20-50 mg of fibers were used at a time, a smaller experimental setup was utilized with a 10mg reaction vessel. The obtained contents were characterized by FTIR, S-TEM and photoluminescence (PL).

5.5 Preparation of Nanocomposites.

To the previously mentioned copolymerization processes (solution and emulsion 5.3.1.2) nanofillers (both silica and Gd₂O₃:Eu³⁺@SiO₂) 5% (w/w relative to the initial monomer) were dispersed in a solution of PAATTC (80% conversion), ethanol/water and relative quantities of the butyl acrylate monomer, and the contents were allowed to polymerize (in-situ). The samples were dried in a ventilated oven over night at 60°C and stored in desiccator. The final product was characterized by FTIR-ATR, SEM, PL, EDS etc.

5.5.1 Nanocomposites in emulsion (5:10 Ratio)

Hybrid latex particles were synthesized by emulsion polymerization carried out in a 25 mL round bottom flask. 0.0125g of silica@ APS or MPS spheres were taken and dispersed in deionized water (10.2 ml) and sonicated for 20 minutes. The initiator 4,4 azobis (4 cyanopentanoic acid) (6.37 mg) was added along with the RAFT copolymer (37.5 mg) and stirred. The round bottom flask was sealed with a rubber stopper and stirred in an icebath until complete dissolution of the RAFT copolymer was obtained. It was then degassed by bubbling nitrogen gas for 20 minutes. The

monomer MMA/BuA in the ratio 7:3 (2.35 g) was added and the reaction was carried out at 70° for 2:00 hours [3].

5.6 Preparation of Polymer Films

5.6.1 Casting

In order to study the surface structure and morphology of polymeric materials, nanocomposite films were prepared. The nanocomposite (0.5 g) was taken in a beaker and chloroform (15 ml) was added and the contents were stirred under nitrogen for 24:00 hours. A Teflon mould was utilized and the above solution was spread evenly on the surface. This was left to dry for 48 hours in the fume hood and then left over night in a ventilated oven at 85°C . The films formed were carefully peeled off and stored in a desiccator until further use.

5.6.2 Spin Coating

The glass slide was initially cleaned with absolute ethanol and NaOH solution to ensure the complete removal of contaminants. It was dried over night in a ventilated oven at 110°C. A glass slide was taken and was tightly secured on a spin coating apparatus by making use of duct tape. The sample was carefully spread on the glass slide making sure that the entire slide was covered with the polymeric solution. The machine was made to run for 2 minutes at a speed of 500-800 rpm.

5.7 Sample Preparation Techniques

5.7.1 Preparation of Polymeric Samples for GPC Analysis: Methylation Process

The sample (10 mg) which was needed to be analyzed was dissolved in 2-3 ml of methanol. Three reaction vessels with a gas inlet and outlet were taken. In the first two vessels 20-30 ml of di-ethyl ether was taken and in the third, acetic acid. A mixture of sodium hydroxide or potassium hydroxide (0.5 g) and ethanol (10 ml) was added alongside 5 ml of distilled water (to improve the solubility) to the 1st reaction vessel. In order to start the reaction (2.2 g) di-azo methane was added to the 1st reaction vessel and nitrogen gas was allowed to pass through the entire system. A brisk reaction is observed followed by the formation of a brisk brown colored solution. Care should be taken, as this reaction is highly explosive in nature. Contents from the second vessel are taken, and is added to the polymer sample. This is then evaporated under nitrogen flow and the sample is now ready for GPC.

5.7.1.1 The GPC analysis

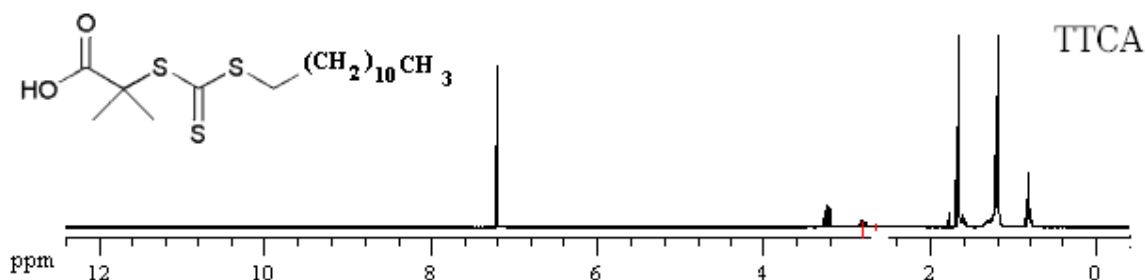
5 mg of polymer was dissolved in 500 µl of DMA/THF solution at 20°C during 30 min and further filtered through a 0.3 µm filter reaching a sample concentration of about 1.0% (10 mg/mL). The SEC analysis was carried out on two PLgel 10 µm MIXED B 300 x 7.5 mm columns protected by a PLgel 10 µm pre-column (Polymer Laboratories, UK) using a PL-GPC 110 system (Polymer Laboratories, UK). The columns, injector system and the detector (RI) were maintained at 70°C during the analysis. The eluent (DMA/THF) was pumped at a flow rate of 0.9 mL/min. The analytical columns were calibrated with polystyrene standards (Polymer Laboratories, UK) in the range 1.7-100.0 kDa. The injected volume was 100 µl.

5.8 Bibliography

1. Ferguson C.J, Hughes R.J, Pham B.T.T, Hawkett B.S, Gilbert R.G, Serelis A.K, and Such C.H, “Effective ab Initio Emulsion Polymerization under RAFT Control”, *Macromolecules*, 2002, 35, 25, 9243-9245.
2. Timmons A.B , Charleaux B, in UPMC, Paris, [unpublished data].
3. Ali S.I, Heuts J.P.A, Hawkett B.S, Herk A.M, “Polymer Encapsulated Gibbsite Nanoparticles: Efficient Preparation of Anisotropic Composite Latex Particles by RAFT-Based Starved Feed Emulsion Polymerization”, *Langmuir*, 2009, 25, 18, 10523–10533.
4. Stöber, W, Fink A, Bohn E, “Controlled growth of monodisperse silica spheres in the micron size range”. *Journal of Colloid and Interface Science*, 1968, 26, 1, 62-69.
5. Miyaji, F., et al., “Organic Crystal Templating of Hollow Silica Fibers”, *Chemistry of Materials*, 1999, 11, 11, 3021-3024.
6. Bourgeat-Lami E, Lang J, “Encapsulation of Inorganic Particles by Dispersion Polymerization in Polar Media: Silica Nanoparticles Encapsulated by Polystyrene.” *Journal of Colloid and Interface Science*, 1998, 197, 2, 293-308.
7. Peixoto, S.M.R, “Síntese e caracterização de nanocompósitos funcionais”, Departamento de Química, 2008, Universidade de Aveiro, Msc Thesis-2009, 1-139.
8. Esteves A.C.C, “Nanocompósitos de matriz polimérica do tipo SiO₂/polímero e CdS/polímero”, in Departamento de Química. 2002, Universidade de Aveiro, MSc Thesis, 1-174.
9. Foschiera J.L, T.M.P.a.E.V.B., “FTIR Thermal Analysis on Organofunctionalized Silica Gel”, *Journal Of The Brazilian Chemical Society*, 2001, 12, 159-164.
10. Olivera F.C, PhD Thesis “Preparation and Characterization of Novel Nanocomposites of Inorganic/Polysaccharide Type”, University of Aveiro, Department of Chemistry July, 2010.
11. Liu L, Ma E, Li R, Liu G, Chen X, “Effects of phonon confinement on the luminescence dynamics of Eu³⁺ in Gd₂O₃ nanotubes”, *Nanotech*, 2007, 18 015403.
12. Macedo A.G, Martins M.A, Fernandes S.E.M, Timmons A.B, Trindade T, Rocha J, “Luminescent SiO₂-coated Gd₂O₃:Eu³⁺ nanorods /poly (styrene) nanocomposites by in situ polymerization”, *Optical Materials*, 2010, 32, 1622–1628.

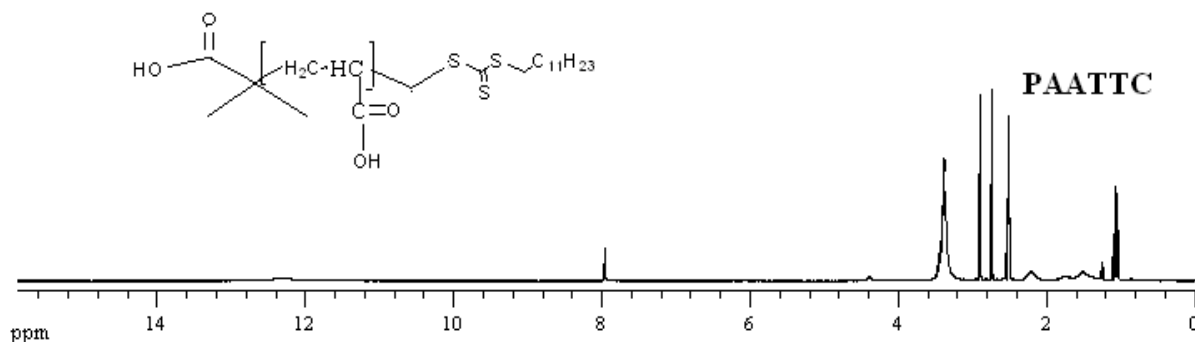
Annex 1: ¹H NMR Studies

a) ¹H NMR of TTC-A



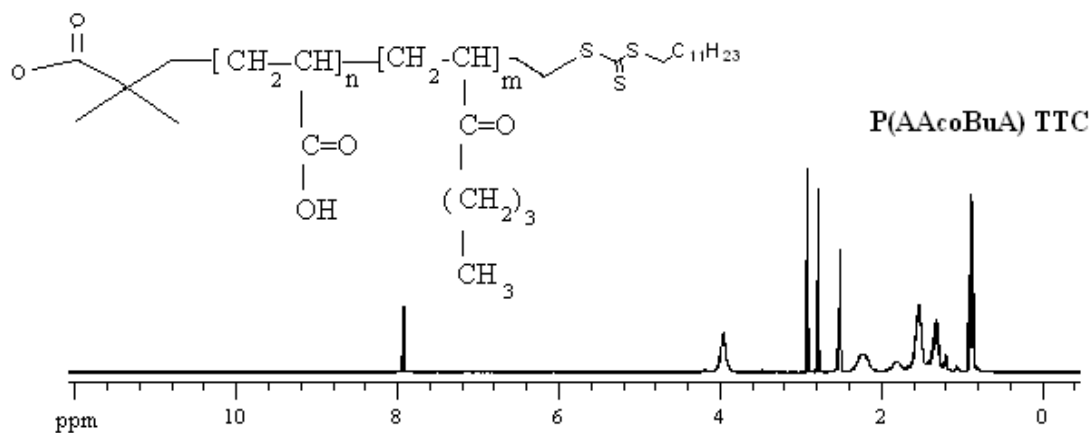
The obtained TTC-A was initially characterized using NMR-¹H. These results were compared with the data obtained from Jutta Rieger *et al.*[1]. The peaks of the ¹H-NMR in CDCl₃ in δ ppm were as follows 0.86 (t, 3H, -CH₂CH₃), 1.23 (m, 18H, -CH₂(CH₂)₉CH₃), 1.67 (s, 6H, -C(CH₃)₂-SC(S)S-), 3.24 (t, 2H, -SC(S)CH₂CH₂-).

b) ¹H NMR of PAATTC



PAATTC-80% was also characterized by ¹H-NMR in CDCl₃ and DMSO in δ ppm. These results were compared with the data obtained from Jutta Rieger *et al.* [1] for the RAFT agent TTC-A. The corresponding peaks at 0.86 (t, 3H, -CH₂CH₃), 1.23 (m, 18H, -CH₂(CH₂)₉CH₃), 1.67 (s, 6H, -C(CH₃)₂-SC(S)S-), 3.24 (t, 2H, -SC(S)CH₂CH₂-) were obtained. For the PAA system the work of Fred O. Garces *et al.* [2] was used for comparison and two peaks at 2.08 and 1.53 ppm corresponding to the H_α and H_β values of the methine group were obtained. The remaining peaks at 2.7 and 3.6 ppm could be due to the presence of DMF, ethanol and other impurities.

c) ^1H NMR of P(AAcoBuA) TTC



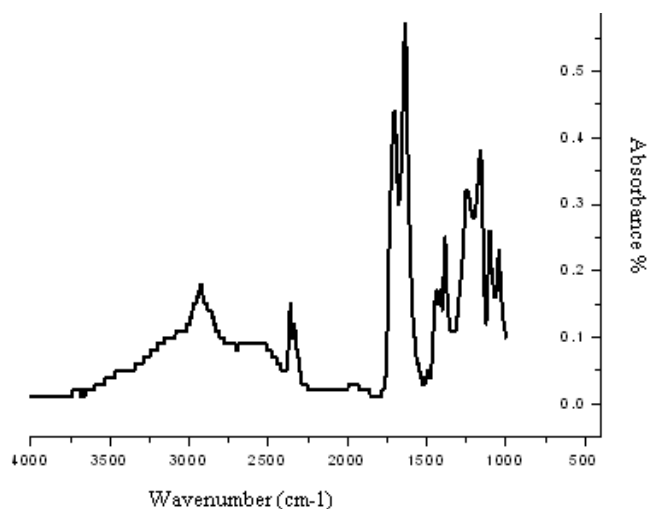
The copolymer obtained was characterized using NMR- ^1H in CDCl_3 and DMSO. These results were then compared with the data obtained from Jutta Rieger *et al.* [1] for TTCA where the peaks were found at 0.86 (t, 3H, $-\text{CH}_2\text{CH}_3$), 1.23 (m, 18H, $-\text{CH}_2(\text{CH}_2)_9\text{CH}_3$), 1.67 (s, 6H, $-\text{C}(\text{CH}_3)_2-\text{SC}(\text{S})\text{S}-$), 3.24 (t, 2H, $-\text{SC}(\text{S})\text{CH}_2\text{CH}_2-$). For the PAA system, peaks were compared to the work of Fred O. Garces *et al.* [2] and two peaks at 2.08 and 1.53 ppm corresponding to the H_α and H_β values of the methine group were obtained. Also for PBuA, from [3] the peak at 4.1 ppm corresponds to the ester methyl protons present in PBuA and the trivalent methine signal can be found in the region 1.8 is due to the resonance in the ester group. The remaining peaks at 2.7 and 3.6 ppm could be due to the presence of solvents such as DMF, ethanol and other impurities.

References

1. Rieger J, Stoffelbach F, Bui C, Alaimo D, Jerme C, Charleux B, "Amphiphilic Poly(ethylene oxide) Macromolecular RAFT Agent as a Stabilizer and Control Agent in *ab Initio* Batch Emulsion Polymerization", *Macromolecules* 2008, 41,12, 4065-4068.
2. Garces F.O, Sivadasan K, Somasundaran P, Turro N.J, "Interpolymer complexation of poly(acrylic acid) and polyacrylamide: structural and dynamic studies by solution- and solid-state NMR", Department of Chemistry, Columbia University, New York, New York 10027, *Macromolecules* 1994,27, 272-278.
3. Ibrahim K, Lofgren B, Seppaa J, "Synthesis of tertiary-butyl acrylate polymers and preparation of di block copolymers using atom transfer radical polymerization" *European Polymer Journal*, 2003, 39 2005–2010.

Annex 2: FTIR-ATR analysis

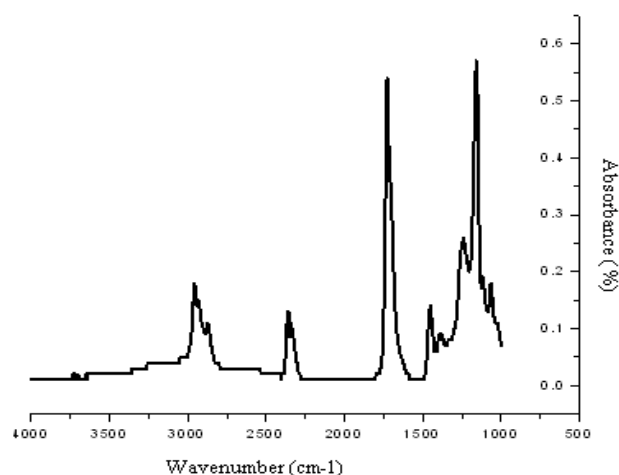
a) FTIR-ATR of PAA-TTC



FTIR-ATR spectrum of PAATTC (80% conversion)

FTIR-ATR spectroscopy was carried out on the sample and the spectrum was obtained from 500 cm⁻¹ to 4500 cm⁻¹. Absorption bands were noticed at 1700 cm⁻¹ which correspond to the stretching of the C=O bond. The bands at 1238 cm⁻¹ and 1167 cm⁻¹ correspond to the C-O stretching. The band at 2600-3500 cm⁻¹ is attributed to the O-H stretching vibration of the PAA dimers which is a characteristic of carboxylic acid. The remaining bands correspond to the TTC-A. [1, 2]

b) FTIR-ATR of P(AAcoPBuA)

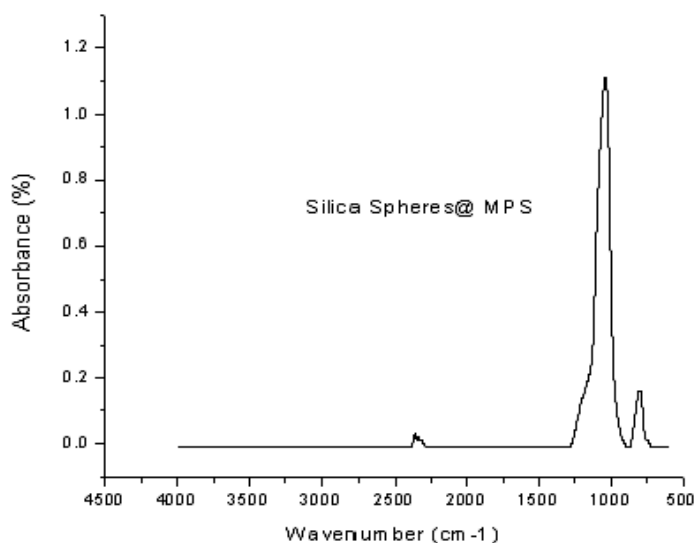


FTIR-ATR spectrum of P(AAcoPBuA)TTC

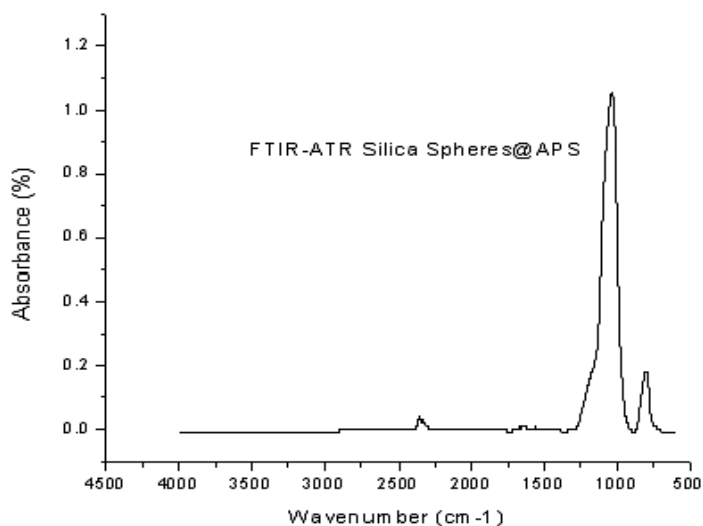
The copolymer was also studied by FTIR-ATR and the spectrum was obtained from 500 cm⁻¹ to

4500 cm^{-1} . An absorption bands were noticed at 1700 cm^{-1} which corresponds to the C=O stretching. The bands at 1238 cm^{-1} and 1167 cm^{-1} correspond to the C-O stretching vibration. The band at 3000-3500 cm^{-1} is attributed to the O-H stretching vibration in the PAA dimers which is characteristic of carboxylic acid. The band at 2961 cm^{-1} corresponds to the C-H stretching of the C-H bonds of the aliphatic chain of PBUA, and the low frequency bands at 1466 and 1375 cm^{-1} belong to the methyl group present in PBUA. The remaining bands correspond to TTC-A. [1, 2]

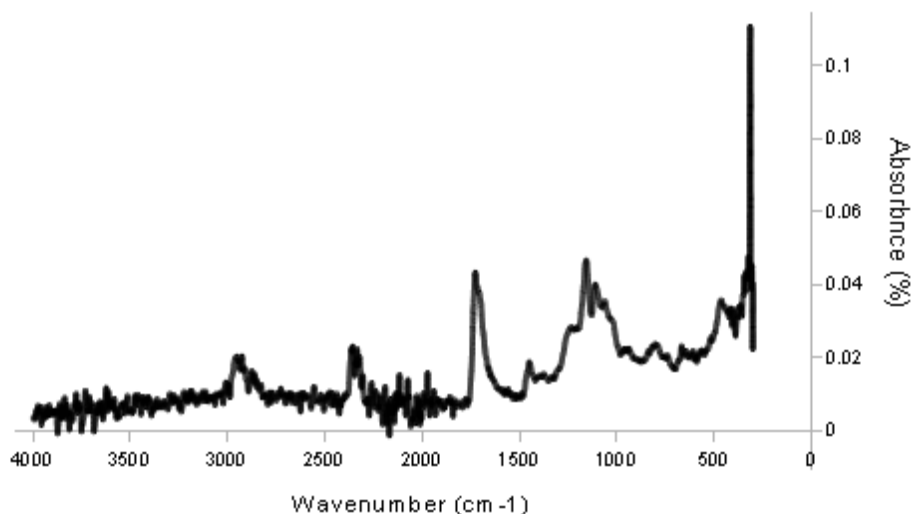
c) FTIR-ATR analysis of SiO_2 @MPS spheres (300nm)



d) FTIR-ATR analysis of SiO_2 @APS spheres (300nm)



e) FTIR-ATR on Silica Fiber nanocomposites



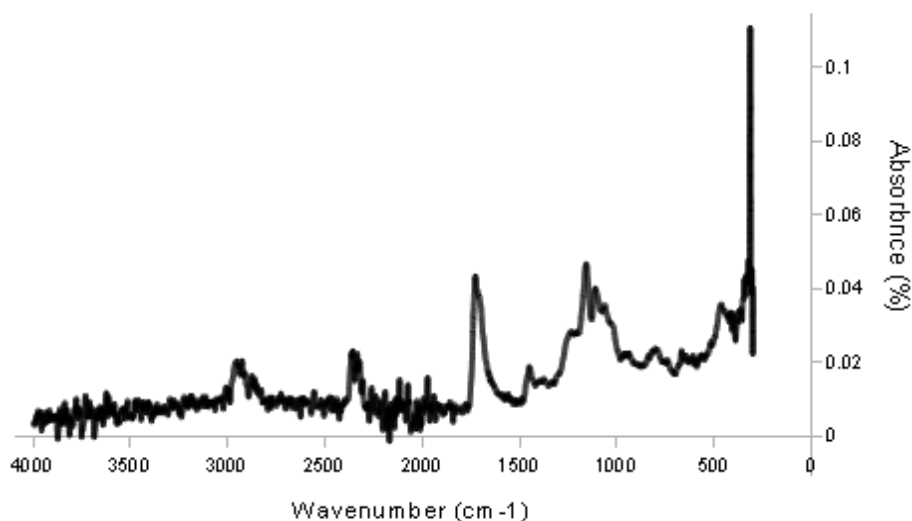
FTIR-ATR spectrum of Silica@APS Nanocomposites (fibers)

FTIR-ATR analysis was performed and a spectrum was obtained from 400 cm⁻¹ to 4500 cm⁻¹. An absorption band were noticed at 1700 cm⁻¹ which corresponds to the C=O stretching. The bands at 1238 cm⁻¹ and 1167 cm⁻¹ correspond to the C-O stretching. The band at 3000-3500 cm⁻¹ is attributed to the O-H stretching vibration in the PAA dimers which is a characteristic of carboxylic acid. The band at 2961 cm⁻¹ corresponds to the C-H stretching in the aliphatic chain of PBUA, and the low frequency 1466 and 1375 cm⁻¹ are characteristic of the methyl group present in PBUA. The bands at 1432 cm⁻¹ and 807 cm⁻¹ correspond to the bending of the Si-CH₂ bond and the N-H bonds of APS. Other bands encountered at 1600 and 2360 cm⁻¹ correspond to the adsorption bands of tartaric acid. The remaining bands corresponds to the TTC-A and the silica. [1-5]

f) FTIR-ATR on Gd₂O₃:Eu³⁺@Silica nanocomposites

FTIR-ATR analysis was performed and a spectrum was obtained from 400 cm⁻¹ to 4500 cm⁻¹. The bands of Gd₂O₃:Eu³⁺ were witnessed at 336, 386 and 431 cm⁻¹ respectively. An absorption band were noticed at 1700 cm⁻¹ which corresponds to the C=O stretching. The bands at 1238 cm⁻¹ and 1167 cm⁻¹ correspond to the C-O stretching. The band at 3000-3500 cm⁻¹ is attributed to the O-H stretching vibration in the PAA dimers which is a characteristic of carboxylic acid. The band at 2961 cm⁻¹ corresponds to the C-H stretching in the aliphatic chain of PBUA, and the low frequency 1466 and 1375 cm⁻¹ are characteristic of the methyl group present in PBUA. The bands at 1432 cm⁻¹ and 807 cm⁻¹ correspond to the bending of the Si-CH₂ bond and the N-H bonds of APS. Other bands encountered at 1600 and 2360 cm⁻¹ correspond to the adsorption bands of tartaric acid. The

remaining bands corresponds to the TTC-A and the silica. [1-7]



FTIR-ATR analysis of Gd₂O₃:Eu³⁺@Silica nanocomposites

References

1. Jiang X, Schoenmakers P.J, Lou X.W, Lima V.G.R, van Dongen J.L.J, Brokken-Zijp J.C.M, Separation and characterization of functional poly(n-butyl acrylate) by critical liquid chromatography, *The Journal of Chromatography A*, 2004, 1055, 1-2, 123-133.
2. Ibrahim K, Lofgren B, Seppaa J, "Synthesis of tertiary-butyl acrylate polymers and preparation of di block copolymers using atom transfer radical polymerization" *European Polymer Journal*, 2003, 39 2005–2010.
3. Foschiera J.L, Pizzolato T.M, Benvenuti E.V, "FTIR Thermal Analysis on Organofunctionalized Silica Gel", *Journal of the Brazilian Chemical Society*, 2001. 12: p. 159-164.
4. Bourgeat-Lami E, Lang J, "Encapsulation of Inorganic Particles by Dispersion Polymerization in Polar Media: Silica Nanoparticles Encapsulated by Polystyrene. *Journal of Colloid and Interface Science*, 1998, 197, 2, 293-308.
5. Olivera F.C, PhD Thesis "Preparation and Characterization of Novel Nanocomposites of Inorganic/Polysaccharide Type", University of Aveiro, Department of Chemistry July, 2010.
6. Söderlind F, Pedersen H, Petoral R.M, Käll P.O, Ovdal, "Synthesis and characterisation of Gd₂O₃ nanocrystals functionalised by organic acids", *The Journal of Colloid and Interface Science*, 2005, 288, 140.
7. Macedo A.G, Martins M.A, Fernandes S.E.M, Timmons A.B, Trindade T, Rocha J, "Luminescent SiO₂-coated Gd₂O₃:Eu³⁺ nanorods /poly (styrene) nanocomposites by in situ polymerization", *Optical Materials*, 2010, 32, 1622–1628.

Annex 3 DSC data

a) DSC : PAATTC Additional attempts

Attempt 2:

Sample	T _g (°C)
PAATTC 100 % conversion	-7.45
PAATTC 80% conversion	-10.32

Attempt 3:

PAATTC (80%- conversion)	T _g (°C)
Test 1	-10.12
Test 2	-10.04
Test 3	-7.66
Test 4	1.58
Test 5	2.13

b) DSC : P(AAcoBuA)TTC : Additional attempts

Attempt 2:

Sample Analyzed	T _g (1)°C	T _g (2)°C
P(AAcoBuA)TTC (100%)	-49.04	-3.06
P(AAcoBuA)TTC (80%)	-51.46	-
P(AAcoBuA)TTC (50%)	-48.22	-

